ABSTRACT

Title of Dissertation:	THE LONG-TERM CHANGE OF CHESAPEAKE BAY HYPOXIA: IMPACTS OF EUTROPHICATION, NUTRIENT MANAGEMENT AND CLIMATE CHANGE
	Wenfei Ni, Doctor of Philosophy, 2019
Dissertation directed by:	Professor Ming Li, Horns Point Laboratory, University of Maryland Center for Environmental Science

Eutrophication-induced coastal hypoxia can result in stressful habitat for marine living resources and cause great economic losses. Nutrient management strategies have been implemented in many coastal systems to improve water quality. However, the outcomes to mitigate hypoxia have been mixed and usually small when only modest nutrient load reduction was achieved. Meanwhile, there has been increasing recognition of climate change impacts on estuarine hypoxia, given estuaries are especially vulnerable to climate change with multiple influences from river, ocean and the atmosphere. Due to the limitation of observational studies and the lack of continuous historical data, long-term oxygen dynamics in response to the changes of external forces are still not well understood. This study utilized a numerical model to quantitatively investigate a century of change of Chesapeake Bay hypoxia in response

to varying external forces in nutrient inputs and climate. With intensifying eutrophication since 1950, model results suggest an abrupt increase in volume and duration of hypoxia from 1950s-1960s to 1970s-1980s. This turning point of hypoxia might be related with Tropical Storm Agnes and consecutive wet years with relatively small summer wind speed. During 1985-2016 when the riverine nutrient inputs were modestly decreased, the simulated bottom dissolved oxygen exhibited a statistically significant declining trend of ~0.01 $mgL^{-1}yr^{-1}$ which mostly occurred in winter and spring. Warming was found to be the dominant driver of the long-term oxygen decline whereas sea level rise had a minor effect. Warming has overcome the benefit of nutrient reduction in Chesapeake Bay to diminish hypoxia over the past three decades. By the mid-21st century, the hypoxic and anoxic volumes are projected to increase by 10-30% in Chesapeake Bay if the riverine nutrient inputs are maintained at high level as in 1990s. Sea level rise and larger winter-spring runoff will generate stronger stratification and large reductions in the vertical oxygen supply to the bottom water. The future warming will lead to earlier initiation of hypoxia, accompanied by weaker summer respiration and more rapid termination of hypoxia. The findings of this study can help guide climate adaptation strategies and nutrient load abatement in Chesapeake Bay and other hypoxic estuaries.

THE LONG-TERM CHANGE OF CHESAPEAKE BAY HYPOXIA: IMPACTS OF EUTROPHICATION, NUTRIENT MANAGEMENT AND CLIMATE CHANGE

by

Wenfei Ni

Dissertation submitted to the Faculty of the Graduate School of the
University of Maryland, College Park, in partial fulfillment
of the requirements for the degree of
Doctor of Philosophy
2019

Advisory Committee:
Professor Ming Li, Chair
Professor William C. Boicourt
Professor Jeffery Cornwell
Professor Raymond G. Najjar
Associate Professor Jeremy M. Testa

Acknowledgements

After over five years of graduate student life at Horn Point Lab, there are so many people that I want to thank for their generous help, guidance and friendship. I will start off by thanking my advisor, Dr. Ming Li for his guidance over the past several years and his patience in getting me through my PhD study. I have gained a lot from every meeting with him, not only on the discussion of scientific questions, but also the philosophy of research. I appreciated his patience and numerous efforts on my first publication, and his guidance on my research proposal. As an ancient Chinese proverb said, "Give a man a fish, and you feed him for a day; show him how to catch fish, and you feed him for a lifetime." I believe that the training that I have received from Ming over the past several years will serve me well throughout my future career. I would like to thank my committee members, Dr. Raymond Najjar, Dr. Jeremy Testa, Dr. Bill Boicourt and Dr. Jeff Cornwell for their insight and guidance. I would like to give special thanks to Ray and Jeremy for the inspired discussions and being helpful on my publications. I also very much enjoyed the wisdom in the chats with Bill and Jeff. There are several people outside my committee and Horn Point Lab who also made contributions to my research: Dr. Andrew Ross from Penn State University provided me with bias-corrected climate model output; Dr. Qian Zhang from Chesapeake Bay Program shared processed nitrate concentration data of the Susquenhanna River; Dr. Rebacca Murphy offered help on the statistical analysis. I also would like to thank my office mates, Dr. Xiaohui Xie, Dr. Fan Zhang, Dr. Wei Liu and Dr. Greg Silsbe, who always provided first aid help when I hit rocks during research. I could not have gotten

through PhD study without the friendship and support from many people. Yini Shangguan, Michelle Lin, Hannah Morrissette, Carol Kim and Catherine Fitzgerald shared a lovely house and a lot of laughter with me during the past five years. I also enjoyed the time hanging out with Emily Russ, Pinky Liau, Sophia Ann, Lexy McCarty and all the Horn Point communities. Finally, I want to give special thanks to my parents who provided me with lots of love and support far away. This PhD study has been supported by UMCES Presidential Fellowship, HPL travel grant, NSF (CBET-1360285) and NOAA-OAP (NA15NOS4780184).

Table of Contents

List of Tables

List of Figures

Chapter 1: Introduction

Ocean deoxygenation refers to the loss of oxygen from the oceans (Keeling et al., 2010) and has attracted extensive attention in recent decades. Long-term ocean monitoring records reveal that oxygen concentration in the open ocean have declined during the 20th century and will most likely continue to decrease with projected climate change. However, in estuaries and the coastal ocean, strongly influenced by the watershed where expanding human population and extensive agricultural activities take place, the oxygen declines (or deoxygenation) have been mostly caused by the increasing loadings of nutrients (nitrogen and phosphorus) and organic matter (Diaz et al., 2008; Breitburg et al., 2018). When the oxygen level becomes low enough (hypoxia), it generates undesirable effects on marine ecosystem including loss of habitat for bottom-dwelling fish and benthic fauna, increasing mortality, altering trophic interaction and energy transfer, and interrupt ecosystem function by changing nutrient cycling and bioturbation (Rabalais et al., 2002).

Several literature reviews have summarized the hypoxia features and processes in various coastal systems, including estuaries, continental shelves, upwelling regions, fjords and semi-enclosed basins, and how these systems responses to the changes in nutrient loads and other forces (Diaz, 2001; Kemp et al., 2009; Rabalais et al., 2010; Zhang et al., 2010; Fennel and Testa, 2018). The following chapters in this dissertation address hypoxia in Chesapeake Bay as a prototype, to investigate the system response to historical eutrophication, recent nutrient management and future climate changes, from the perspective of long-term change of hypoxia. The findings of this study can be

instructive to managers in setting loading targets to restore water quality and serve as a reference to other hypoxic coastal environments faced with similar issues.

1.1 Chesapeake Bay hypoxia and eutrophication

Hypoxia was first observed and reported in Chesapeake Bay during summer between Patuxent River and Annapolis as early as 1930s (Newcombe and Horner, 1938). However, recurring hypoxia was considered to develop after the 1950s, when anthropogenic nutrient loading began to rise rapidly, and hypoxia expanded ~2 fold during the following four decades (Hagy et al., 2004). Previous studies have mostly focused on the biological and physical processes in the seasonal development of hypoxia (Taft et al. 1980; Malone, 1986; Boicourt, 1992; Sanford et al, 1990; Testa et al., 2014), and the factors controlling the interannual variation of hypoxia (Zhou et al., 2014; Li et al., 2016; Scully, 2016; Du et al., 2018) in Chesapeake Bay. Only limited studies probed into the long-term change of eutrophication status and hypoxia condition in Chesapeake Bay over the past half century (Hagy et al., 2004; Murphy et al., 2011; Harding et al., 2015; Kemp et al., 2009). The major constraining factor is the lack of long-term, continuous and extensive observational data of water quality over the whole bay.

With the insufficient observational data from Chesapeake Bay Institute (prior to 1984) and Chesapeake Bay Program (after 1984), a regime shift of hypoxic volume in response to the increasing nitrogen load of the Susquehanna River was discovered by several studies (Kemp et al., 2009; Murphy et al., 2011). This increased sensitivity of hypoxia with nutrient loading also has been found in other coastal environments,

such as the northern Gulf of Mexico and Danish Straits (Kemp et al., 2009; Conley et al., 2007). However, although several factors might contribute to the abrupt change in hypoxia response to nutrient loading, including the alterations in physical environment, nutrient cycling and ecosystem characteristics, the primary cause and dominant process is still unclear.

1.2 Nutrient management and coastal hypoxia in past decades

With increasing knowledge of the causes and consequences of hypoxia, nutrient management strategies have been implemented worldwide in recent decades to improve water quality and mitigate hypoxia. Actions have been taken in coastal hypoxic systems around world to reduce anthropogenic nutrient loads by controlling the sources of pollution in the watershed (HELCOM, 2007, 2013; USEPA, 2010). However, the outcome of watershed nutrient management on load reduction and hypoxia mitigation greatly varied among the systems (Conley et al., 2009; Mee et al., 2006; Van Meter et al., 2018). Unless the nutrient load reduction is large enough and surpasses other factors, the remediation of hypoxia is not easily achieved, especially in large and open systems where climatic influences are prominent.

Chesapeake Bay has been subject to extensive efforts to reduce nutrient inputs since the 1980s. In 1987, a commitment was made to reduce controllable sources of both nitrogen (N) and phosphorous (P) by 40% by the year 2000. Although the actual implementation fell short of the goals, there were appreciable declines of dissolved nitrogen, widely reported by Zhang et al. (2015), Murphy et al. (2011), Testa et al. (2018), and Harding et al. (2015). However, no long-term trends in the magnitude of

summer hypoxia in Chesapeake Bay were found in previous retrospective studies based on the water quality monitoring data since 1984. Only some shifts in the seasonal cycle of hypoxia, an increase in early summer and a decrease in late summer, have been revealed.

The outcome of nutrient management practice in Chesapeake Bay appears to be modest, since the secular change is relatively small compared to the large seasonal and interannual variability of oxygen condition. In addition to nutrient loading, climate forces, such as freshwater discharge, wind and temperature, can also generate significant influences on the short-term and long-term change of hypoxia, by controlling the physical supply of oxygen to bottom water and biological consumption of oxygen. Freshwater discharge can not only sustain the stratification that contributes to the formation of summer hypoxia, but also determine the nutrient loads into estuaries that stimulates oxygen consumption (Justić et al., 1993; Boicourt, 2000; Hagy et al., 2004; Hetland & DiMarco, 2008). Both wind direction and speed can affect vertical mixing of oxygen by altering stratification and advection, and manipulate hypoxia from short to longer time scale (Scully 2010, 2013; Yu et al., 2015; O'Donnell et al., 2008). Therefore, there have been rising concerns about climate change impacts on coastal hypoxia paralleling the nutrient reduction. The influences of climate change may become even more significant in larger hypoxic marine systems receiving nutrient inputs from vast drainage basins.

The key question missing in previous observational studies is that they could not separate the individual effects of nutrient reduction and climate change, and determine the driving force for the long-term trend in hypoxia in Chesapeake Bay since the 1980s. Process-based numerical models are alternative research tools that have yet to be used to address this question. However, the comprehensive modeling study to quantify the relative importance of recent nutrient reductions and climate change on the long-term changes of oxygen in Chesapeake Bay is still lacking.

1.3 Future regional climate change impacts on coastal hypoxia

Although coastal deoxygenation and hypoxia formation have been mainly linked to increases in nutrient loading, there is increasing recognition of climate change influences on the long-term variation of hypoxia in estuaries and coastal waters (Justic et al., 2003; Carstensen et al., 2014; Meier et al., 2017). Numerical model simulations and climate projection models have been widely applied to estimate the future climate change impact in various coastal hypoxic systems, especially in European waters. Bendtsen and Hansen (2013) found that future warming will significantly increase the hypoxic bottom areas in Baltic Sea-North Sea transition zone. Using an ensemble of coupled physical-biogeochemical models driven by global climate model outputs, Meier et al. (2011) projected considerable expansion of hypoxic and anoxic areas in the Baltic Sea. It should be noted that the competing effects between a changing climate and nutrient reduction in future hypoxia can still be uncertain (Meier et al., 2011; Sariva et al., 2019b; Irby et al., 2018; Ni et al., 2019).

Chesapeake Bay is experiencing rapid climate change. The surface water temperature in the bay increased at the rate of 0.05 to 0.10 °C/yr during the past 30 years (Ding and Elmore, 2015). Sea level rise rate has accelerated over the last century in the bay and reached 4-10mm yr^{-1} in 2011 (Ezer and Corlett, 2012). The future climate projections suggest these changes would most likely continue in the Chesapeake Bay region in the 21st century and potentially generate large impacts on the bay (Najjar et al., 2000, 2010). Therefore, there is increasing recognition and concern about climate change impacts on Chesapeake Bay.

Two recent modeling studies have examined the impacts of future climate change on hypoxia in Chesapeake Bay (Irby et al., 2018; Wang et al., 2017). Those studies imposed simplified climate changes on the model boundary and tested the response of Chesapeake Bay hypoxia to each individual force or combined forces. Although these studies were the first attempt to investigate climate change impacts on Chesapeake Bay hypoxia, their method was generally considered as sensitivity analysis rather than making future projections. The natural climate variability and connections within the climate system (e.g., the relationship between temperature, precipitation/evapotranspiration, and river discharge change) were also missing in their studies. Therefore, further integrated modeling study on future change of Chesapeake Bay hypoxia that combine regional climate projections and coupled physical-biogeochemical model is needed.

1.4 Motivations and thesis structure

In summary, the overall motivation of this research is to utilize a numerical model to understand the over a century time scale change of Chesapeake Bay hypoxia in response to the varying external forces, including the drastic increase of nutrient loading from 1950s to 1980s, the slight nutrient load reduction with rapid climate changes from 1980s to 2010s, and projected future climate changes imposed on the current high nutrient inputs in mid-21st century. The findings of this research, generated with the use of a numerical model, will provide comprehensive insights on the oxygen dynamics of estuaries over long time scales.

This dissertation is organized as follows: retrospective simulation of Chesapeake Bay hypoxia with eutrophication from the 1950s to 1980s is presented in Chapter 2, followed by the study to discern the effects of warming, sea level rise and nutrient management on the long-term hypoxia trend in Chesapeake Bay in Chapter 3; Chapter 4 investigates the projected future climate change in the mid-21st century on Chesapeake Bay hypoxia; and Chapter 5 summarizes the findings, identifies remaining questions, and suggested future research directions.

Chapter 2: Retrospective simulation of Chesapeake Bay hypoxia with eutrophication

Preface

This chapter is a reproduction of work will soon appear in the *Journal of Geophysical Research: Oceans* with coauthors Ming Li. The right to reuse this work was retained by the authors when publication rights and nonexclusive copyright were granted to the American Geophysical Union.

Ni, W., Li, M. (In prep). Retrospective simulation of Chesapeake Bay hypoxia with eutrophication. Journal of Geophysical Research: Oceans.

2.1 Introduction

The occurrence and intensity of hypoxia in estuaries and coastal waters has been expanding in recent decades coincident with eutrophication due to excess riverine nutrient inputs. Previous reviews found varying oxygen responses to nutrient loading in coastal aquatic system worldwide (Kemp et al., 2009; Zhang et al., 2010). In small and well mixed systems where point source organic matter input dominates, such as Laajalahti Bay and Scheldt estuary, hypoxia usually changes linearly with inorganic and organic nutrient loads (Kauppila et al., 2005; Soetaert et al., 2006). In large stratified systems where ecosystem structure is complex and physical processes play a key role in oxygen depletion, the responses of hypoxia to nutrient load can be non-linear, i.e. with a threshold above which a relatively small change in nutrient input causes an abrupt increase in hypoxia (Kemp et al., 2009). Some large coastal marine ecosystems, such as Chesapeake Bay, Danish coastal waters and the Northern Gulf of Mexico, exhibit a likely regime shift with increase in susceptibility of hypoxia in more recent decades (Conley et al., 2009).

For the long-term change of hypoxia with eutrophication in Chesapeake Bay since 1950s, when the riverine nutrient load grew rapidly and regular water quality measurement in the main bay began, there have been some key studies to detect the long-term trend of hypoxia and identify the relation between hypoxia and Susquehanna River nutrient loading. With the intermittent measurements made during 1950-1980, Flemer et al. (1983) found a drastic increase in hypoxia during this period while Selger&Boggs (1988) suggested there was not sufficient evidence for the long-term

increase and interpreted the variation mostly as interannual difference. Hagy et al. (2004) extended the oxygen dataset by combining Chesapeake Bay Program monitoring data in 1984-2001 and concluded that summer hypoxic volume expanded substantially from 1950 to 2001, with ~2-fold increase of nitrate loading (Figure 2.1b). During the same period, there has been a significant increase of phytoplankton biomass in the main stem of Chesapeake Bay (Harding & Perry, 1997; Harding et al., 2015).

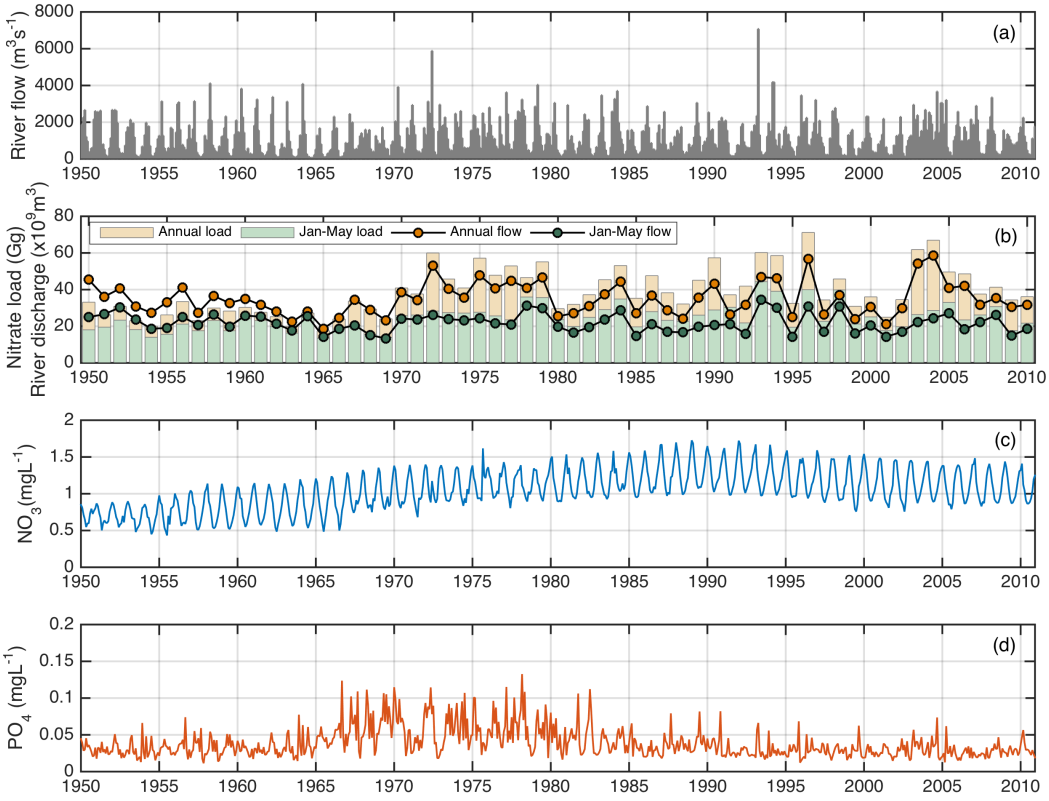

Figure 2.1 (a) Monthly freshwater discharge of Susquehanna River during 1950-2010. (b) Jan-May and annual average river discharge/nitrate load of Susquehanna River. (c) Estimated monthly average nitrate concentration of Susquehanna River during 1950-2010 from Zhang et al. (2013). (d) Reconstructed monthly average phosphate concentration of Susquehanna River during 1950-2010.

Chesapeake Bay has been found to be more susceptive to hypoxia in recent years; that is, for a given nitrate loading more hypoxia would occur after the 1980s than earlier decades. In the Kemp et al. (2009) defined this change as regime shift with

threshold in the hypoxia response to nutrient loading. The turning point for the shift in the hypoxia-nutrient load relationship was detected by Conley et al. (2009), which occurred in 1986. The ecological changes associated with eutrophication in Chesapeake Bay, such as the loss of benthic habitat and submerged plants, may have caused the shift by reducing the efficiency to retain nutrients and a supporting planktonic environment that ferment hypoxia (Kemp et al., 2005). The positive feedback between water column-sediment recycling of dissolved nutrients and hypoxic may also account for the increased hypoxia volume generated per unit nitrogen loading during 1965-2007 (Testa & Kemp, 2012). In addition to ecological and biogeochemical changes, the abrupt changes in physical forcing can affect the long-term hypoxia by altering the oxygen supply to the bottom water. Murphy et al. (2011) suggested the long-term trend of increasing stratification could be a driver for the observed increase of hypoxic volume per nitrogen loading. The change of salt influx into Chesapeake Bay due to sea level rise, shift in Gulf Stream position, and the change of summer prevailing wind direction and intensity are other physical factors that which may have induced the shift in hypoxia-nutrient loading relation (Kemp et al., 2009). However, none of these biogeochemical or physical process has been proved to be deterministic or significant enough to cause this hypoxia regime shift.

This study uses retrospective numerical simulations to reproduce and investigate the long-term change of hypoxia with increasing nutrient load from 1950 to 1989. The historical nutrient concentration in the major tributaries of Chesapeake Bay is reconstructed from an up-to-date watershed study and reasonable assumption. The

development of hypoxia and the varying relation to nutrient loading is analyzed and inspected based on the simulation results. The potential causes for the shift are also discussed.

2.2 Method

2.2.1 Reconstruction of historical riverine nutrient concentrations

The Susquehanna River is the largest single contributor among the non-tidal rivers feeding Chesapeake Bay in terms of river flow (62%), total nitrogen (TN) load (65%), total phosphorus (TP) load (46%), and Suspended Sediment (SS) load (41%) during the period of 1979-2012 when abundant observing data was available (Zhang et al., 2015) (Figure 2.1). Thus, Susquehanna River dominates the temporal trend of the riverine nutrient loads and freshwater discharge into Chesapeake Bay. Also, Susquehanna River is the only tributary that drains directly into the main stem of Chesapeake Bay without its own estuary. The nutrient loads from other tributaries are substantially reduced by their own estuaries before reaching the main bay (Boynton et al., 1995). Thus, the hypoxia was found to be positively correlated with nitrate loading from Susquehanna River during 1950-2001 (Hagy, et al., 2004). Since the measurement of nutrient concentration was insufficient and discontinuous before 1980s when USGS River Input Monitoring Program and Chesapeake Bay Program began, the reconstruction of historical nutrient concentration of Susquehanna River is an important first step to conduct retrospective simulation.

The monthly nitrate plus nitrite concentration (NOx) at the USGS Conowingo Station from 1950 to 1985 was obtained from Zhang et al. (2013) using the "Weighted Regressions on Time, Discharge, and Season" (WRTDS) method (Figure 2.1c). This method considers varying concentration-flow relation and seasonal trends, which can produce better temporal variations in concentration and load (Hirsch et al., 2010). The NOx concentration data at Harrisburg from 1945 to 1978 was converted to the concentration at Conowingo Dam, which is just above the head of tide, using monthly ratios from Hagy et al. (2004). This estimated data, together with observational NOx data at Conowingo during 1978-2011 constituted the full records at Conowingo during from 1945 to 2011.

The total phosphorus (TP) data at Conowingo and Harrisburg station was firstly combined during 1971-1989, using the monthly average scaling factor between these two stations. Since the TP data before 1971 was missing, we attempted to reconstruct this data referring the observed nutrient trend in upper Chesapeake Bay. A "rise-then-fall" pattern was observed in phosphate concentration in oligohaline region during 1960s-1990s from Harding et al. (2015), mostly due to the implementation of a ban on phosphate in detergents. Thus, we assumed there was a cosine-shaped trend in TP between 1965 and 1985 (peak in 1974, about 2.5 times of low TP level during 1985-1990), and TP maintained low level as 1985-1989 before 1965. After the TP was re-constructed during 1950-1989, phosphate and other phosphorus nutrients (i.e. particulate organic phosphorus and dissolved organic phosphorus) were calculated from the climatology of monthly scaling factors with TP during 1985-1989. For the

estimation of other forms of nitrogen nutrients (e.g. ammonium, particulate organic nitrogen and dissolved organic nitrogen), we used similar method with monthly scaling factors with NOx, assuming the factors remained unchanged between 1985-1989 and 1950-1984 (Figure 2.1c,d).

In addition to the Susquehanna River, the Potomac River also contributes to large portion of freshwater discharge and nutrient loads to the main stem of Chesapeake Bay. However, the data records of NOx inputs of Potomac River before 1985 was mostly absent. A simple assumption was made that the Potomac River had same long-term trend in NOx as the Susquehanna River during 1950-1989. To acquire long-term trend, a Butterworth low-pass filter was used to remove the seasonal and interannual variations of NOx during 1945-2011 in Zhang et al. (2013). Then the time series was normalized to 0-1 by the average value of a high concentration period (1985-1989). Combining the averaged NOx concentration of the Potomac River during high level period (1985-1989) and normalized time series of the Susquehanna River, the historical NOx concentration of Potomac River during 1950-1985 was generated. The extended PO_4 concentration of Potomac River during 1950-1985 was estimated based on Jaworski et al. (2007).

For the other major tributaries, which most of the nutrient input records before 1980s are missing, we just assumed they had similar trend in NOx and PO_4 as Susquehanna River. The historical NOx and PO_4 concentration during 1950-1985 were created using the same method above for Potomac River. For Potomac River and other

major tributaries, the concentrations of other forms of nitrogen and phosphorus nutrients were estimated by the method assuming constant monthly ratio during 1985-1994 in each tributary as Susquehanna River.

2.2.2 Coupled physical-biogeochemical model (ROMS-RCA)

In this study, the coupled physical-biogeochemical model is used to implement the retrospective simulation from 1950 to 1989 with constructed historical riverine nutrient loading. Regional Ocean Modeling System (ROMS) model provided the simulations of hydrodynamics in Chesapeake Bay, which has been developed and validated against the observations in previous studies from tidal to seasonal time scales (Li et al. 2005; Zhong and Li, 2006; Cheng et al., 2013, Xie and Li, 2018). The model has 120×80 horizontal grids (~1-2 km resolution) and 20 layers in vertical sigma-coordinate (Figure 2.2). The ROMS model configuration is the same as the one used for climate projection simulations (Ni et al., 2019) . Atmosphere, river and ocean forcing at the boundaries of model domain are required to drive the ROMS simulation.

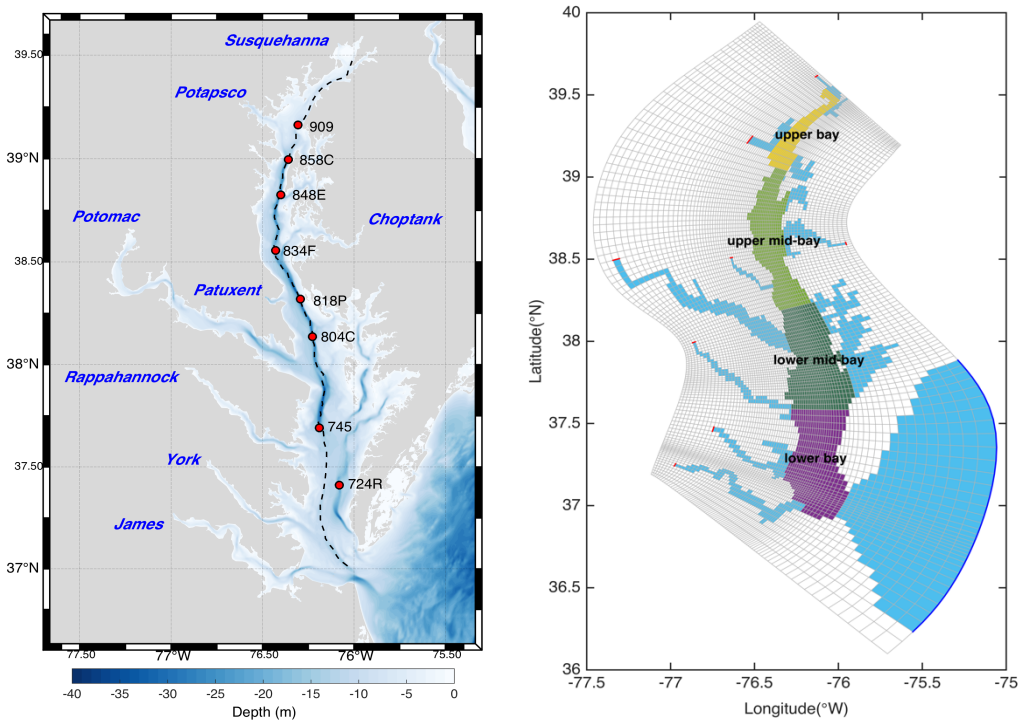

Figure 2.2 (a) Chesapeake Bay Institute monitoring station and (b) ROMS-RCA model domain, showing definitions of upper, upper-mid, lower-mid and lower portions of the main stem bay.

North American Regional Reanalysis (NARR) in 1978, a new dataset from NOAA-CIRES-DOE (National Oceanic and Atmospheric Administration-Cooperative Institute for Research in Environmental Sciences-Department of Energy) Twentieth Century Reanalysis (20CR) project (https://www.esrl.noaa.gov/psd/data/20thC_Rean/) is utilized to provide the essential atmosphere variables. 20CR combines a data assimilation system with surface pressure observations and generates global atmospheric dataset of weather spanning 1851 to 2014 (V2c) at 3-hourly interval across 2° latitude x 2°longitude global grid. Only wind speed is bias-corrected and scaled by month to NARR as a reference. The air-sea fluxes of momentum and heat across the

surface are calculated based on standard bulk formula (Fairall et al., 2003) from the atmospheric variables, including surface air pressure, downwelling longwave radiation and net shortwave radiation, relative humidity and air temperature at 2m above surface, and wind velocity at 10 m above surface. The tidal component of water level at the east open boundary during 1950-1989 is generated by harmonic analysis from Oregon State University global inverse tidal model TPXO7 (Egbert and Erofeeva, 2002). The non-tidal component during 1978-1989 is calculated from de-tided water level at Duck, NC (NOAA station ID: 8651370). For the non-tidal component during 1950-1977 when Duck data are absent, we assume it repeats the period of 1978-2015 with half of the sea level rise rate during this period. The salinity and temperature at ocean boundary is interpolated from World Ocean Atlas (WOA) 2013 decadal average from 1955 to 2012. The freshwater discharge of each major tributary during 1950-1989 is obtained from daily record at USGS monitoring stations using similar scaling method as Hagy et al. (2004) when the data is incomplete. For the water temperature at each tributary, we calculate the monthly averages during 1985-1989 at CBP stations and simply use the average annual cycle to replace the missing data during 1950-1984.

The biogeochemical model Row-Column AESOP (RCA) is forced with ROMS hydrodynamic output at the same model grid. RCA includes both eutrophication model in water column (Isleib et al., 2007) and a two-layer sediment model (Di Toro, 2001; Testa et al., 2013; Brady et al., 2013). The coupled ROMS-RCA model has been utilized to investigate the interannual variation of O_2 and ecosystem metabolism in Chesapeake Bay (Li et al., 2016; Shen et al., 2019). Two phytoplankton groups are

included in RCA model, the winter-spring species (optimal growth rate at 10°C) and the summer species (optimal growth rate at 25°C). The turnover of particulate and dissolved forms of organic carbon, organic and inorganic nutrients (nitrogen, phosphorus) and O_2 is simulated in the eutrophication model. The bottom sediment receives fluxes of particulate organic matter and oxygen from water column and exchanges dissolved nutrients and mineralized end-product. The RCA model is described in detail in Testa et al. (2014) and the configuration in this study is consistent with Li et al. (2016). The river inputs of phytoplankton, particulate and dissolved organic carbon, organic and inorganic nutrients are linearly interpolated from Chesapeake Bay Program bi-weekly monitoring data at the major tributaries during 1985-1989 (https://www.chesapeakebay.net/what/data). For the period of 1950-1984, the nutrient inputs are acquired based on other data sources or assumptions described in Section 2.2.1. The ocean boundary concentrations nitrate and phosphate are acquired from WOA 2013 decadal average and from Filippino et al. (2011). The atmospheric deposition is neglected in this study.

2.2.3 Retrospective simulation during 1950-1989

The model simulation was implemented for the years 1950 to 1989, when both the nitrate loading of Susquehanna River and hypoxic volume of main Chesapeake Bay increased substantially. The ROMS model was initiated in year 1949 as spin-up, then run continuously in the following 40 years with output at hourly interval. The RCA model was run on the same grid as ROMS model at computational time-step of 450 seconds and the output was saved at 4-hourly interval. Since most of the organic matter generated in Chesapeake Bay is consumed within annual cycle (Cowan and Boynton,

1996), RCA model was initiated every year with the spatial-interpolated condition of pervious December from the CBP observation during 1985-1989. The averaged initial condition of 1985-1989 was set as the initial condition for 1970-1984 when the river nutrient and organic matter input was at high level; it was scaled by 0.5 for 1950-1969 when the river input was at relatively low level.

The model output of bottom O_2 and hypoxic volume was calculated and compared with limited measurements at Chesapeake Bay Institute monitoring stations (Figure 2.2). The along-channel and cross-channel development of hypoxia over each decade during 1950-1989 were investigated. The statistical GAM model was utilized to identify the spatial and temporal change of bottom O_2 during this period. To discover the causes for the change in hypoxia with nutrient loading, we further examined the change in surface chlorophyll-a and the hypoxic volume vs. nutrient load relation.

2.3 Results

2.3.1 Model validation of bottom O_2 and hypoxia volume

The model output of bottom O_2 is compared with limited historical observational data during 1950-1989 along the central channel of Chesapeake Bay. Prior to the initiation of Chesapeake Bay Program (CBP) in 1984, the water quality measurement was conducted by the Chesapeake Bay Institute (CBI) during 1949-1982 at multiple stations in the main stem and major tributaries. The historical observation data from CBI was inconsecutive and sampled less than once a month. CBP performs bi-weekly on-site measurements between March and October since 1984,

however, at different locations as CBI. To facilitate the comparison between model results and difference sources of observation, we selected 8 CBI monitoring stations which are close to CBP stations along the central channel of Chesapeake Bay (Figure 2.2).

The model simulation well captured the seasonal variation of bottom O_2 at these stations (Figure 2.3). The correlation coefficient between model outputs and observation ranged from 0.79-0.87 at varying stations, and the Root-Mean-Square-Error (RMSE) was relatively small compared to the variance. In addition, the model showed excellent agreement with observation in the spatial difference of summer bottom O_2 along the main stem, that the middle bay was more hypoxic than the lower bay and Station 745 (CB5.5) marks the south end of hypoxic zone in the summer. The model results also displayed the similar long-term decline in summer bottom O_2 as the observation from 1950-1969 to 1970-1989, especially in upper bay station (909) and lower bay station (745). Additional interannual variation of bottom O_2 in the observation can be clearly seen in the model output. Therefore, the model did a great job to simulation the temporal and spatial change of Chesapeake Bay O_2 with increasing nutrient loads. The validation on bottom O_2 supports the subsequent quantitative analysis on the development of hypoxia and its relation with nutrient loads.

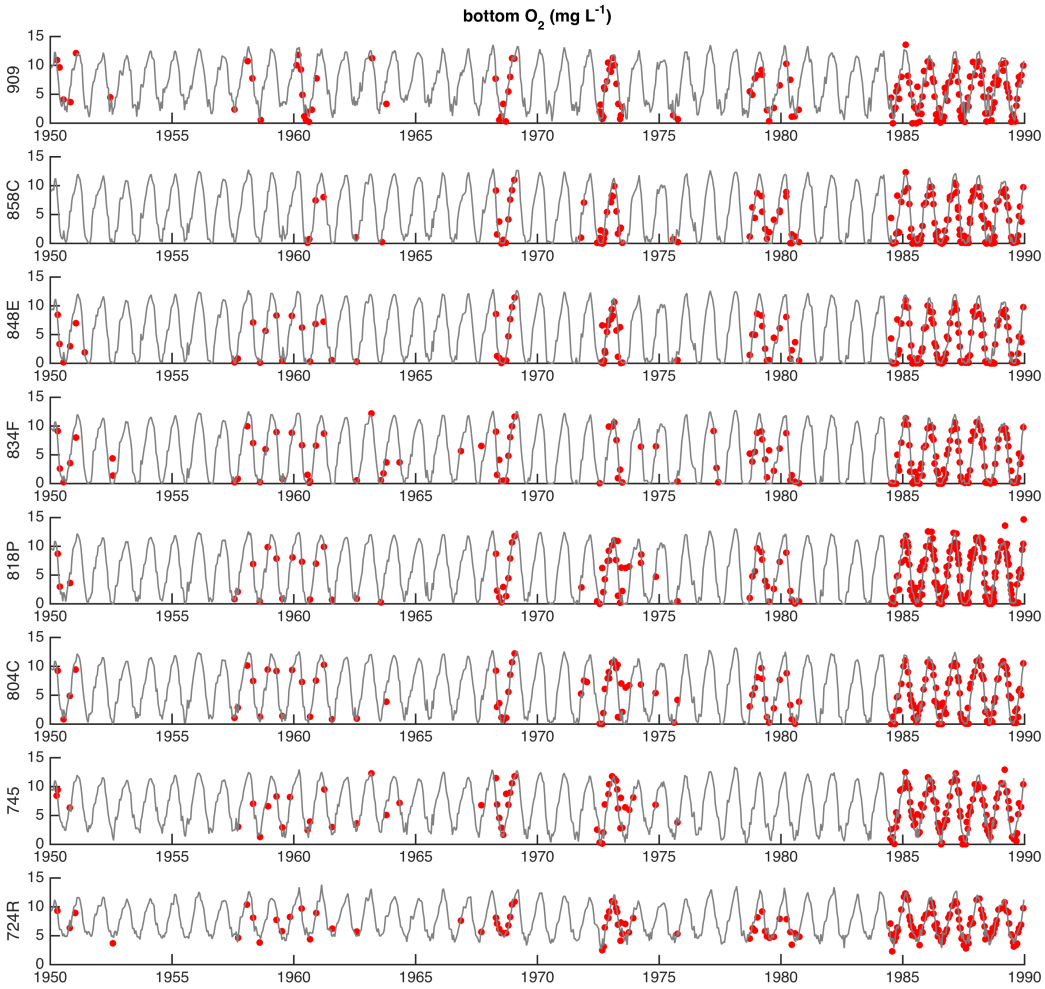

Figure 2.3 Model validation of bottom O_2 at CBI monitoring stations along central channel of main Chesapeake Bay (stations location see Figure 2.1)

In addition, the hypoxia volume (O_2<2mg L^{-1}) of main Chesapeake Bay was calculated based on the model outputs and compared with the observed July hypoxic volume from Hagy et al. (2004). Model results showed good agreement with observation in the interannual variation of summer hypoxic volume (Figure 2.4). However, the simulated maximum summer hypoxic volume was 20-70% larger than the observation in July. This mismatch between model simulation and observation may result from the scarce data in both time and space. Thus, the peak volume might not be able to be captured by the monthly snapshot from field survey. Besides, wind event or

other extreme weather can alter the hypoxia drastically within a few days. For example, during Tropical Storm Agnes in 1972, record high freshwater was discharged into Chesapeake Bay from June 20th to July 5th and significantly altered the subsequent oxygen condition in the Chesapeake Bay (Schubel&Cronin, 1977). With more frequent sampling after 1984 by Chesapeake Bay Program, the model could reproduce the observed hypoxic (O_2<2mgL^{-1}) volume and anoxic (O_2<2mgL^{-1}) volume.

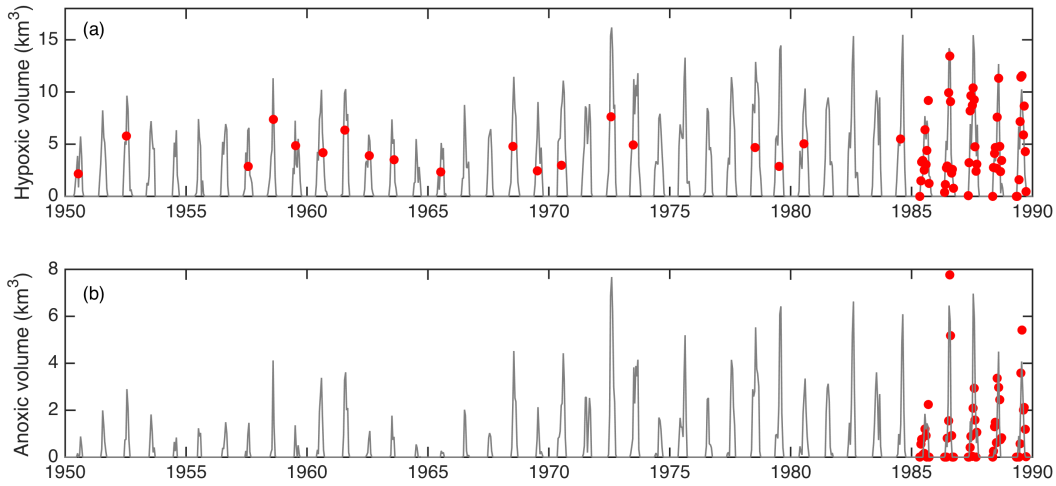

Figure 2.4 (a) Modeled hypoxic volume (O_2<2mg/L) in comparison with estimated hypoxic volume from observation data. (b) Modeled anoxic volume (O_2<0.5mg/L). Model results were averaged at bi-week interval. Anoxic volume data was missing before 1985.

2.3.2 Hypoxia expansion during 1950-1989

In this section, the expansion of hypoxia in Chesapeake Bay is described by decadal average (1950-1959, 1960-1969, 1970-1979,1980-1989) to chronicle the impact of increasing nutrient loads in the retrospective simulation from 1950s to 1980s. The features include hypoxic volume, hypoxia timing, spatial distribution of hypoxic water in the main stem of Chesapeake Bay.

The summer average (June-August) hypoxia expanded modestly from 1950s to 1960s, and the total volume increases from 4.1 km^3 to 4.6 km^3 (Table 2.1). Then the summer hypoxic volume increaseed substantially by ~65% to 7.6 km^3 in 1970s and maintained relatively stable in 1980s. The alternative metrics cumulative hypoxia days (CHD, km^3days) followed similar pattern as summer average hypoxic volume, except that it decreases slightly from 1970s to 1980s by ~8%. The seasonal hypoxia began to develop in early June and terminates in mid-September during 1950s-1960s. In the following 2 decades, the onset of hypoxia shifted earlier to mid-May meanwhile the termination was delayed until early October. The overall duration of hypoxia was prolonged by ~1 month from 1950s-1960s to 1970s-1980s.

Table 2.1 Average summer hypoxic volume, accumulative hypoxia volume days, timing of onset, end and duration of hypoxia (threshold =$0.5\times10^9 km^3$)

	Jun-Aug HV (km^3)	CHD (km^3days)	onset	end	duration
1950-1959	4.1	438	152	264	112
1960-1969	4.6	484	154	265	111
1970-1979	7.6	917	139	279	140
1980-1989	7.5	846	138	277	139

Along the central channel of Chesapeake Bay, hypoxic water in June was primarily confined in the upstream of deep channel and it extends seaward markedly from 38.5°N to 38°N (Figure 2.5). In September, it expanded both landward and seaward from the early decades to more recent decades. The south end of hypoxia area only stretched from the Potomac River to the Rappahannock River in July-August. Over a cross section in the middle bay, the hypoxia water overflowed to the shallow shoal in 1970s-1980s, meanwhile exhibited remarkable vertical expansion in June and

September (Figure 2.6). The change of bottom hypoxia distribution revealed the overall expansion in both longitudinal and lateral direction. The bottom hypoxia area spread most substantially in June and September. In contrast, July-August hypoxia only showed small expansion from 1950s-1960s to 1970s-1980s (Figure 2.7).

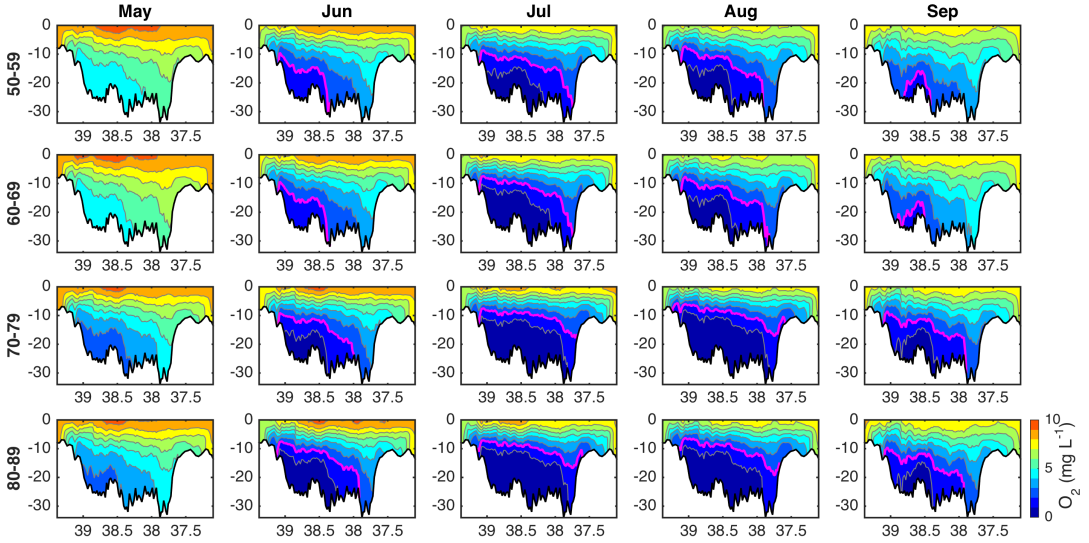

Figure 2.5 Modeled along-channel distribution of O_2 from May to September in four decades (50-59, 60-69, 70-79, 80-89) during 1950-1989.

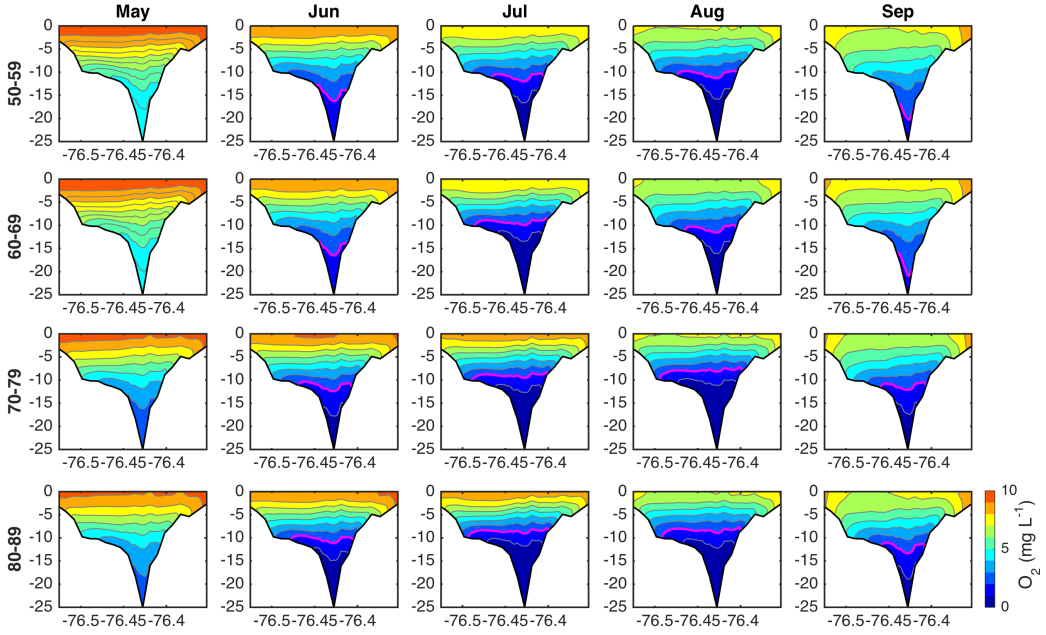

Figure 2.6 Modeled cross-channel distribution of O_2 at upper mid-bay (38.64ºN, -76.72ºW) from May to September in four decades (50-59, 60-69, 70-79, 80-89) during 1950-1989.

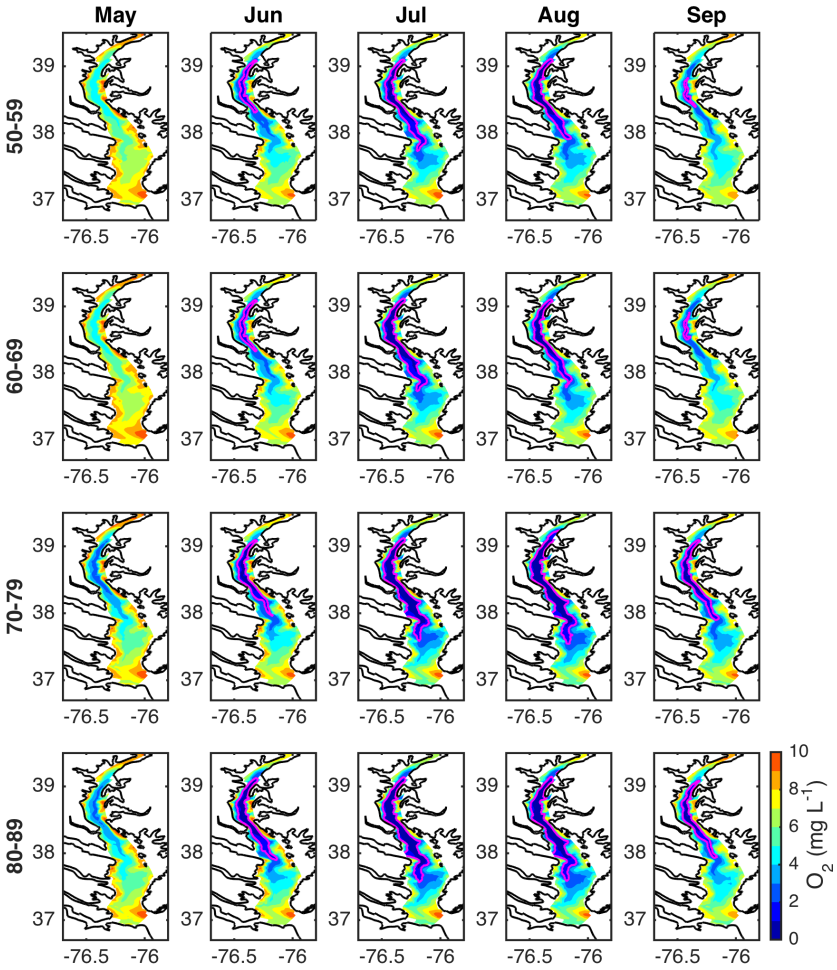

Figure 2.7 Modeled bottom distribution of O_2 from May to September in four decades (50-59, 60-69, 70-79, 80-89) during 1950-1989.

Paralleling to the change of hypoxia, surface chlorophyll-a concentration also presented significant increase from 1950s-1960s to 1970s-1980s in most part of the bay in Jan-May when the spring phytoplankton biomass accumulates (Figure 2.8). The concentrations of chlorophyll-a in the surface mixing layer have increased more drastically in the seaward regions of the main bay than elsewhere. It has increased 1.5- to 2-fold in the middle bay region where the concentration is highest. The time series analysis of sub-regional averaged chlorophyll-a concentration indicated a jump in early 1960s in the upper bay then slightly decrease after mid-1960s (Figure 2.9). However,

this jump appeared several years later in late 1960s in the middle bay and the chlorophyll-a concentration maintained at high level since 1970s. This temporal and spatial variation of phytoplankton biomass was in good agreement with previous observation study of Harding&Perry (1997). Correspondingly, the regional bottom O_2 decreased notably from early 1960s, except for the lower bay which experienced raise-then-fall from 1950s to 1970s (Figure 2.9). In summary, the model simulation results suggested a significant increase in Chesapeake Bay hypoxia and surface chlorophyll-a from 1950s to 1980s, with a jump around 1970.

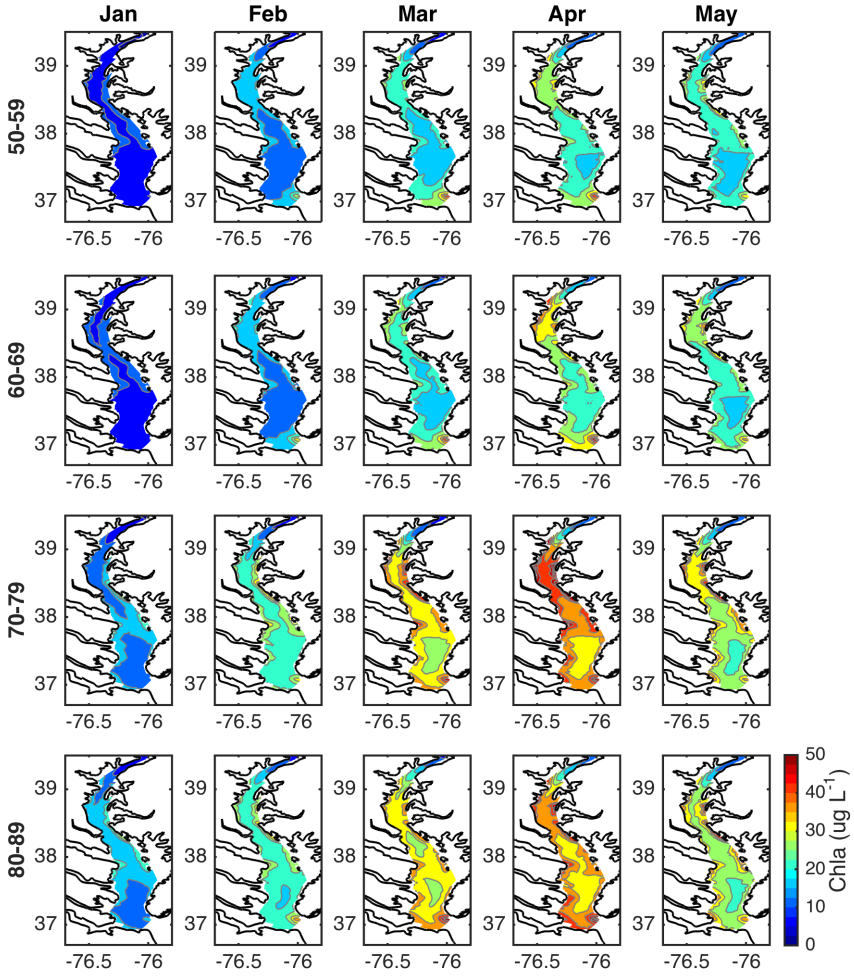

Figure 2.8 Modeled surface distribution of Chlorophyll-a from January to May in four decades (50-59, 60-69, 70-79, 80-89) during 1950-1989.

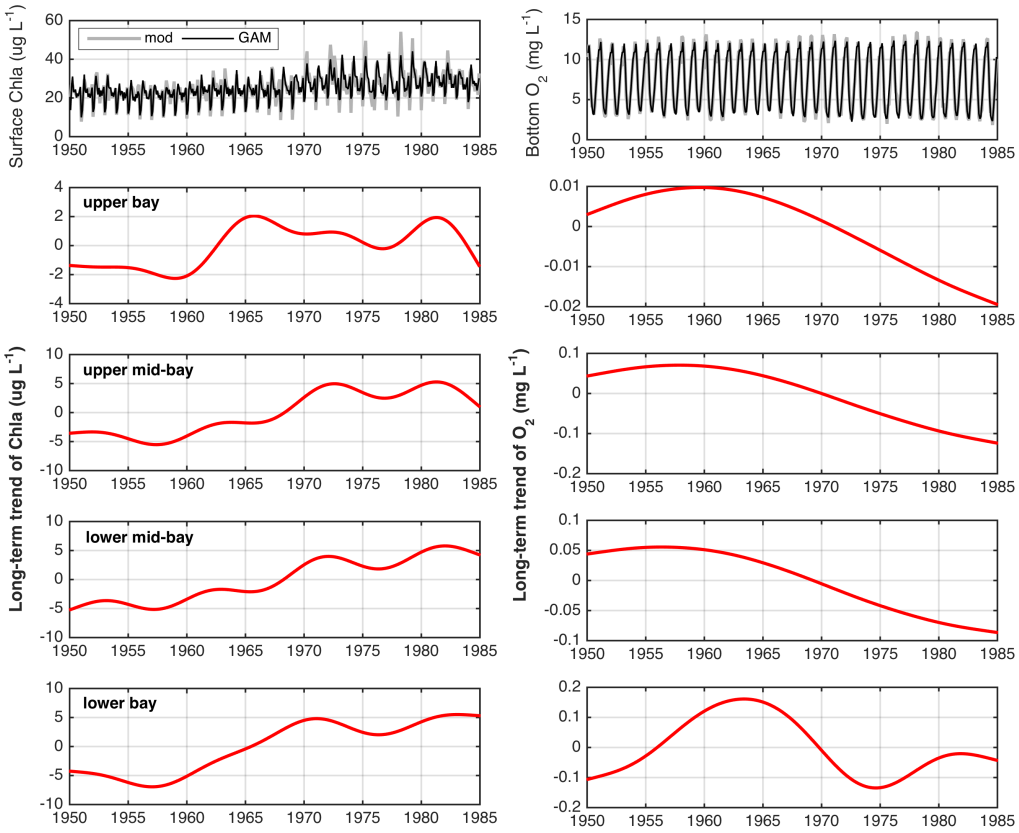

Figure 2.9 GAM fit on modeled surface Chla and bottom O_2 at upper mid-bay (upper panel). The long-term trend in GAM of surface Chla and bottom O_2 at four different sub-regions of Chesapeake Bay (lower panels).

We further inspected the seasonal decline rate of bottom O_2 in upper and lower mid-bay regions where most of the hypoxia occurs in the Chesapeake Bay. A set of predicted GAM models with components reflecting the contributions of time, season and freshwater on the O_2 time series was developed. The long-term trend of bottom O_2 in hypoxia months (May-September) were calculated. The decreasing trend of bottom O_2 is more consistent among the hypoxia months in the upper mid-bay, except for May which exhibits a much faster decline (Figure 2.10). However, the descending of bottom

O_2 becomes slower from May to September in lower mid-bay. This leads to spatial variation in the decrease of O_2 that the upper mid-bay declines more rapidly than the lower mid-bay, except in July-August. It's worth noting that there is notable maximum decline rate around 1970 for all the hypoxia months (Figure 2.11).

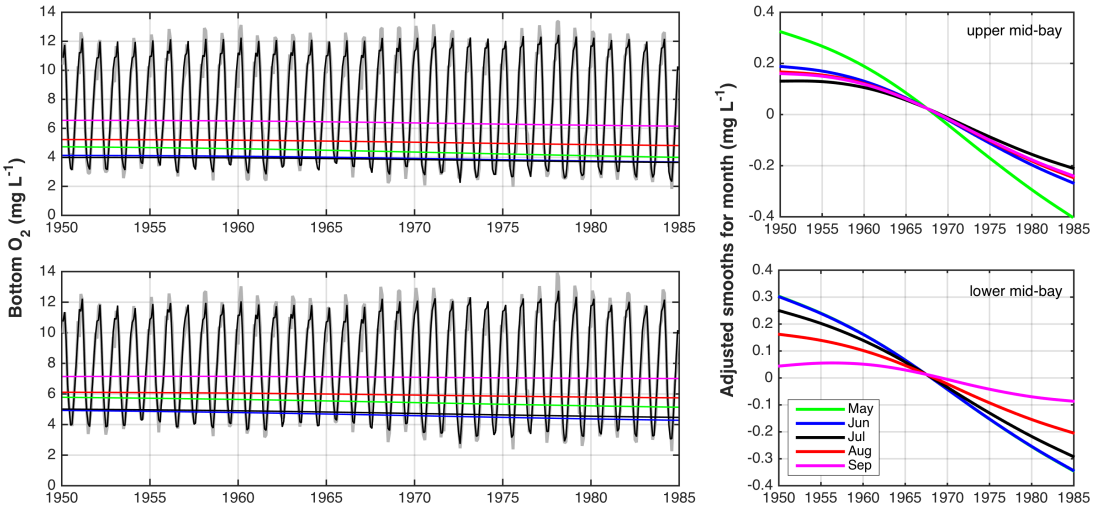

Figure 2.10 GAM fit and adjusted smooths for bottom O_2 from May to September at upper mid-bay and lower mid-bay.

2.3.3 Hypoxia vs. nutrient loading

The relation between Chesapeake Bay hypoxia and nitrate input of Susquehanna River from 1950s to 1980s is analyzed in this section. The value of annual hypoxia per unit Jan-May nitrate load of Susquehanna River was calculated. The metrics of cumulative hypoxia days (CHD) is used since it reflects the expansion of hypoxia in both space and time. The calculated time series suggested a significant shift in the relation between hypoxia and nitrate load in late 1960s to early 1970s (Figure 2.12a). An approximate half more CHD was produced per unit nitrate load on average during 1968-1989 compared to 1950-1967. There were two separate positive correlations between nitrate load and summer average hypoxia volume over these two

periods with more hypoxic volume per nitrate load in more recent period (Figure 2.12b).

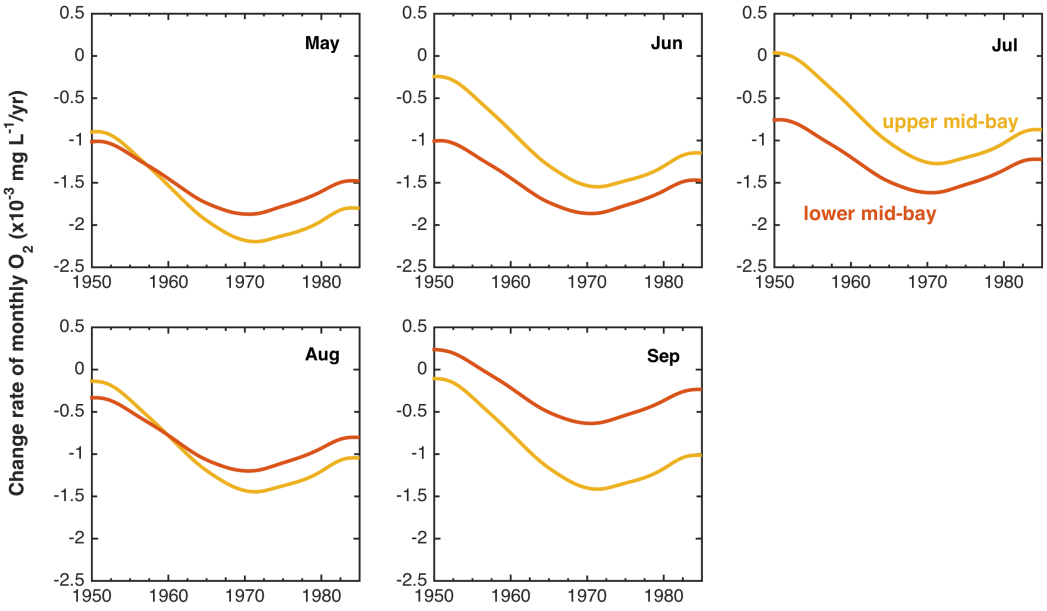

Figure 2.11 Monthly change rate of adjusted smooth of bottom O_2 from May to September at upper mid-bay and lower mid-bay.

Comparing 5-year averaged summer hypoxic volume to the Jan-May Susquehanna River nitrate load revealed varying responses of hypoxia to the nitrate input (Figure 2.13). From 1950 to 1969, the nitrate load wiggled around 20 Gg/yr with slowly expanding hypoxic volume, since the increase of nitrate concentration was small and superimposed with alternative dry/wet hydrological years. During 1970-1979, there was a sharp rise in nitrate load with simultaneously significant increase of late summer (August-September) hypoxic volumes, while the increase in early summer (June-July) was relatively modest. This agreed with previous observation studies from Hagy et al. (2004) and Murphy et al. (2011) concluding that the persistence of hypoxia during late summer is mainly controlled by nutrient loading. The nitrate load remained

at high level but decreases slightly in 1980-1984 due to the end of wet hydrological cycle in 1970s and slower increase in nitrate concentration. The hypoxic volumes of each month were mostly consistent with late 1970s.

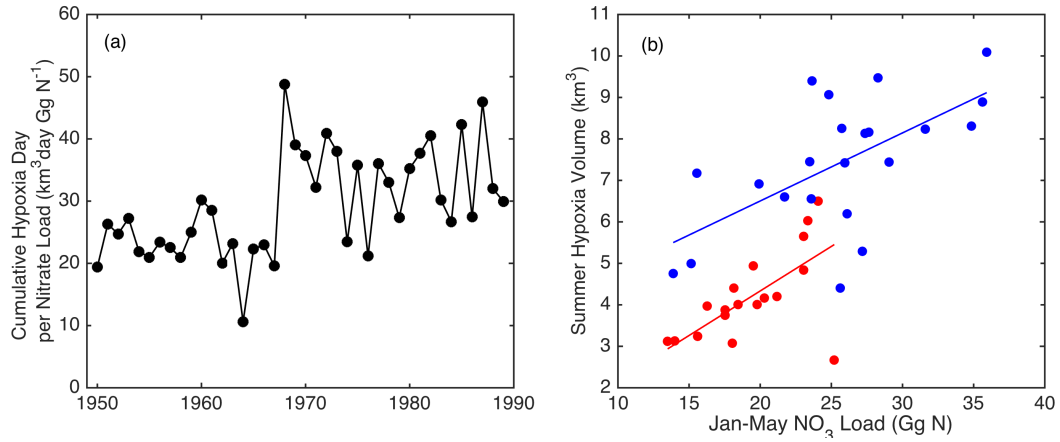

Figure 2.12 Time series of cumulative hypoxia days per unit Jan-May nitrate load during 1950-1989 (left). Relation between summer average hypoxic volume with Jan-May nitrate load during 1950-1989 (right), blue color indicates 1968-1989 and red color indicates 1950-1967.

2.4 Discussion and conclusion

The long-term retrospective simulation of Chesapeake Bay in this study successfully reproduces the deterioration of oxygen condition in the bottom water with increasing nutrient loading from 1950 to 1989. The summer hypoxia expanded modestly from 1950s to 1960s, while the hypoxic volume increases substantially by ~65% from 4.6 km^3 to 7.6 km^3 in 1970s and maintains relatively stable in 1980s. The hypoxia duration was also prolonged by ~1 month from 1950s-1960s to 1970s-1980s with both earlier onset and later termination for about two weeks. The bottom oxygen concentration declined most rapidly around 1970s in the mid-Chesapeake Bay, paralleling the significant increase of winter-spring chlorophyll-a concentration from 1950s-1960s to 1970s-1980s. Therefore, more hypoxic water was produced per unit

Jan-May nitrate load of Susquehanna River since ~1970 and the hypoxic volume in the Chesapeake Bay maintains at high level until late 1980s.

In Chesapeake Bay, an abrupt increase of hypoxic volume per unit spring nitrogen load of Susquehanna River was demonstrated in the observational studies, and the turning point was detected in 1986 (Kemp et al., 2009; Conley et al., 2009). The possible factors that contributed to this regime shift of hypoxia summarized in Kemp et al. (2009) included: (1) a rapid increase in water temperature around 1985, (2) changes in atmospheric forcing due to climate variability, (3) the positive feedback in benthic nitrogen cycling between summer bottom ammonium concentration and hypoxia, and (4) a sharp decrease in oyster population and associated filtration capacity. However, a notable finding from the retrospective simulation in this study suggested a more rapid decline of bottom O_2 around 1970 and significant expansion of hypoxia from 1950s-1960s to 1970s-1980s. The significant increase of hypoxia volume per nitrate load occurred around 1970s instead of 1986. The timing of detected shift mismatched with the conclusion of previous studies.

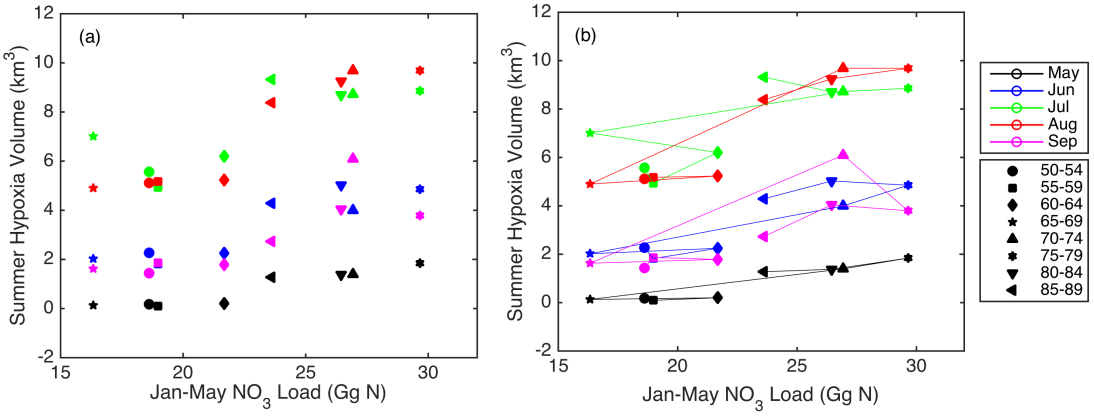

Figure 2.13 Monthly hypoxic volume from May to September responses to Jan-May Susquehanna nitrate load, with points representing 5-years average.

Essential difference existed between current and previous studies in the aspect of methodology. This study relied on the numerical model simulation instead of observation data to reconstruct the development of hypoxia with increasing nutrient loading in Chesapeake Bay. With proper validation, although model can never be perfect replications of reality, it can represent the response of the system when the external forcing changes with high-resolution data in both time and space. Thus, model simulation is less sensitive to the sampling bias as observation as described in Section 2.3.1. One fact should be mentioned that regular water quality monitoring of Chesapeake Bay Program initiated in 1984 with continuous monthly to bi-weekly sampling in the main Chesapeake Bay. Therefore, there was a rapid increase of data availability after 1984 which co-occurred with shift timing observed in the previous studies.

The possible causes for the rapid decline of bottom O_2 and shift in hypoxia volume per nitrate loading around 1970s is not clear yet. However, several key events coincide with this prominent change might contribute to the hypoxia increase. First, during June 1972 Tropical Storm Agnes released record amounts of rainfall on the watersheds of most of the major tributaries of Chesapeake Bay. It generated a marked effect on the hydrology of Chesapeake Bay in the consecutive years (Figure 2.14a). The vertical averaged stratification in the main bay in the summer of 1972 was abnormally high which made for usual high hypoxic volume after the storm (Schubel&Cronin, 1977) (Figure 2.14b). The low bottom salinity at the bay mouth in

1972 also reflected this extreme event (Figure 2.14c). In addition, the abundance of submerged aquatic vegetation (SAV) bed decreased drastically after Agnes (Gurbisz&Kemp, 2018). The abrupt decline of benthic production triggered the transition from benthic- to planktonic-dominated ecosystem with less efficiency to retain nutrient in Chesapeake Bay (Kemp et al., 2005). Over the longer term, there was a transition from dry period to wet period from 1960s to 1970s, which resulted in higher summer stratification to incubate hypoxia (Figure 2.14a-b). The summer wind speed was below averaged condition from 1968 to 1975 and favored the hypoxia expansion (Figure 2.14d). The bottom salinity at the bay mouth also exhibited long-term increase, associated with sea level rise and shift in Gulf Stream, which might increase the stratification in the bay (Figure 2.14c).

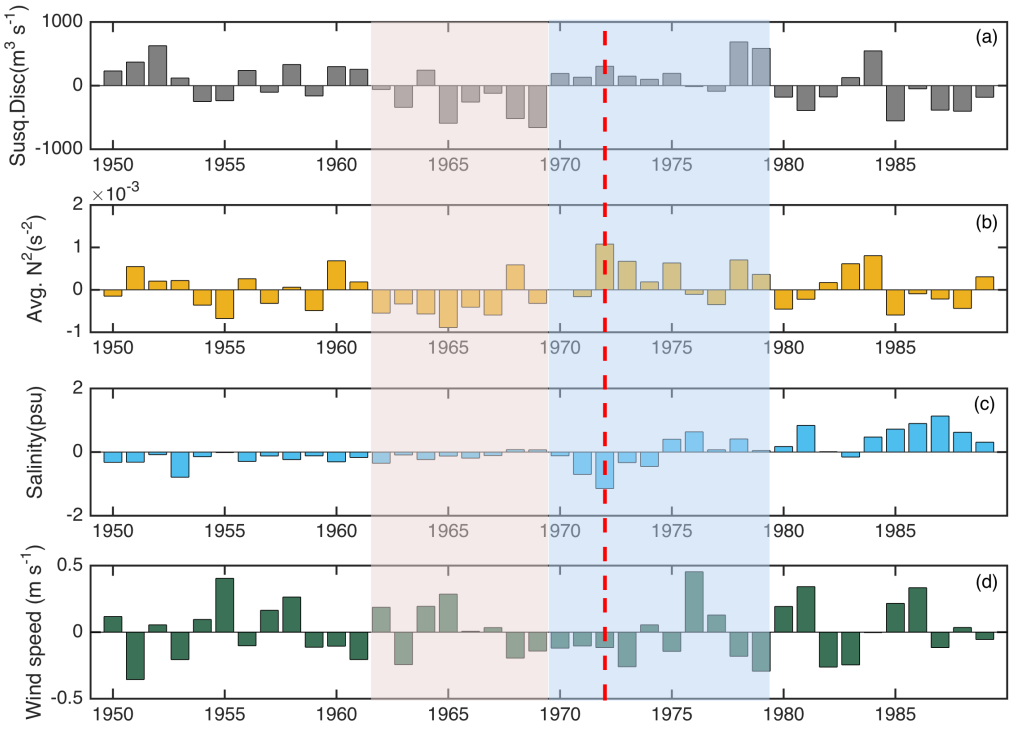

Figure 2.14 Time series of anomaly (relative to mean condition during 1950-1989) of Jan-May average Susquehanna River flow (a) Jun-Aug average N^2 in the main stem of Chesapeake Bay (b) Jun-Aug average bottom salinity at Chesapeake Bay month (c) Jun-Aug average wind speed over the main bay. The red dashed line indicates Tropical

Storm Agnes. The red shading and blue shading area indicates the relative dry and wet period respectively.

Second, the rising of nitrate and phosphate concentration in Susquehanna River was fastest in late 1960s (Figure 2.15a). The phosphate concentration reached the highest in early 1970s then fell back to low level after 1980s. The coincidence of rapid increase of both nitrate and phosphate loading from Susquehanna River, coupled with the above-average-flow condition in 1970s, resulted in a steep rise of phytoplankton biomass in the Chesapeake Bay around 1970, particularly in the middle bay (Figure 2.15b). Accordingly, the water column respiration (WCR) in the bottom water increased rapidly during the same period and maintained at high level afterwards (Figure 2.15c). Furthermore, the lateral and longitudinal expansion of bottom hypoxia area can enhance water-column and sediment recycling of dissolved nitrogen and phosphorus nutrient and favored further generation of hypoxia. The shift in hypoxia-nutrient load relation also indicates that with the same amount of nitrate load, the earlier period featured with low riverine nitrate concentration and high river flow tended to produce less hypoxic volume than the later period with high nitrate concentration and low river flow. Although higher river flow would generate larger stratification and consequent less vertical ventilation of oxygen to bottom, it also enhanced the exchange flow in the bottom which brought oxygen rich water to the hypoxic zone upstream.

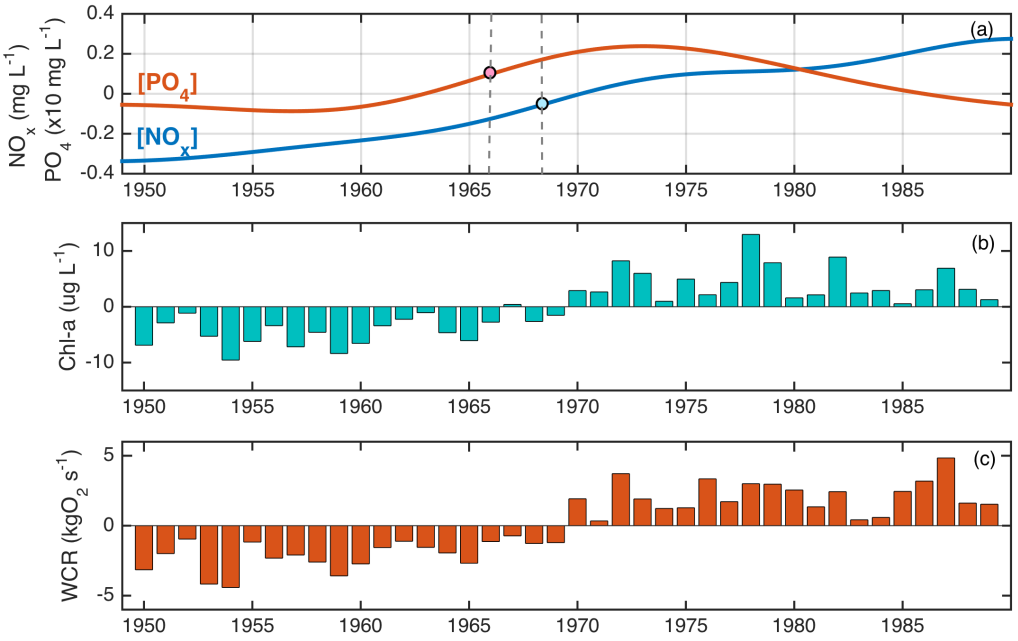

Figure 2.15 Time series of anomaly (relative to mean condition during 1950-1989) of long-term trend of nitrate+nitrite concentration and phosphate concentration of Susquehanna River (a), average surface chlorophyll-a concentration in the mid-bay (b) and bottom water column respiration rate in the mid-bay (c). Dashed lines and dots in (a) indicate the most rapid increase.

Although it is the first modeling effort to reproduce eutrophication driven hypoxia development in Chesapeake Bay, long-term ecological change due to eutrophication is not considered in the model, this study successfully reproduced the expansion of hypoxic water with a possible regime shift ~1970s. More thorough study on the changes of biogeochemical cycling and physical process and their impacts on hypoxia will be needed in the future.

2.5 Acknowledgments

We are grateful to NSF (CBET-1360285) and NOAA Ocean Acidification Program (NOAA-OAP; Award NA15NOS4780184) for the financial support. Model outputs can be acquired upon request.

Chapter 3: Discerning effects of warming, sea level rise and nutrient management on long-term hypoxia trend in Chesapeake Bay

Preface

This chapter aims to study the ongoing climate change impacts in comparison to the nutrient reduction on Chesapeake Bay hypoxia. It is a reproduction of work will soon appear in the *Journal of Geophysical Research: Oceans* with coauthors Ming Li and Jeremy Testa. The right to reuse this work was retained by the authors when publication rights and nonexclusive copyright were granted to the American Geophysical Union.

Ni, W., Li, M., Testa, J.M. (In prep). Discerning effects of warming, sea level rise and nutrient management on long-term hypoxia trend in Chesapeake Bay. *Journal of Geophysical Research: Oceans.*

3.1 Introduction

Anthropogenic nutrient enrichment of estuaries has contributed to the degradation of water quality by fueling phytoplankton production and associated depletion of oxygen (hypoxia) from bottom waters in coastal systems worldwide (Diaz and Rosenberg, 2008; Kemp et al., 2009; Zhang et al., 2009; Breitburg et al. 2018). Despite the fact that many coastal regions have made major public commitments to reduce nutrient loading and reverse this trend of declining water quality and habitat conditions, estuaries in the U.S. and around the world continue to experience hypoxia and deteriorating water quality (Conley et al., 2009; Duarte et al., 2009; Scavia et al., 2017; Fennel and Testa, 2019). A major impediment to achieving restoration successes is the complicating effect of climate variability and climate change. Large interannual fluctuations in river flows result in highly variable nutrient loading and strong interannual variability in hypoxia (Justic et al., 2003; Hagy et al., 2004; Bever et al., 2013; Li et al., 2016). Longer-term climate changes, such as warming and sea level rise, exert more subtle controls on biogeochemical processes, and their effects on hypoxia in estuarine and coastal systems are not well understood.

There has been worldwide implementation of nutriment management strategies in the coastal hypoxic regions. In Baltic Sea, continuous efforts have been made to reduce anthropogenic nutrient load since the late 1980s by Helsinki Commission (HELCOM) and an international agreement of Baltic Sea Action Plan (BSAP; HELCOM, 2007, 2013) was reached in 2007 with nutrient reduction target for each

country. With modest reduction in nitrogen and phosphorus loads over the past decades, there was only local recovery of water quality (Conley et al., 2009). In northern Gulf of Mexico, although the action plan was released by Mississippi River/Gulf of Mexico Watershed Nutrient Task Force in 2001, little sign of reduction in nutrient load as well as the extent and intensity of hypoxia has been revealed lately (Rabalais et al., 2010; Van Meter et al., 2018). In contrast, major improvement of oxygen condition has been reported in Tampa Bay, Northwest Black Sea and northern Adriatic Sea, where substantial decrease of anthropogenic nutrient inputs occurred (Greening&Janicki, 2006; Mee et al., 2006; Giani et al., 2012). However, there are exceptional coastal regions, such as Bohai Sea and Pearl River Estuary, where the anthropogenic eutrophication is still ongoing (Xin et al., 2019; Qian et al., 2018). Expanded and more severe seasonal hypoxia has been emerging in these regions in recent decades (Zhai et al., 2019). The above cases with distinct changes of nutrient load (i.e. modest, little, large reduction and increase) suggest that unless the nutrient load reduction is sufficiently significant and overtakes other factors, the remediation of hypoxia is difficult to be fully achieved, especially in large and open systems where the climatic influences are prominent.

Climate change related sea level rise, warming, altered pattern of precipitation and wind can generate varied effects on coastal hypoxia (Altieri and Gedan, 2015). In Baltic Sea, North Sea and Chesapeake Bay, sea level rise may lead to reinforced salt influx and stronger vertical stratification with consequent oxygen decline in bottom water (Meier et al., 2017; Meire et al., 2013; Ni et al., 2019). The warming could

increase the temporal and spatial extent of hypoxia via reduced oxygen solubility, enhanced oxygen consumption and intensified internal nutrient cycling (Meier et al., 2011; Lake&Brush, 2015; Irby et al., 2018). More than 30% of observed decrease of oxygen in Long Island Sound during the past two decades can be attributed to the increased temperature (Staniec&Vlahos, 2017). Wind and river discharge can significantly affect coastal hypoxia with modification of physical supply of oxygen through circulation and vertical mixing (O'Donnell et al., 2008; Scully, 2010; Hetland&DiMarco, 2008). Changes in wind speed, direction and freshwater discharge play a crucial role to control the interannual and long-term variation of hypoxia in addition to nutrient loads (Wilson et al., 2008; Feng et al., 2012; Scully, 2010, 2016; Zillén et al., 2008). Therefore, the climate forces can generate comparable impact with nutrient loads on coastal hypoxia, and changes of climate can possibly overcome nutrient reduction effects (Meier et al., 2011).

Retrospective analysis of water quality monitoring data in Chesapeake Bay have found no long-term trends in the magnitude of summer hypoxia but an apparent early shift of the seasonal hypoxia cycle. Murphy et al. (2011) analyzed 60-year records of hypoxic volume since 1950s. They found significant increases in early summer hypoxia but a slight decrease in late summer hypoxia between 1985 and 2009. Zhou et al. (2014) reached a similar conclusion that the timing of the maximum hypoxic volume shifted from late to early July but there was no long term trend in the seasonal-maximum of the hypoxic volume. No significant trend was found in the timing of hypoxia onset while the termination of hypoxia moved from October to September

during 1985-2010. On the other hand, Testa et al. (2018) suggested a speed-up of the seasonal hypoxia cycle due to warming: larger early summer hypoxic volume but smaller late summer hypoxic volumes in recent decades. Testa et al. (2018) also suggested that spring phytoplankton biomass in the lower Bay was reduced due to modest reduction of nitrate input. However, including extended data prior Chesapeake Bay Program in 1984, Harding et al. (2016) found little sign of decreasing annual integrated chlorophyll-a in the lower Chesapeake Bay. The modeling studies from Scully (2016) and Du et al. (2018) suggested the importance of physical processes on Chesapeake Bay hypoxia, and indicated a worsened physical condition over the past few decades. However, they only utilized physical model with simple assumption on oxygen and the complete hypoxia-related biogeochemical processes were lacking in their studies.

Coordinated plans to control point and nonpoint sources of pollution and improve water quality of Chesapeake Bay initiated in 1983. The Total Maximum Daily Load (TMDL) was developed in 2010 to set pollution limits to meet water quality in the Chesapeake Bay and its tidal tributaries (USEPA, 2010). The nitrate concentration of Susquehanna River, which is the major source of nutrient inputs, has been reduced by ~15% over the past three decades (Zhang et al., 2015). Meanwhile, Chesapeake Bay has been experiencing rapid climate changes, including both warming and sea level rise (Ding and Elmore, 2015; Boon&Mitchell, 2015). However, previous studies have not found significant alleviation of long-term summer hypoxia in Chesapeake Bay, although some seasonal changes have been noted. The key question missing in previous

observational studies is that they could not separate the individual effects of nutrient reduction and climate changes, and determine the driving force for the long-term trend in hypoxia in Chesapeake Bay. Also, limited by the sparse measurement data, the estimations from observational studies might be biased and not entirely reliable. As an emerging tool in marine science research, numerical model can generate high resolution data in both time and space and provide mechanistic insight of the changes in marine system.

Therefore, the objective of this study is to use numerical model to quantify the relative importance of recent nutrient reduction and climate changes on the long-term changes of oxygen in Chesapeake Bay. The coupled physical-biogeochemical model is adopted to implement both hindcast and scenario simulations of Chesapeake Bay during 1985-2016. We apply sophisticated statistic model to analyze the simulated oxygen and other properties in four sub-regions of Chesapeake Bay main stem, considering the non-linear trend and large seasonal variations. Then scenario-based simulations removing individual forcing of sea level rise, warming and nutrient reduction are conducted in comparison with the hindcast simulation. The effect of each forcing on seasonal hypoxia and long-term trend are further investigated. The results of this study can help managers to assess the effectiveness of current nutrient reduction to alleviate hypoxia in Chesapeake Bay, and propose adaptive management strategies under climate change background.

3.2 Methods

A coupled hydrodynamic-biogeochemical model was used to conduct hindcast simulations of dissolved oxygen in Chesapeake Bay between 1985 and 2016. The model outputs were analyzed to identify long-term trends in hypoxia. Additional model runs were designed to discern mechanisms that drove the long-term changes.

3.2.1 Coupled hydrodynamic-biogeochemical models (ROMS-RCA)

The hydrodynamic submodel is based on Regional Ocean Modeling System (ROMS) model (Shchepetkin and McWilliams, 2005; Haidvogel et al., 2008), which has been configured for Chesapeake Bay (Li et al. 2005) and validated against a wide variety of observational data (Li et al. 2005, 2006; Zhong and Li, 2006; Xie and Li, 2018). The model has 120×80 horizontal grids (~1-2 km resolution) and 20 sigma-coordinate layers in the vertical direction (Figure 3.1b). MPDATA advection scheme is employed for temperature and salinity (Smolarkiewicz and Margolin, 1998). The vertical eddy viscosity and diffusivity are calculated using the *k–kl* turbulence closure scheme (Warner et al., 2005) with the background diffusivity and viscosity set at 5×10^{-6} m^2 s^{-1}. A quadratic stress is implemented at the sea bed, assuming that the bottom boundary layer is logarithmic with a roughness height of 0.5 mm (Xu et al., 2012).

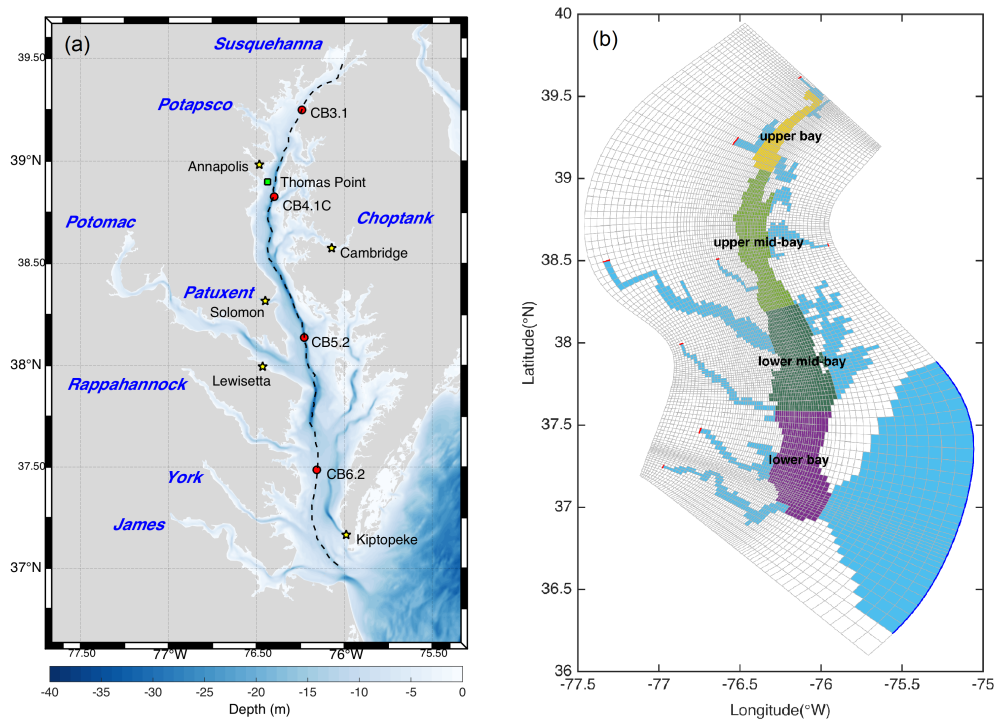

Figure 3.1 (a) Map of Chesapeake Bay. The yellow stars mark NOAA tidal gauge stations, the green squares mark NOAA buoys, and the red dots mark EPA Chesapeake Bay Program (CBP) monitoring stations. The eight major rivers are highlighted in dark blue letters. (b) ROMS-RCA model grid. The yellow, light green, dark green and purple regions indicate four subregions in the estuary: upper bay, upper middle-bay, lower middle-bay and lower bay. The red and blue lines show the river and ocean boundaries of the model.

ROMS model is driven by the atmospheric, riverine and oceanic forcing at the boundaries (Figure 3.1b). Across the sea surface, the air-sea fluxes of momentum and heat were calculated by applying the standard bulk formula (Fairall et al., 2003) to the atmospheric products from the North American Regional Reanalysis (NARR) (Mesinger et al., 2006). The atmospheric variables include surface air pressure, relative humidity and air temperature at 2 m above surface, downwelling longwave radiation and net shortwave radiation at surface, and wind speed at 10 m above the sea surface. At the offshore boundary, the model is forced by open-ocean sea level, temperature and salinity. The sea level includes both tidal and non-tidal components. The former was

calculated from 10 harmonic constituents (M_2, S_2, N_2, K_2, K_1, O_1, P_1, Q_1, M_f and M_m) interpolated from the Oregon State University global inverse tidal model TPXO7 (Egbert and Erofeeva, 2002). The later was obtained from de-tided water level at Duck, NC (NOAA station ID: 8651370). Temperature and salinity at the offshore boundary were interpolated from the World Ocean Atlas (WOA) climatological averages. At the upstream boundaries of eight major tributaries (Figure 3.1a), the freshwater discharge were obtained from daily measurements at USGS gauging stations (http://nwis.waterdata.usgs.gov/nwis). Daily temperature at the tributaries was interpolated from Chesapeake Bay Program monitoring stations (https://www.chesapeakebay.net/).

The biogeochemical model is based on Row-Column AESOP (RCA) which includes a water column component (Isleib et al., 2007) and a sediment component (Di Toro, 2001; Testa et al., 2013; Brady et al., 2013). The water-column model includes state variables representing dissolved inorganic nitrogen, phosphorus, and silica, particulate and dissolved organic nitrogen and phosphorus, two phytoplankton groups and dissolved oxygen (O_2). The sediment model has one aerobic layer and one anaerobic layer, and simulates the cycling of carbon, O_2, nitrogen, phosphorus and sulfur. RCA is driven by loads of dissolved and particulate nutrients from river and ocean. Riverine concentration of phytoplankton, particulate and dissolved organic carbon, organic and inorganic nutrients were obtained from Chesapeake Bay Program (CBP) bi-weekly monitoring data at the eight tributaries. Nutrient concentration at the offshore ocean boundary were acquired from the WOA 2013 climatology and Filippino

et al. (2011). The atmospheric deposition of dissolved inorganic nutrient on the estuary's surface was less than 3% of the riverine nutrient loading and thus not considered in this study (Li et al., 2016). ROMS-RCA was previously used to predict the seasonal development and interannual variation of hypoxia in Chesapeake Bay (Testa et al., 2014; Li et al., 2016; Shen et al., 2019).

In this paper ROMS-RCA was used to make hindcast simulations over 3 decades: 1985- 2016. EPA CBP have carried out regular monitoring cruises since 1985 and collected measurements of water quality parameters such as dissolved oxygen at a number of monitoring stations, providing a rich data set to compare with the model results. ROMS was initialized on 1 January 1984 and run continuously until 31 December 2016. Results from the spin-up period of 1984 were not analyzed. ROMS outputs were saved at hourly intervals and then used to drive RCA in an offline mode. RCA was initialized on 1 January every year using the water-quality data collected in the preceding month. RCA was run on the same grid as ROMS with a time-step of 450 seconds, and RCA outputs were saved at 4-hour intervals.

3.2.2 Statistical analysis approaches

Water quality parameters such as salinity, dissolved oxygen and chlorophyll-a in Chesapeake Bay display large seasonal and interannual variations. To detect long-term trends, we used the Generalized Additive Model (GAM) (Hastie and Tibshirani 1986, 1990). GAM is preferable over the generalized linear regression model due to its flexible specification of the response's dependence on the covariates (Wood, 2006). It also incorporates features such as non-Gaussian distributions, correlated errors and

random effects. GAM was previously used to analyze long term trends in Chlorophyll-a (*Chl-a*), nutrient concentration and dissolved oxygen in Chesapeake Bay using the monitoring data collected by CBP and others (Harding et al., 2015; Testa et al., 2018; Murphy et al., 2019).

Time series extracted from the model outputs were analyzed using GAM as below:

$$y_t \sim y_{t-1} + s(dnum) + s(doy) + s(sal) + ti(dyear, doy) + ti(dyear, sal) + ti(dyear, doy, sal) \quad (3.1)$$

where y_t represents the response variables as O_2 and Chlorophyll-a, y_{t-1} represents the same variables at the preceding time step to account for the autocorrelation, *dnum* is the number of month relative to the reference time (e.g. 1 for Jan. 1985), *doy* is the number of month in a year (e.g. 1 for January), and *sal* is the monthly averaged salinity representing the influence of flow. Among the functions used in GAM, *s*() is a smooth function with thin plate regression splines [*s*(*doy)* was fitted with cyclic cubic spline to ensure a smooth seasonal cycle], *ti*() represents tensor product of two smooth functions to account for the interaction between these two variates. In Equation (1), *s*(*dnum*) represents the long-term residual, *s*(*doy*) represents the seasonal cycle, and *s*(*sal*) is meant to capture the effects of salinity on the interannual variabtions. The high-order term *ti*(*dyear, doy*) allows the seasonal cycle to change over time. In the GAM model built for salinity, the river discharge was used in Equation (3.1) instead of salinity, since it has been shown to be strongly influenced by flow (Beck and Murphy, 2017) and the residence time of Chesapeake Bay is of the order of months. Only the term *s*(*dnum*), *s*(*doy*) and *ti*(*dyear, doy*) were considered in the GAM model for temperature, since

Chesapeake Bay is a relative shallow system dominated by air-sea fluxes exchange. The objective of GAM is to minimize the generalized cross-validation (GCV) score and maximize the model R^2 and percentage of deviation explained. The GAM structure in Equation (3.1) considered the pattern of response variables in long-term trend ($s(dnum)$), seasonal cycle ($s(doy)$), relation with flow ($s(sal)$) and changing seasonal cycle/flow with time ($ti()$).

In addition, an adjusted GAM model was constructed for the summer averaged bottom O_2 from 1985 to 2016:

$$y_{an} \sim s(dyear) + s(flow\_JM) + s(temp\_JA) \quad (3.2)$$

where y_{an} represents the summer averaged bottom O_2, $s()$ stands for the smooth function with thin plate regression splines, *dyear* represents the number of years since 1985, *flow_JM* represents the averaged January-May Susquehanna River discharge, *temp_JA* represents the summer averaged (June to August) temperature. The predicted GAM model was run with repeated mean *flow_JM* and mean *temp_JA* over 1985-2016 as flow and temperature adjusted GAM, while other variates were allowed to vary. The resulting predictions show what O_2 would have been if the river flow and temperature had remained unchanged.

To investigate estuary-wide responses, we calculated the spatial averages over different regions of the Bay. The main stem of Chesapeake Bay was divided into four sub-regions: upper bay (oligohaline), upper and lower mid-bay (mesohaline), and lower bay (polyhaline), following Irby et al. (2018) (Figure 3.1b). The mid-bay was split into

two subregions to better account for the bathymetric and hydrodynamic controls of hypoxia. In each region, temperature, salinity, O_2 and Chlorophyll-a in the surface layer and bottom layer were calculated from ROMS-RCA and averaged at monthly intervals. The R package 'mgcv' of version 1.8-15 (https://cran.r-project.org/web/packages/mgcv/index.html) was used to develop the GAM for each sub-region. Degrees of smoothing (knots=k) in each smooth function were selected by the program to minimize the GCV score.

The non-parametric Mann-Kendall (MK thereafter) trend test was applied to the time series to statistically assess if there is a monotonic upward or downward trend of a variable over time (Mann, 1945; Kendall, 1975; Gilbert, 1987). A monotonic upward/downward trend means that the variable consistently increases/decreases through time, but the trend may or may not be linear. A key assumption in the MK trend test is that the data points are not serially correlated over time. This would require that the time between two samples be sufficiently large so that there is no correlation between data collected at different times. The MK test was applied to both the external forcing such as air temperature and offshore sea level time series as well as state variables such as sea level, temperature, salinity, O_2 and hypoxic volume in Chesapeake Bay. Since these variables exhibit large seasonal and interannual variations, care is needed when applying the MK test to detect the long-term trend. We either calculated monthly averages or used the GAM model to remove the short term signals. To calculate the linear trends of the time series, we used the non-parametric Theil-Sen estimator or Sen's slope estimator (Theil, 1950; Sen, 1968; Wilcox, 2001). The

estimator is a method for robustly fitting a line to sample points in a plane by choosing the median of the slopes of all lines through pairs of points. The significance level α was set as 0.05 for both tests.

3.2.3 Model scenarios

Warming, sea level rise and nutrient management are the three major factors driving the long-term changes in Chesapeake Bay. Although the river flows displayed strong interannual variations, they showed no long term trend between 1985 and 2016 (Figure 3.2d). To tease out how each of these external factors affected the hypoxia in the estuary, we conducted three scenario model runs in which the long-term trend in temperature (DtrTEMP run) or sea level (DtrSLR run) or nutrient loading (DtrNut run) was removed in the model forcing. The hindcast run is hereafter denoted as the Base run.

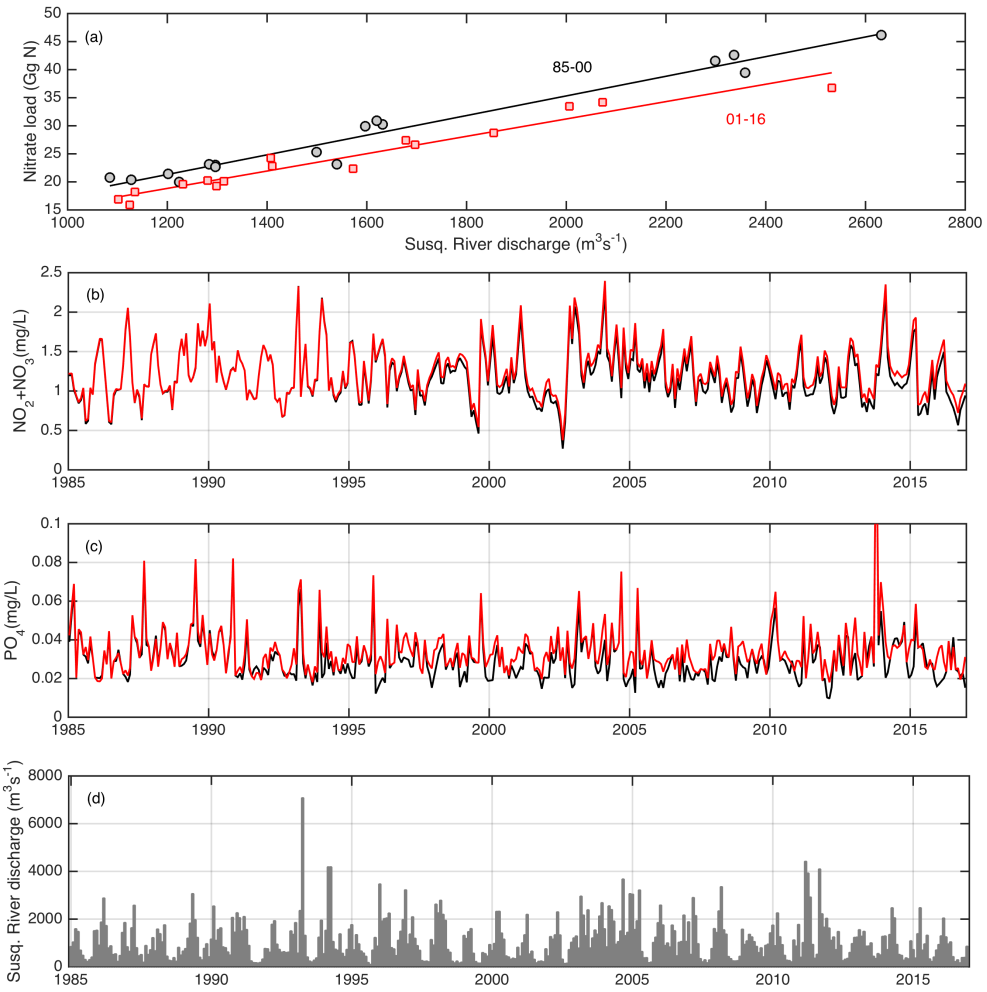

Figure 3.2 (a) Relationship between winter-spring (January-May) Susquehanna River flow and nitrate loading during 1985-2000 (black) and 2001-2016 (red). (b)-(c) Monthly NO_{23} and PO_4 concentrations (black lines) and detrended NO_{23} and PO_4 concentration (red lines) in the Susquehanna River. (d) Monthly averaged Susquehanna River discharge.

Both the air temperature over Chesapeake Bay and the riverine temperature in the tributaries have increased over the past several decades (Ding and Elmore, 2015; Rice and Jastram, 2015). The riverine temperature influences the estuarine temperature through river inflows while the air temperature affects it through the air-sea heat fluxes. To remove the long-term trends in temperature forcing in DtrTEMP run, Mann-Kendall trend test (M-K test) was applied to the temperature time series at the upstream

boundary of the eight major tributaries as well as the heat flux-related variables (air temperature, humidity, solar radiations) at NARR grids over Chesapeake Bay:

$$T_{detrend} = T_{original} - Slope_T \times (Time - 1/1/1985) \quad (3.3)$$

where $T_{original}$ represents the original time series of each variable (i.e. river temperature, surface air temperature, humidity, downwelling long-wave radiation and net short wave radiation), $T_{detrend}$ represents the detrended variables. $Slope_T$ is the Theil-Sen slope calculated from the original data. Eq. (3.3) was only applied to the grids or tributaries when the p-value of M-K test was less than 0.4. Temperature in the Mid-Atlantic Bight also increased over the past few decades (Lentz, 2017), but no long-term temperature series were available near the mouth of Chesapeake Bay. The Base run, which was forced by the climatological temperature and salinity at the offshore boundary, accurately simulated the observed warming inside the Bay (see the next section).

To remove the sea level rise in DtrSLR run, we removed the linear trend of the observed de-tided sea level time series at Duck, North Carolina. The detrended non-tidal sea level component was then added to the tidal sea level to produce the sea level time series at the offshore boundary:

$$SL_{detrend} = H_{Duck} - Slope_H \times (Time - 1/1/1985) + SL_{tide} \quad (3.4)$$

where H_{Duck} represents the de-tided sea level time series at Duck, N.C., $Slope_H$ is the Theil-Sen slope obtained from the de-tided time series at Duck, SL_{tide} is the tidal sea level and $SL_{detrend}$ represents the detrended sea level.

Riverine nutrient concentration in the Susquehanna River and other tributaries have shown not only seasonal and interannual variations due to river flows but also long term changes due to nutrient management practices (Langland et al., 2007; Zhang et al., 2015) (Figure 3.2). At the same flows from the Susquehanna River, the nitrate loading in 2001-2016 was appreciably lower than in 1985-2000 (Figure 3.2a), as reported in Testa et al. (2018). To examine how the nutrient management affected the long-term trend in hypoxia, we conducted DtrNut run in which the long-term trends in the river nutrient concentration were removed (Figures 3.2b-c). Since the hypoxia in Chesapeake Bay is mostly caused by autochthonous primary production fueled by riverine inorganic nutrients, only the time series of nitrate+nitrite and phosphate concentration from the Susquehanna River were detrended. Because the nutrient loads were highly influenced by streamflow and season, we applied the additive approach based on the flow-normalized nutrient concentration from USGS Chesapeake Bay Nontidal Monitoring Program (https://cbrim.er.usgs.gov). The monthly averaged maximum concentrations during 1985-1989 ("peak period") were estimated, and the differences in the nutrient concentration between this peak period and each year in 1985 to 2016 were calculated. These differences were then added to the original riverine nutrient concentration:

$$C_{detrend} = C_{original} + (CF_{peak\ period} - CF) \quad (3.5)$$

where $C_{detrend}$ and $C_{orginal}$ are the detrended and original riverine nutrient concentration respectively, CF is the flow-normalized nutrient concentration during 1985-2016 and $CF_{peak\ period}$ is the monthly averaged nutrient concentration during 1985-1989. Finally,

the M-K test was applied to the newly-generated nutrient time series to ensure that no decreasing trend remained.

3.3 Model-simulated long-term changes and comparison with observation

Results from the 30-year (1985-2016) hindcast model simulation (Base run) are presented, with a focus on identifying long term trends in dissolved oxygen and hypoxia. To support the use of model simulations to quantify trends, we first evaluated the model-predicted sea level, temperature and O_2 in Chesapeake Bay against long-term observations.

3.3.1 Sea level rise and warming

Model-predicted monthly averaged water levels at selected NOAA tidal gauging stations (locations marked in Figure 3.1a) were compared with monthly averaged observations in Figure 3.3. The model accurately captured the seasonal and interannual sea level variations in the estuary. The correlation coefficient between the predicted and observed monthly sea levels is around 0.95 and the standard deviations of the predicted and observed sea level are very close to each other (Figure 3.4a). Mann-Kendall trend test indicate that both the modelled and observed sea levels show a statistically significant upward trend, with small p-values (Table 3.1). The Theil-Sen estimator was used to calculate these linear trends. The modelled sea levels at the tidal gauge stations rose at a rate of 4.7-4.9 mm/year while the observed sea level rise rate varied from 4.3 to 6.6 mm/year between 1985 and 2016. The ROMS model is forced by the offshore sea level at Duck, North Carolina, which rose at a rate of 4.5 mm/year. Land subsidence associated with glacial isostatic adjustment (Engelhart et al., 2009;

Miller et al. 2013) and ground water extraction produced non-uniform relative sea level rise rates in Chesapeake Bay (Boesch et al., 2018). This was not considered in our model runs. Nevertheless, the difference between the predicted and observed long-term trend over the past 30 years was relatively small and should not significantly affect hypoxia simulations.

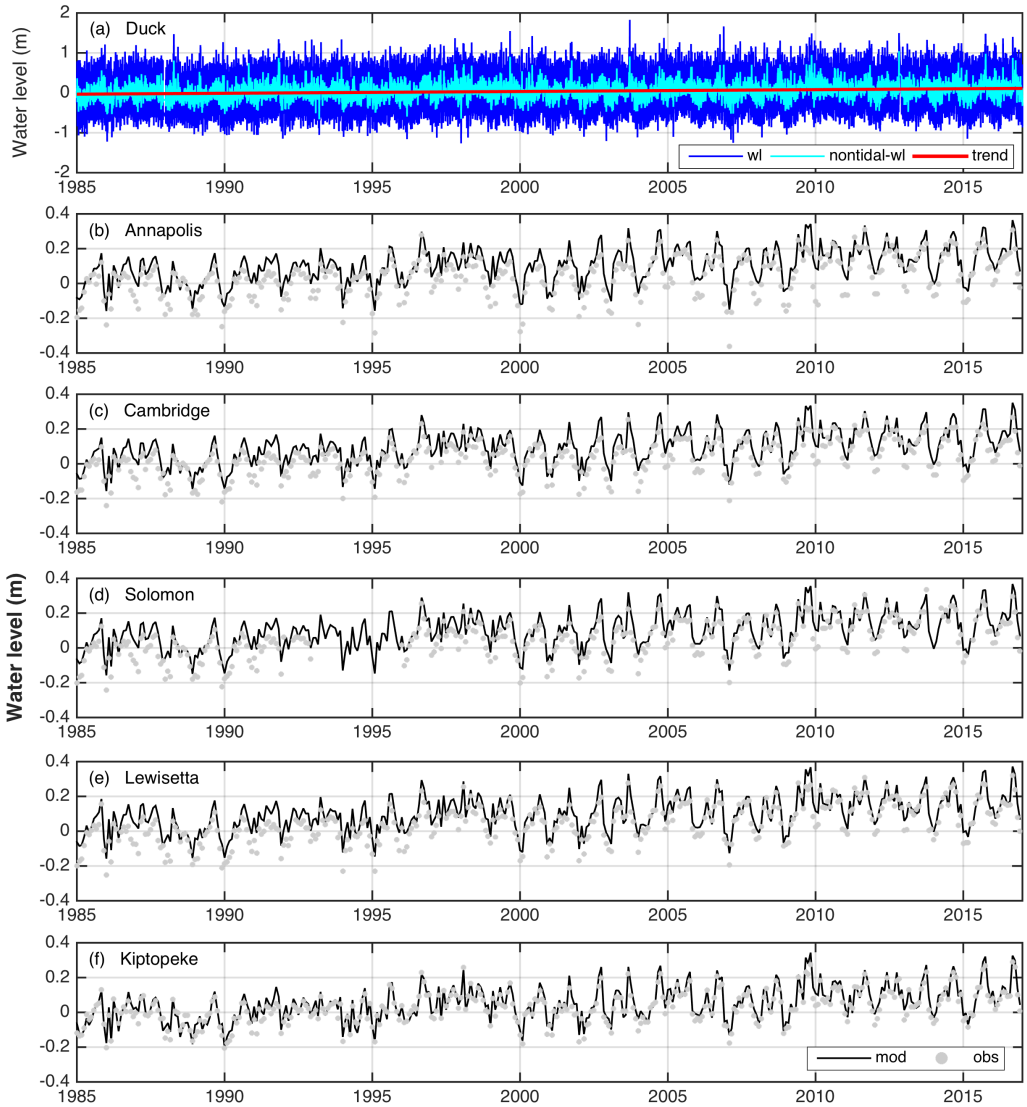

Figure 3.3 (a) Time series of water level of Duck, North Carolina used to forced the ROMS model. The blue line shows the hourly observations, the cyan line shows de-tided water level and the red line is the linear trend. (b)-(f) Modeled (black line) and observed (grey dots) monthly averaged water level at NOAA gauge stations in Chesapeake Bay.

Table 3.1 Sen's slope, significance and RMSE of monthly observation and modeled water level at NOAA gauge stations.

	obs mm/yr	obs p-value	mod mm/yr	mod p-value	RMSE (m)
Baltimore	4.3	<0.01	4.7	<0.01	0.149
Annapolis	4.9	<0.01	4.7	<0.01	0.081
Cambridge	5.1	<0.01	4.8	<0.01	0.066
Solomon	6.2	<0.01	4.8	<0.01	0.066
Lewisetta	6.6	<0.01	4.8	<0.01	0.064
Kiptopeke	4.4	<0.01	4.9	<0.01	0.035

The model-predicted surface water temperature compared well with the observations at the NOAA tidal gauging stations (Figure 3.5). Temperature at the tidal gauge stations was sampled at hourly intervals and averaged to produce monthly averaged temperature. The model not only captured the annual cycle but also the long term warming trend. The correlation coefficient is 0.99 and the normalized standard deviation is close to 1 (Figure 3.4b). We used the Theil-Sen estimator to calculate the linear trends in the temperature time series: the observation showed an average temperature increase of 2.0 ^{o}C among these five stations and the modelled temperature showed an average warming of 1.8 ^{o}C (Table 3.2). However, the p-value for both the observed and modelled time series are larger than 0.05, indicating that this warming trend is not statistically significant when compared against large annual cycle.

Table 3.2 Sen's slope, significance of Mann-Kendal trend test and RMSE of monthly observation and modeled surface water temperature at NOAA tidal gauge stations.

	obs °C/32yr	obs p-value	mod °C/32yr	mod p-value	RMSE (°C)
Tolchester	1.95	0.45	1.52	0.24	1.29
Thomas Point	1.40	0.25	1.99	0.11	1.50
Solomon	1.51	0.46	2.02	0.10	1.57
Lewisetta	2.10	0.34	2.03	0.08	1.59
Kiptopeke	3.08	0.11	1.29	0.23	1.84

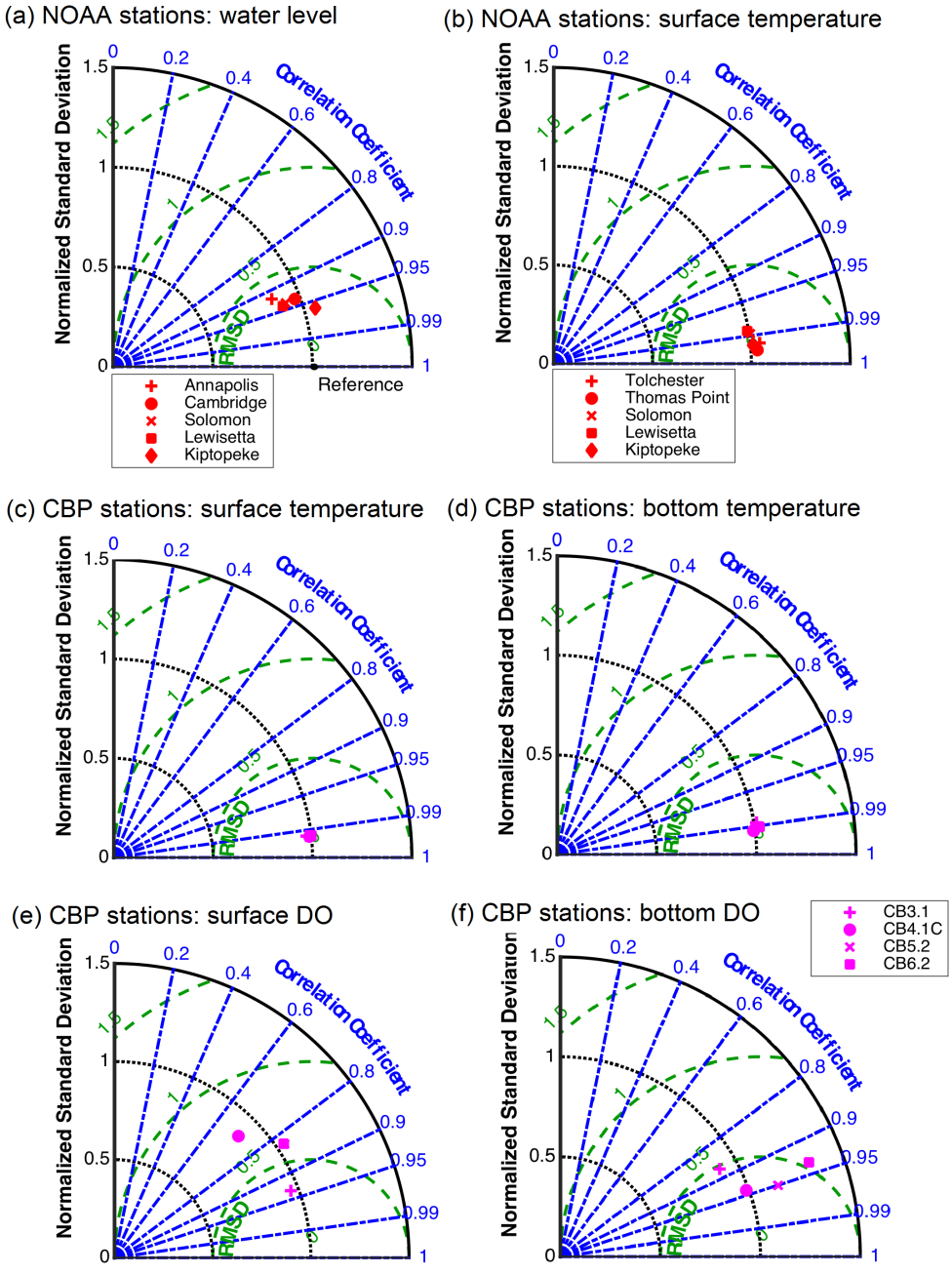

Figure 3.4 Taylor diagram for comparing the modelled and observed water level (a) and surface temperature (b) at NOAA tidal gauge stations, and surface (c)/(e) and bottom (d)/(f) temperature/O_2 concentration at CBP monitoring stations.

Table 3.2 Sen's slope, significance of Mann-Kendal trend test and RMSE of monthly observation and modeled surface water temperature at NOAA tidal gauge stations.

	obs °C/32yr	obs p-value	mod °C/32yr	mod p-value	RMSE (°C)
Tolchester	1.95	0.45	1.52	0.24	1.29
Thomas Point	1.40	0.25	1.99	0.11	1.50
Solomon	1.51	0.46	2.02	0.10	1.57
Lewisetta	2.10	0.34	2.03	0.08	1.59
Kiptopeke	3.08	0.11	1.29	0.23	1.84

Next we compare the predicted and observed surface and bottom water temperature at a few stations arrayed along the center deep channel of the Bay (Figure 3.6, Table 3.3). The CBP monitoring cruises collected temperature measurements at these stations at bi-weekly or monthly intervals. These data are directly compared with hourly model output. Once again the model accurately captured the observed temperature time series in both surface and bottom waters (Figures 3.4c-d), although the model tended to slightly overestimate temperature by ~1.2°C. Both the long-term monthly averages from observations and model simulation show clear increasing trends from 1985 to 2016 (Figure 3.6). Over the 32-year time period, surface water temperature is increased by ~1.4-2.1°C at most stations.

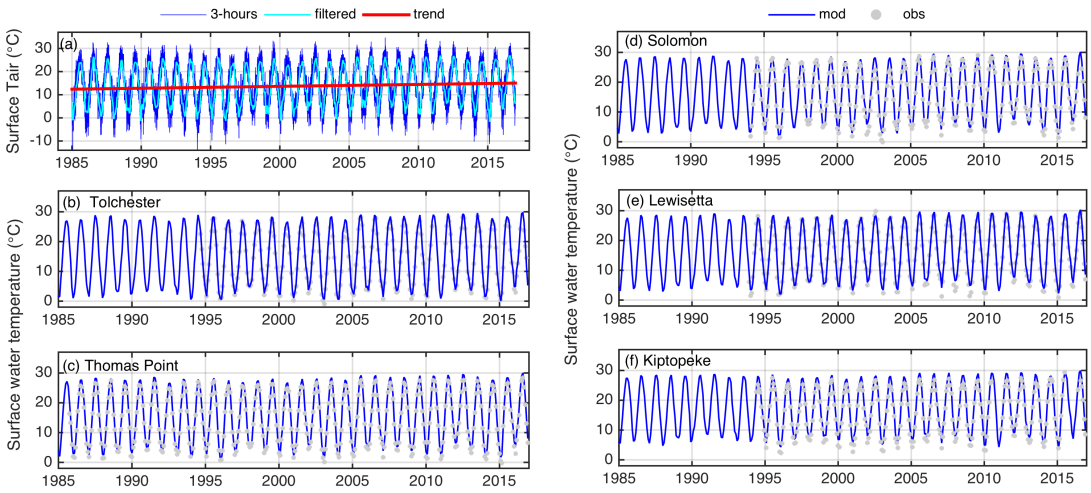

Figure 3.5 (a) Surface air temperature at a mid-bay location obtained from NARR (see Figure 3.1b for its location). The blue line indicates 3-hourly reanalysis outputs, the cyan line shows monthly filtered data and the red line is the linear trend. (b)-(e) Modeled (hourly, thin blue lines) and observed (grey dots, monthly) surface temperature at NOAA tidal gauge stations.

Further inspection on the simulation results suggests that the water temperature of every sub-regions in Chesapeake Bay is increasing and the trend is statistically significant (Table 3.4). The surface water temperature is generally increased by 1.3-1.8°C at different sub-regions over the past 32 years from 1985 to 2016. The simulated increases fall into reasonable range compared with the study of Ding and Elmore (2015) using remote sensing images to estimate the trend of Chesapeake Bay surface water temperature. The simulated results also suggest that the Chesapeake Bay salinity increases by ~0.3psu during 1985-2016 with sea level rise (Table 3.3). The increasing trend is statistically significant in both surface and bottom water and becomes weaker in the lower bay. It is very close to the estimation from Hong and Shen (2012) with experimental sea level rise.

Table 3.3 Theil-Sen's slope, significance of M-K trend test of observed water temperature and monthly averaged model results at CBP stations and Root-Mean-Square-Error(RMSE) between model results and observation data

		obs °C/32yr	obs p-value	mod °C/32yr	mod p-value	RMSE (°C)
surface	CB3.1	1.78	0.09	1.46	0.22	1.03
	CB4.1C	1.52	0.17	2.05	0.1	1.18
	CB5.2	1.48	0.16	2.18	0.08	1.17
	CB6.2	2.07	0.05	1.86	0.12	1.52
bottom	CB3.1	1.46	0.14	1.65	0.12	1.47
	CB4.1C	1.47	0.13	1.9	0.09	1.51
	CB5.2	1.35	0.18	1.76	0.1	1.6
	CB6.2	1.6	0.09	1.61	0.11	1.63

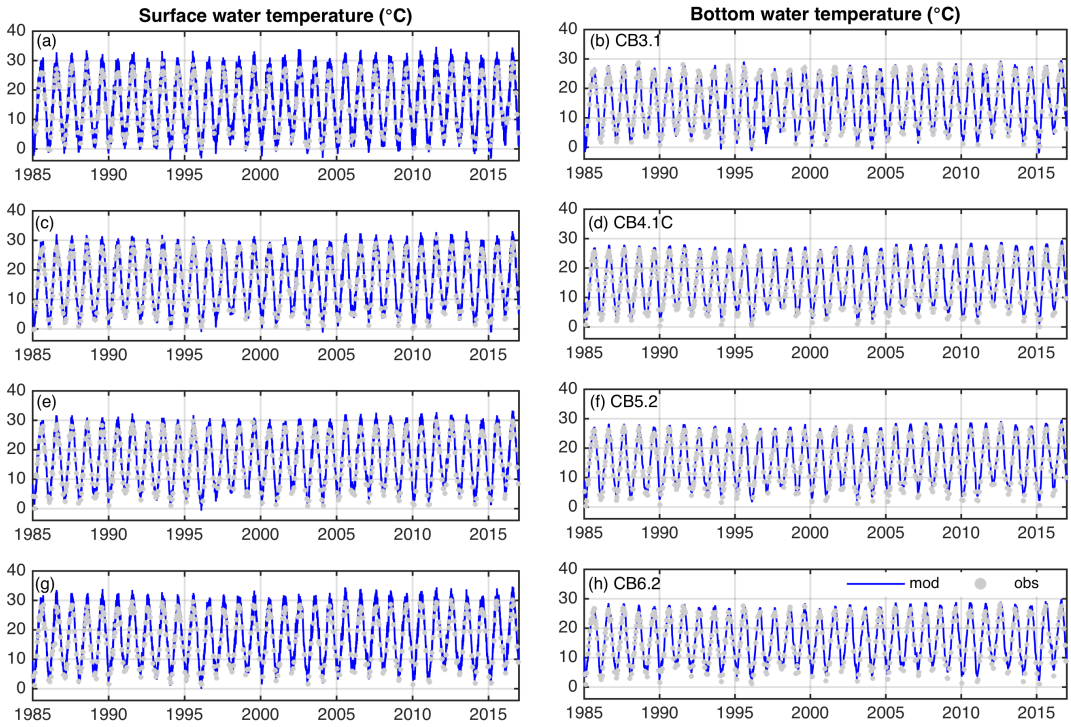

Figure 3.6 (a)-(h) Modeled (hourly, blue lines) and observed (grey dots) surface/bottom temperature at the CBP monitoring stations.

Table 3.4 Sen's slope and significance of monthly modeled surface and bottom water temperature, salinity at upper, upper-mid, lower-mid and lower Chesapeake Bay region in Base run

		Temperature (°C)		Salinity (psu)	
		MK-p	Sen-32yr	MK-p	Sen-32yr
surface	upper	<0.01	1.31	1.58E-03	0.30
	up-mid	<0.01	1.80	5.90E-02	0.30
	low-mid	<0.01	1.77	1.35E-02	0.30
	lower	<0.01	1.23	3.65E-01	0.12
bottom	upper	<0.01	1.34	2.10E-02	0.24
	up-mid	<0.01	1.65	2.28E-02	0.30
	low-mid	<0.01	1.57	1.68E-02	0.20
	lower	<0.01	1.08	7.98E-02	0.16

3.3.2 Long-term changes in O_2 and hypoxic volume

Figure 3.7 shows a comparison between the modelled and observed O_2 concentration in the surface and bottom waters at the CBP monitoring stations over the 32 year period. The model outputs are saved at 4-hourly intervals while the sampling data were collected at bi-weekly or weekly intervals. Clearly the model captured the seasonal cycle of dissolved oxygen as well as the interannual variations. For the surface O_2, the correlation coefficient ranges from 0.70 to 0.95 and the normalized standard deviations is around 1 except that it falls to 0.85 at station CB 4.1C (Figure 3.4e). For the bottom O_2, the correlation coefficient ranges from 0.87 to 0.95 and the normalized standard deviations is around 1 at stations CB 3.1 and CB 4.1C but is 1.1/1.3 at stations CB 5.2/CB 6.2 where the model-predicted variance is larger than the observed (Figure 3.4f). At station CB 6.2, the model did not always capture the observed seasonal minimum, which occasionally dropped below 2 mg/L.

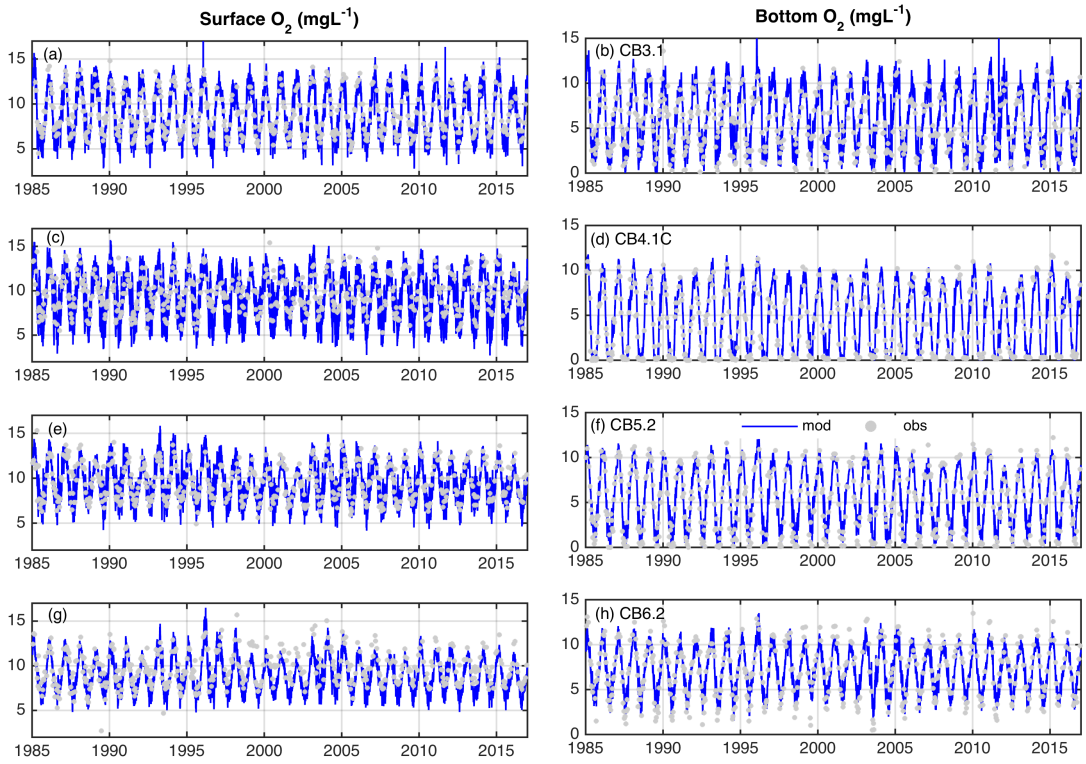

Figure 3.7 Modeled (4-hourly, blue line) and observed (grey dots) surface (right column) and bottom (left column) O_2 concentration at CBP monitoring stations.

To identify long term O_2 trends, we averaged O_2 concentration over the four subregions and obtained the regionally averaged O_2 concentrations for both the surface and bottom waters. The GAM model was used to fit these time series, as illustrated in Figures 3.8a-b. GAM fits represented the data with high skill, with the adjusted regression coefficient R^2 ranging from 0.91 to 0.96. After the seasonal cycle was removed, the residuals displayed large interanuual variations, as reported in previous studies (e.g. Li et al., 2016). However, O_2 declined in all four subregions, with larger reductions in surface waters than in bottom waters (Table 3.5). Surface O_2 decreased by ~0.3 mg/L in the upper and lower Bay between 1985 and 2016, but it decreased by ~0.5 mg/L (67% larger) in the mid-Bay regions. For comparison, we calculated

saturation concentration and found that it decreased by 0.13-0.29 mg/L over the same period. The surface O_2 reduction in the mid-Bay clearly exceeded this. The bottom O_2 declined by ~0.3 mg/L in the upper and mid-Bay but ~0.15 mg/L in the lower Bay. Mann-Kendall tests were conducted to determine the statistical significance of these long term trends in the time series of the regionally averaged O_2. All the O_2 decline trends were statistically significant, with the *p*-value much less 0.01 (Table 3.5).

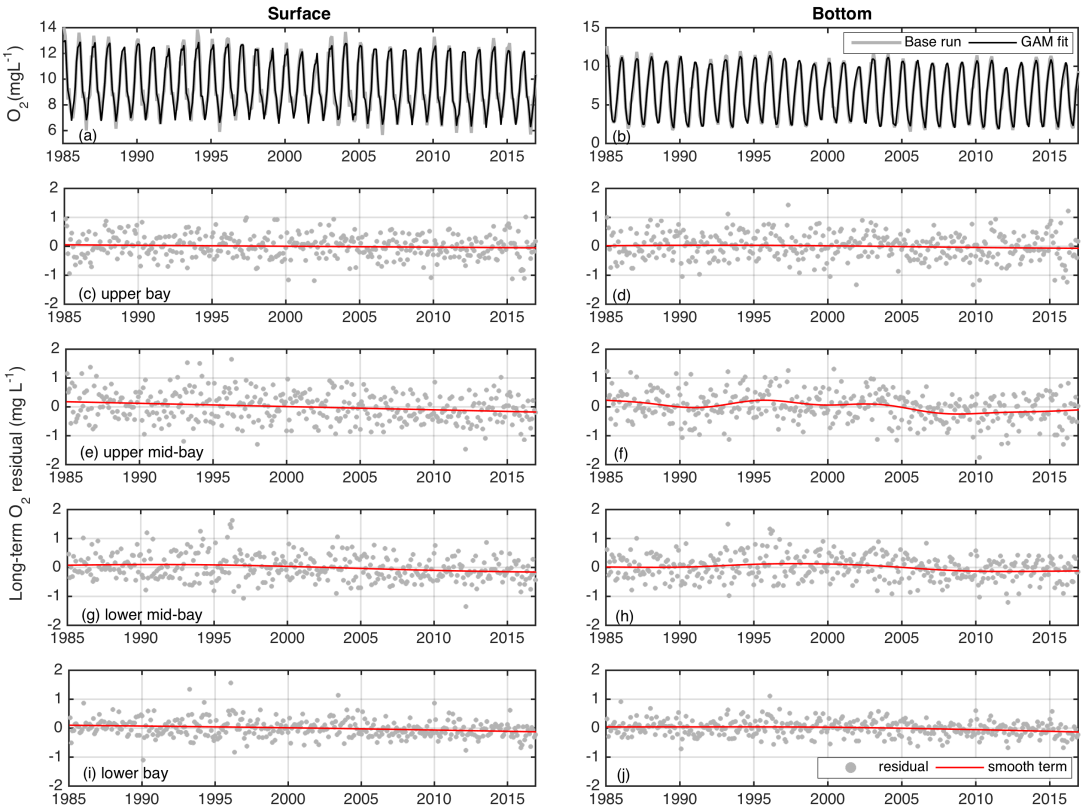

Figure 3.8 Time series of modeled monthly (grey line) and GAM fitted (black line) surface (a) and bottom (b) O_2 concentration averaged in the upper-mid bay. (c)-(j) Long-term O_2 residuals (grey dots) and their linear trends (red line) in four subregions of Chesapeake Bay.

Table 3.5 Sen's slope, significance monthly modeled surface and bottom O_2 at upper, upper-mid, lower-mid and lower Chesapeake Bay region in Base run

		DO-Base(mg/L)		DO-DtrTEMP(mg/L)		DO-DtrSLR(mg/L)		DO-DtrNut(mg/L)	
		MK-p	Sen-32yr	MK-p	Sen-32yr	MK-p	Sen-32yr	MK-p	Sen-32yr
surface	upper	4.95E-04	-0.28	6.50E-01	0.04	2.23E-03	-0.25	1.51E-03	-0.26
	up-mid	3.38E-09	-0.53	4.22E-01	-0.07	5.86E-09	-0.53	2.36E-07	-0.48
	low-mid	3.65E-08	-0.50	3.20E-02	-0.18	1.06E-07	-0.49	6.02E-08	-0.49
	lower	1.91E-06	-0.32	8.00E-02	-0.12	2.23E-06	-0.32	7.11E-07	-0.34
bottom	upper	4.26E-03	-0.29	7.35E-01	0.03	3.32E-02	-0.22	3.58E-03	-0.30
	up-mid	2.25E-03	-0.34	3.67E-01	0.10	7.41E-03	-0.30	5.06E-04	-0.39
	low-mid	2.75E-03	-0.28	3.87E-01	0.08	1.29E-02	-0.23	2.29E-04	-0.33
	lower	1.08E-02	-0.15	3.16E-01	0.06	2.05E-02	-0.14	1.38E-03	-0.18
surface saturation	upper	3.10E-08	-0.28	3.00E-03	-0.14	5.83E-06	-0.22	-	-
	up-mid	2.20E-05	-0.29	2.80E-02	-0.15	3.24E-04	-0.25	-	-
	low-mid	4.30E-06	-0.23	3.70E-02	-0.11	1.44E-04	-0.20	-	-
	lower	1.30E-03	-0.13	1.75E-01	-0.06	7.08E-03	-0.11	-	-

Monthly averaged hypoxic volumes (with O_2 concentration less 2 mg/L) were calculated for May-September and their variations in 1985-2016 are shown in Figure 3.9. The non-parametric MK test was applied to the time series of the hypoxic volume to identify possible monotonic long term trends. The Sen's slope in the September hypoxic volume was -0.028, amounting to a reduction of 0.9 km^3 over the 32-year period. In comparison, the Sen's slope in the July hypoxic volume was 0.014, amounting to an increase of 0.46 km^3. The Sen's slope in May, June and August hypoxic volume was less than 0.01, indicating no apparent long term trend. However, the MK test showed that none of these trends are statistically significant, with all p-values exceeding 0.05 (Figure 3.9). This suggests that the long-term trend was insignificant when compared with the large interannual variations in the hypoxic volume.

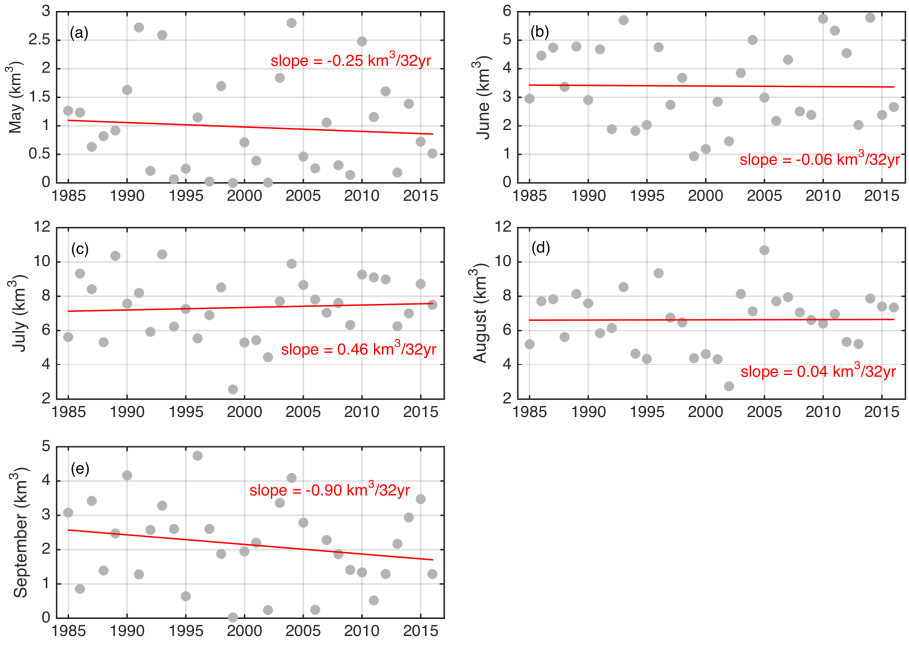

Figure 3.9 Variations in monthly hypoxic volume calculated from ROMS-RCA: May (a), June (b), July (c), August (d), September (e). The red line marks a linear fit through the data.

The apparent contradiction between Figures 3.8 and 3.9 motivated us to examine the seasonal averaged O_2, as shown in Figure 3.10 for the bottom O_2 in the upper mid-Bay where hypoxia generally occurs. O_2 declined by 0.61 mg/L in winter and by 0.54 mg/L in spring between 1985 and 2016. In contrast, O_2 declined by 0.35 in summer but increased by 0.13 in fall over the same period. In summary, the dissolved oxygen declined by an average value of 0.3 mg/L over the past 3 decades, but at much faster rates in winter and spring seasons. On the other hand, O_2 increased slightly in the fall, resulting in a smaller hypoxic volume.

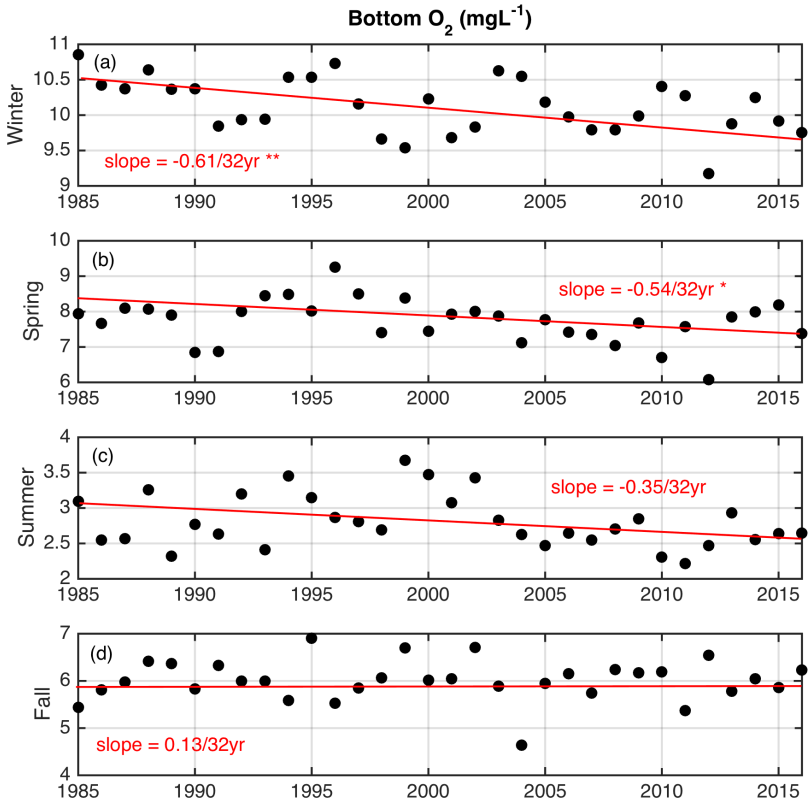

Figure 3.10 Variations in seasonal bottom O2 in upper mid-bay calculated from ROMS-RCA: Winter (a), Spring (b), Summer (c), Fall (d). The red line marks a linear fit through the data.

3.4 Model-scenario analysis to discern driving mechanisms

To discern the roles of warming, sea level rise and nutrient management in driving the long-term trends in hypoxia in Chesapeake Bay, we analyzed the three scenario model runs DtrTEMP, DtrSLR and DtrNut and compared them with the Base run.

The long-term residual in the GAM fit to the regionally averaged O_2, namely *s(dnum)*, is shown in Figure 3.11. First, in all the four subregions and in both surface and bottom waters, there were no detectable differences in *s(dnum)* between the Base run and DtrSLR run. This suggests that removing sea level rise had little effects on the long-term O_2 trend in Chesapeake Bay between 1985 and 2016. Second, DtrTEMP run showed the largest difference from the Base run. For example, in the DtrTEMP runs, surface O_2 showed no linear trends in the upper Bay and upper mid-Bay over the 32 years. It increased slightly in the lower mid-Bay and lower Bay between 1985 and 1995 and decreased slightly between 1995 and 2016, but the net reduction over the 32 years was considerably smaller than surface O_2 in the Base run. Bottom O_2 showed no linear trend in the upper Bay and a weak trend in the lower Bay. In the bottom water of two mid-Bay subregions, O_2 in the DtrTEMP run trended upwards in 1990-2000, downwards in 2000-2010 and upwards again after 2010, but did not display a definition direction for change. In comparison, *s(dnum)* in the Base run displayed an overall declining trend over the 32 years, even though it showed oscillations at decadal periods. Thus, the widespread reductions in oxygen in the Base run disappeared or were highly muted when temperature increases were removed. Third, the DtrNut run showed

relatively small differences from the Base run. In general, O_2 showed smaller declines in DtrNut run than in the Base run, where there were virtually no differences in the lower Bay and lower mid-Bay and the differences (smaller declines) were most clear in the upper Bay and upper mid-Bay. Thus, the effect of removing the nutrient load reduction was to lead to higher oxygen levels relative to the Base run in northern Bay regions in proximity to the Susquehanna River.

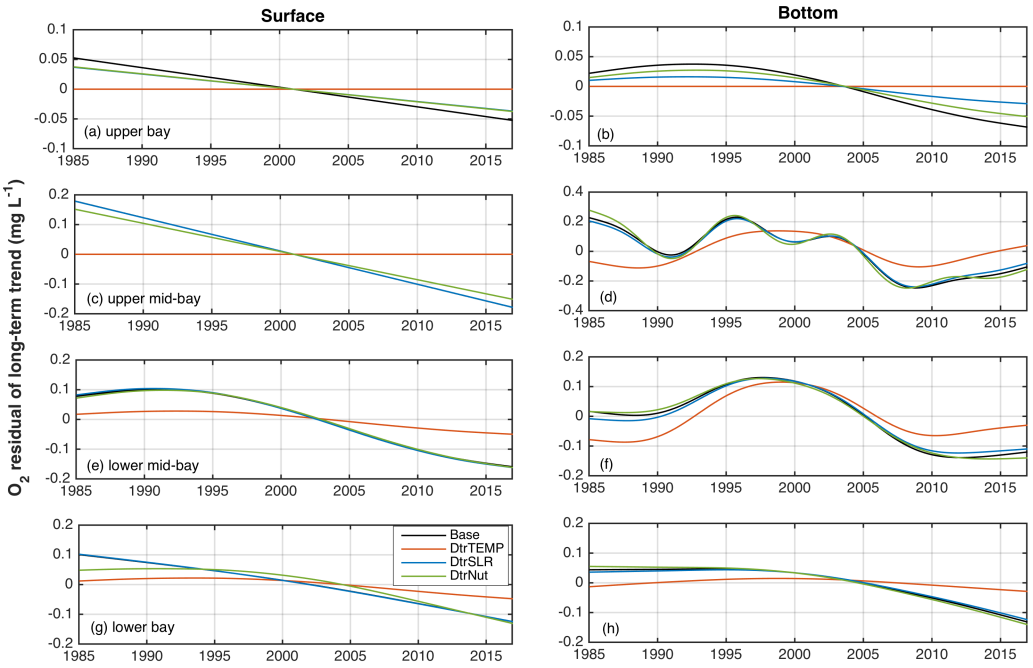

Figure 3.11 The smooth term representing long-term trend of surface (left) and bottom (right) O_2 obtained from the hindcast model run and scenario model runs removing temperature increase, sea level rise and nutrient management factors. O_2 is averaged over (a)(b) upper bay; (c)(d) upper mid-bay; (e)(f) lower mid-bay; (g)(h) lower bay.

Another way to tease out the individual effects of sea level rise, warming and nutrient reduction is to compare the regionally averaged concentration O_2 in bottom water between the beginning and end of the 32-year period. To filter out interannual fluctuations, we averaged O_2 over two decadal periods: 1985-1994 (Period 1) and 2007-

2016 (Period 2). Figures 3.12a-d show the differences ΔO_2 between Period 1 and Period 2 from the Base run and three scenario runs. In the Base run, O_2 decreased during most of times in a year, except during late summer and early Fall (August-October) when O_2 showed a slight increase (< 0.1 mg/L) in the middle and lower Bay. This is consistent with the declining September hypoxic volume shown in Figure 3.9. In contrast, ΔO_2 was negative in other seasons, reaching (-0.2 to -0.4) mg/L in the lower and upper Bay and (-0.5 to -0.7) mg/L in the two mid-Bay regions. It is interesting to note that the O_2 reduction was considerably larger during winter and spring. This resolves an apparent contradiction between Figures 3.8 and 3.9 because the largest O_2 reduction occurred during the non-hypoxic seasons.

We further compared the ΔO_2 between Period 1 and Period 2 in three detrended scenario runs (Figure 3.12a-d). Compared with Base run, ΔO_2 in the upper bay from DtrSLR run exhibited overall upward shift, indicating a smaller decline in winter-summer and larger increase in fall. ΔO_2 in the mid and lower Bay regions did not differ from the Base run. O_2 decline in the upper bay from DtrNut run was smaller in the winter but larger in late spring when compared with Base run. In the middle and lower bay, ΔO_2 was even negative during summertime. The most dramatic difference with the Base run still came from DtrTEMP run, where the O_2 decline during winter to early spring was substantially reduced in mid and lower bay regions. ΔO_2 even became positive from late spring to fall, implying that the bottom O_2 concentration increased without warming. In DtrTEMP run, bottom O_2 in the upper bay decreased in late winter and summer but increased in spring and fall.

Since the O_2 concentration was similar between the Base run and scenario runs in Period 1, a comparison of the O_2 concentration between the Base and scenario runs in Period 2 shed further light on the effects of the individual forcing (Figures 3.12e-h). Clearly bottom O_2 in DtrTEMP run was much higher than the Base run throughout the year, with the largest difference in winter-spring and the smallest difference in fall. The surplus reached 0.5-0.7 mg/L in the upper Bay and mid-Bay and 0.3 mg/L in the lower Bay. This clearly demonstrated that bottom O_2 would be considerably higher without warming. Bottom O_2 in DtrNut run was somewhat lower than the Base run in the mid-Bay, indicating that O_2 concentration would be ~0.1 mg/L lower without nutrient reduction. Bottom O_2 was greater in the DtrSLR run than in the Base run, particularly in the upper Bay, indicating that O_2 would be higher without sea level rise. In conclusion, the effect of warming is strongest during winter-spring that predominately drives the decline of bottom O_2. It can be one order of magnitude larger than the effects of other two forcings. Both warming and sea level rise caused the decline of bottom O_2, while nutrient loads reduction leads to the recovery of bottom O_2 during summer in the middle bay.

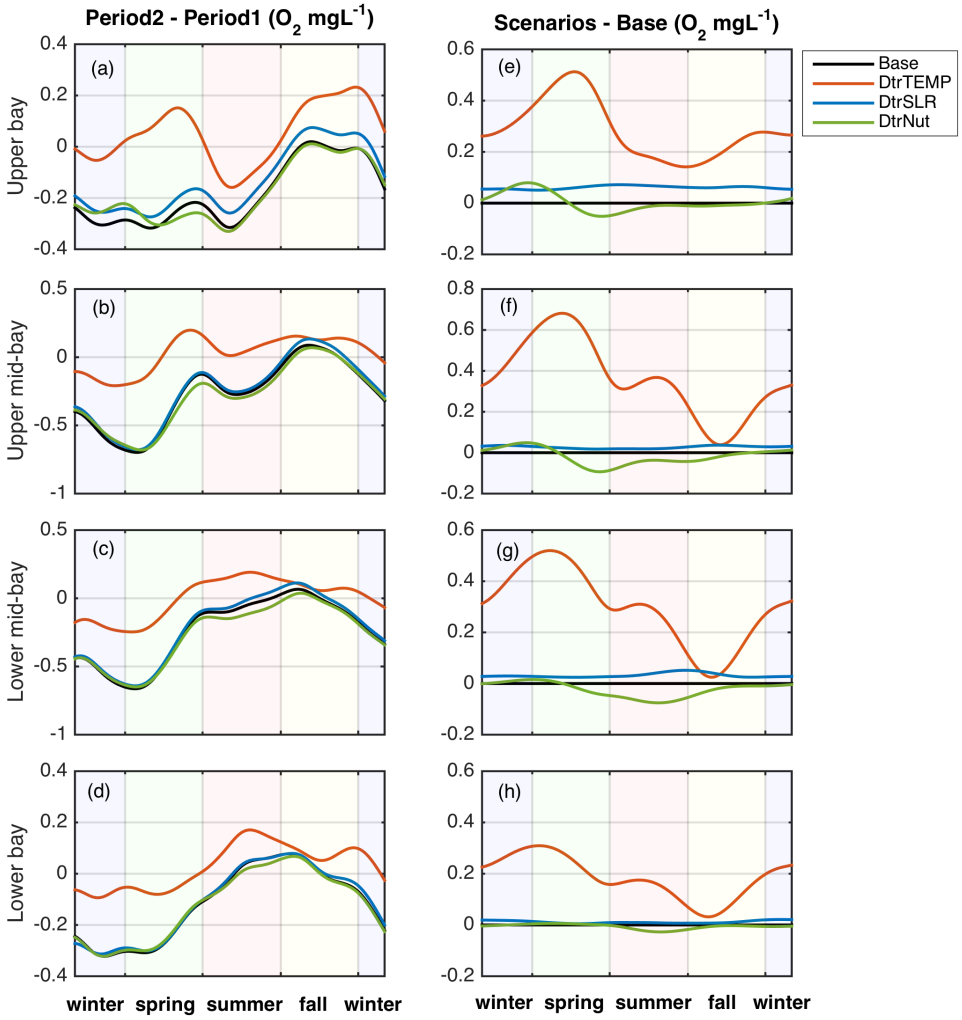

Figure 3.12 (a-d) O_2 differences between Period2 and Period1 in the hindcast run and scenario runs. (e-h) O_2 differences between scenario runs and the hindcast run in Period2. The O_2 time series were low-pass filtered to remove the short-term fluctuations.

In addition to O_2 concentration and hypoxic volume, we examined whether the onset and termination of hypoxia shifted over the past three decades. Using the mid-Bay station CB4.1C as an example, we calculated the day of a year (hypoxia initiation day, T_{ini}) when O_2 first fell below 2 mg/L in spring and the day of a year (hypoxia termination day, T_{ter}) when O_2 rose above 2 mg/L in fall (Figure 3.13). There was large

scatter in T_{ini} spanning from late April to early June, although it most often occurred in the month of May (Figure 3.13a). The MK trend test showed that T_{ini} showed no long term trend in the Base run. No trend in T_{ini} was detected either in DtrSLR and DtrNut runs. On the other hand, T_{ini} in DtrTemp had an appreciable upward trend, with the Sen's slope of 1.8 days/decade. This suggests that the onset of hypoxia would have been delayed by ~6 days without the warming over the past 3 decades. This result can be seen more clearly when we plot the difference in the hypoxia initiation day ΔT_{ini} between the three scenario runs and the Base run. ΔT_{ini} was nearly zero in DtrSRL run, indicating that sea level rise had no effects on hypoxia initiation. ΔT_{ini} was slightly negative (up to 5 days after 2005, with an outlier of 10 days in 2012) in DtrNut run, indicating that nutrient reduction delayed hypoxia initiation in recent years. More strikingly, ΔT_{ini} in DtrTemp reached 5-10 days between 2000 and 2016, suggesting that warming caused the hypoxia to develop 5-10 days earlier in spring.

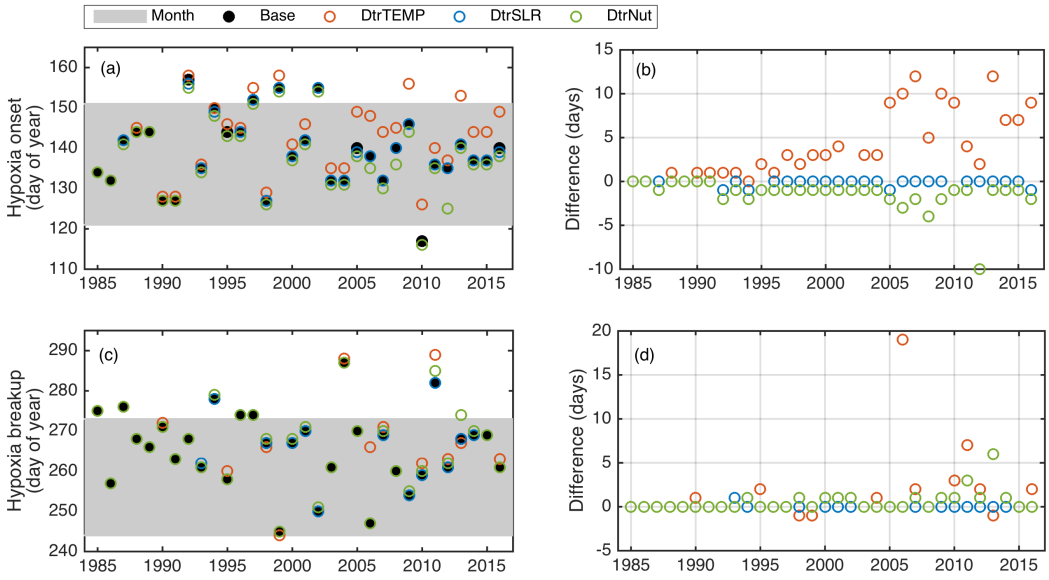

Figure 3.13 Hypoxia onset (a) and breakup (c) timing at CB4.1C during 1985-2016 by Base run (black solid cicle), DtrTEMP run (red empty circle), DtrSLR run (blue empty circle) and DtrNut run (green empty circle). The difference of hypoxia onset (b) and

breakup (d) timing between between DtrTEMP, DtrSLR, DtrNut and Base run correspondingly.

There was also substantial scatter in the hypoxia termination day T_{ter} (Figure 3.13c). The MK trend test showed that T_{ter} shifted earlier in the Base run as well as in the three scenario runs if year 2003 and 2011 were removed due to Hurricane Isabel and Tropical Storm Lee in fall. We also calculated the difference in the hypoxia termination day ΔT_{ter} between the three scenario runs and the Base run (Figure 3.13d). Once again ΔT_{ter} is nearly zero in DtrSLR, indicative of no influence from the sea level rise. ΔT_{ter} in both DtrTemp and DtrNut runs is positive but small. This shows that warming and nutrient reduction have less influence on the hypoxia termination than the hypoxia initiation, although both drove an earlier termination by several days.

3.5 Discussion and conclusion

To investigate long term changes in dissolved oxygen in Chesapeake Bay, we used a coupled hydrodynamic-biogeochemical (ROMS-RCA) model to conduct hindcast simulations between 1985 and 2016 when regular water quality monitoring were available. ROMS-RCA accurately captured the observed O_2 time series at the CBP monitoring stations, with the correlation coefficient around 0.9 and the normalized standard deviation in the range of (0.9-1.1). After the seasonal and interannual variations are removed, the dissolved oxygen in all regions of the estuary showed a statistically significant downward trend: decreasing ~0.3 mg/L over the past three decades. Most of this O_2 decline occurred during the winter and spring seasons, with a magnitude of (0.5-0.6) mg/L. The hypoxic volume in May-August showed no changes. However, over the same period September O_2 increased by 0.13 mg/L, the September

hypoxic volume showed a slight increase (~0.9 km^3), and the hypoxia breakup shifted earlier in the fall.

The model provided high frequency (4-hourly) and fine resolution (1 km, 20 vertical layers) outputs of the three-dimensional fields of O_2 and other physical/biogeochemical state variables, enabling a more robust statistical analysis than what could be achieved on sparse water quality data (biweekly or monthly intervals and 49 stations distributed in the Bay) collected at the CBP monitoring stations. There was general agreement in the direction and magnitude of the long-term trend in oxygen concentration, hypoxic volume, and hypoxia termination day between the modeling and data analysis. The model results showed that the hypoxic volume decreased in September and the hypoxia termination day shifted early by ~5 days over the past three decades. This is consistent with the retrospective data analysis by Murphy et al. (2011) who found a slight decrease in late summer hypoxia. Testa et al. (2018) confirmed this finding and hypothesized that the earlier disintegration of hypoxia resulted from a "speeding up" of organic matter consumption associated with warming in combination with the suppression of spring phytoplankton biomass in the lower Bay due to modest nutrient load reductions. Murphy et al. (2011) also suggested that the hypoxic volume increased in early summer, and Testa et al. (2018) hypothesized that elevated early summer hypoxic volume was linked to increased winter phytoplankton biomass in the upper Bay. The later result is a subject of debate and there is no consensus whether the timing of hypoxia initiation has shifted in spring. Zhou et al. (2014) detected no significant trend in the timing of onset of hypoxia in Chesapeake Bay and did not find

a trend in the seasonal-maximum hypoxic volume itself. In a related study, Harding et al. (2016) found that the annual mean surface chlorophyll stabilized in the lower and upper bay but continued to increase in the mid-Bay since 1980s. All these data analyses were based on the same data set, but the apparent differences in their conclusions reflected different methodological approaches and different time windows for analysis and data aggregation. However, the many analyses of observations also reflect the limitations of the data set itself, such as coarse temporal resolution and sparse coverage over the complex estuarine geometry. A numerical model validated against the observational data can reproduce a high resolution time series as well as spatial averages to deduce system-wide metrics, although it must be cautioned that the model is only an approximate representation of the estuarine system.

The numerical model also afforded an opportunity to probe underlying mechanisms that might have driven the long term changes in O_2. We conducted additional numerical experiments in which we removed trends in each long term driver to discern the separate effects of temperature increases, sea level rise and nutrient reduction. Warming was found to the dominant driver of the long-term oxygen decline whereas sea level rise had a minor effect (Figures 3.11-3.13). In their retrospective data analysis, Murphy et al. (2011) suggested that the increase trend of early summer hypoxia might be related to enhanced stratification in June due to regional sea level rise. We calculated the depth-averaged stratification N^2 in the mid-bay where most of hypoxic water is located. Indeed, N^2 showed a statistically significant upward trend in the upper mid-Bay and an upward trend in the lower mid-Bay (Figure 3.14). However,

there were virtually no differences in between the Base run and DtrSLR run, suggesting that the increasing trend in the June stratification was not caused by the relatively modest sea level rise (~0.15 m over the past three decades). Warming or other physical forcings was more likely a cause for the increased stratification. The comparison between Base run and DtrNut run indicated that extra nutrient loading would result in earlier hypoxia initiation of 2-3 days. This is consistent with the finding of Testa&Kemp (2014) that the timing of hypoxia onset is highly related with chlorophyll-a concentration.

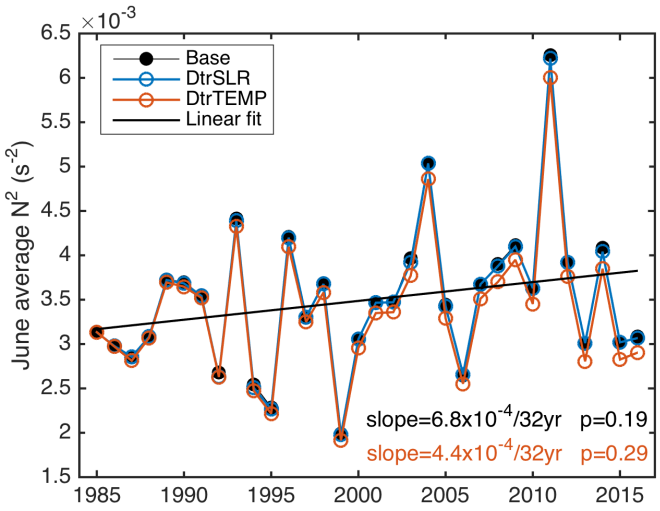

Figure 3.14 June vertical averaged stratification over mid-bay region from Base run, DtrSLR run and DtrTEMP run. Black solid line indicates linear regression of Base run result.

Warming was found to be the dominant force driving the long-term decrease of dissolved oxygen in Chesapeake Bay. Without warming, O_2 concentrations in all regions of the estuary showed no or weak long term trends over the past three decades (Figure 3.11). The magnitude of reduction was about the same as that expected from the solubility effects in the upper Bay but exceeded it in other regions of the Bay (Table

3.5). In the two mid-Bay regions, the bottom O_2 decreased by 0.31 mg/L, which was slightly larger than -0.26 mg/L expected from solubility reduction. In contrast, the surface O_2 decreased by 0.51 mg/L, which was twice as much as the solubility effect. The integrated water column respiration in the mid-bay showed notable reduction from winter to early summer when no warming occurred (Figure 3.15). This suggests that water column respiration in the upper water column increased substantially over the three decades. A similar story emerged in the lower Bay where the bottom O_2 decreased by 0.15 mg/L, slightly larger than the solubility reduction, but the surface O_2 decreased by 0.32 mg/L, twice as much. Relative to 1985-1994, O_2 concentration in 2007-2016 decreased slightly in winter and spring but increased by a similar amount in summer and fall in the absence of warming (Figure 3.12). Comparison between the Base run and DtrTemp showed that warming led to earlier (~6 days) initialization in the spring and earlier disintegration (~ 0.5 days) of hypoxia in the fall (Figure 3.13). This early shift is consistent with Testa et al.'s (2018) hypothesis that warming-induced an early shift in phenology led to speeding-up of the biogeochemical cycling and seasonal hypoxia cycle.

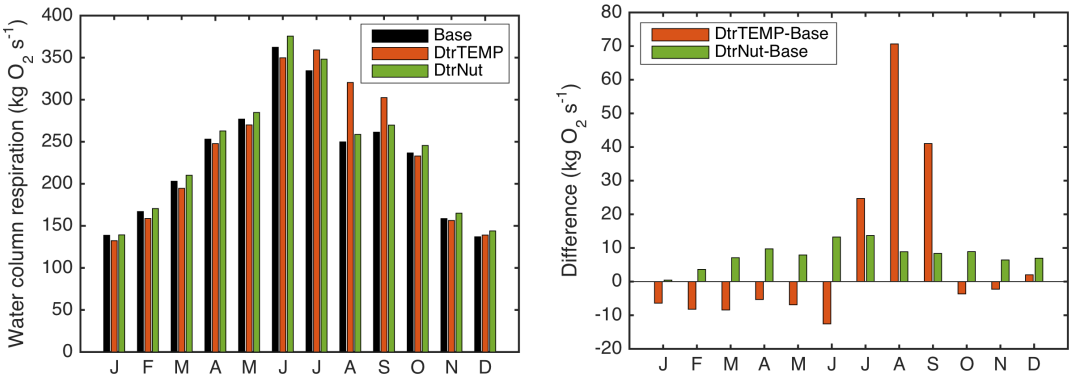

Figure 3.15 Left: monthly averaged water column respiration in mid-bay in Period 2 in the hindcast run and scenario runs. Right: difference of monthly averaged water column respiration in mid-bay in Period 2 between the hindcast run and scenario runs.

Chesapeake Bay has been subject to extensive efforts to reduce nutrient inputs since 1980s. In 1987, a commitment was made to reduce controllable sources of both nitrogen (N) and phosphorous (P) by 40% by the year 2000. Although the actual implementation fell short of the goals, there were appreciable declines of dissolved nitrogen, as shown in Figure 2 and widely reported by Zhang et al. 2015, Murphy et al. 2011, Testa et al. 2018, and Harding et al. 2015. At the same flow of the Susquehanna River, the total nitrate loading was 5-10 Gg smaller in 2001-2016 than in 1985-2000 (see also Testa et al., 2018). However, the model results suggested that this nutrient reduction only played a minor role in driving the long-term O_2 trend over the past three decades. The bottom O_2 increased by <0.1 mg/L in the middle parts of the Bay, which was one third of the O_2 increase due to warming (Figure 3.12). Nutrient reduction delayed the onset of hypoxia by < 5 days (Figure 3.13b), in agreement with Testa et al. (2018)'s hypothesis that modest nutrient reduction suppressed spring phytoplankton biomass in seaward waters. Interestingly, nutrient reduction worked in concert with warming to cause earlier termination of hypoxia in the fall, as shown in Figure 3.13d. It is worth to note that atmospheric deposition and wastewater treatment plants discharge into tidal rivers were not included in the model. The additional reduced nutrient loads from these sources might further contribute to the recovery of oxygen level in the bay.

The main finding of this modeling study is that the warming-induced O_2 decline was nearly three times as large as O_2 increase related to nutrient reduction. This

suggests that climate change (about 1.5 ^{o}C warming) has completely cancelled out potential benefits of nutrient management over the past three decades. The only improvement is the earlier termination of hypoxia in the fall as warming may have caused a phenological shift and the speeding up of the seasonal hypoxia cycle. Assuming that the hypoxia responds linearly to nutrient loading, a three-fold increase in nutrient reduction would have been needed to compensate for the warming-induced deoxygendation. To further clarify the opposing effects of warming and nutrient reduction, we extended the GAM model of summer bottom O_2 to include the effects of both river flow and temperature. The time series of residual O_2 in bottom waters of the upper mid-Bay showed a moderate upward trend after both the temperature effects and river flow were removed (Figure 3.16). This suggests that bottom O_2 could have increased if there was no warming during the past decades. Nutrient reduction in Chesapeake Bay did not lead to a better O_2 condition along the reversed trajectory in relation to changes in nutrient load, and this result is linked to warming, which may have caused a shift in baseline condition and altered the hypoxia response to reduced nutrient loads. With projected warming in the mid-late 21st century, recent modeling studies on future Chesapeake Bay hypoxia also suggest a modest to large decline in bottom oxygen with expanded hypoxic volume (Irby et al., 2018; Ni et al., 2019). Relatively larger nutrient reductions and longer recovery times might be required to fulfil a complete reversal of eutrophication-induced hypoxia.

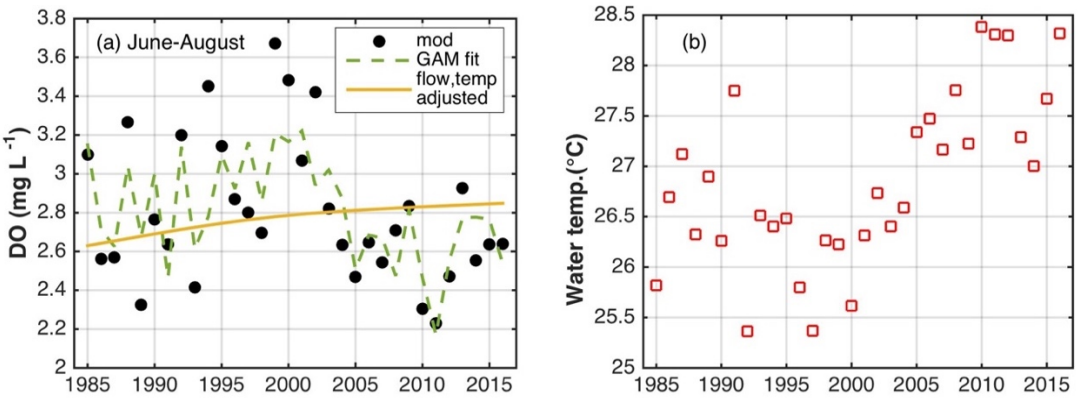

Figure 3.16 (a) June-August averaged bottom DO in upper mid-bay during 1985-2016 (black dots), GAM model fit (green dashed line) and flow and temperature adjust long-term trend (yellow solid line) of Base run. (b) June-August averaged water temperature in upper mid-bay during 1985-2016.

3.6 Acknowledgements

We are grateful to NSF (CBET-1360285) and NOAA Ocean Acidification Program (NOAA-OAP; Award NA15NOS4780184) for the financial support. Model outputs can be acquired upon request.

Chapter 4: Large projected decline in dissolved oxygen in a eutrophic estuary due to climate change

Preface

This chapter is a reproduction of work published in the *Journal of Geophysical Research: Oceans* with coauthors Ming Li, Andrew Ross and Raymond Najjar. The right to reuse this work was retained by the authors when publication rights and nonexclusive copyright were granted to the American Geophysical Union.

Ni, W., Li, M., Ross, A. C., & Najjar, R.G. (2019). Large projected decline in dissolved oxygen in a eutrophic estuary due to climate change. Journal of Geophysical Research: Oceans, 124. https://doi.org/10.1029/2019JC015274

4.1 Introduction

Dissolved oxygen (O_2) concentration has been declining in both the open ocean and coastal waters (Diaz and Rosenberg, 2008; Breitburg et al., 2018). In the open ocean, the oxygen loss is primarily linked to global warming and other climate change effects (Stramma et al., 2008; Schmidtko et al., 2017; Levin, 2018). Among the most relevant deoxygenation drivers, warming reduces ventilation of deeper waters due to stronger stratification in the upper ocean and decreases oxygen solubility (Keeling et al., 2010) while raising microbial metabolic rates and oxygen consumption (Deutsch et al., 2011). In estuaries and coastal oceans, the depletion of oxygen in bottom water has occurred at faster rates than the open ocean (Gilbert et al., 2010) and has been traditionally attributed to nutrient and organic matter loading from the surrounding watershed and rivers (Kemp et al., 2009; Rabalais et al., 2014; Fennel and Testa, 2019). Nevertheless, there is increasing recognition that climate change can also significantly affect hypoxia in estuarine and coastal waters (Justic et al., 2003; Meier et al., 2011; Bendtsen and Hansen, 2013; Altieri and Gedan, 2015; Claret et al., 2018).

Climate change and climate variability can affect physical processes regulating the supply of O_2 to the bottom water. In coastal and estuarine waters, freshwater input sustains the stratification that contributes to the formation of summer oxygen depletion. As a consequence, variations in the hydrologic cycle can affect the extent of hypoxia from interannual to long-term time scales (Zillén et al., 2008; Yu et al., 2015; Du et al., 2018). Wind affects O_2 by regulating mixing and advection of O_2 to the bottom water (Scully 2013, 2016a; Wilson et al., 2008; Feng et al., 2012). Climate change and

climate variability can also affect biogeochemical processes that consume O_2 in the water column and sediment. Nutrient loading from river runoff was shown to drive interannual hypoxia variations by regulating phytoplankton growth and water column respiration (Justic et al., 2002; Li et al., 2016). Similarly, Groβe et al. (2016) found that biological production is a major driver of oxygen deficiency in some parts of the North Sea.

With climate change projected to accelerate in the 21st century, it is important to take into consideration its effects when modeling hypoxia in estuarine and coastal waters and developing nutrient management strategies (Breitburg et al., 2018). Using an ensemble of coupled physical-biogeochemical models driven by regionalized global climate model outputs, Meier et al. (2011) projected that the hypoxic and anoxic areas in the Baltic Sea will increase in the future climate. This regional deoxygenation is caused by reduced oxygen solubility and intensified internal nutrient cycling, both of which result from increased temperature. Model simulations also showed that the warming induced decline of oxygen solubility and intensified stratification will lead to significant decrease of bottom-water O_2 in the North Sea and Gulf of Mexico by the end of 21st century (Meire et al., 2013; Laurent et al., 2018). In a recent modeling study, however, Saraiva et al. (2019a) found that the effects of climate change are smaller than the effects of considered nutrient load changes in the Baltic Sea.

Chesapeake Bay, the largest estuary in the United States, is characterized by high biological productivity and abundant fishery resources. It is a partially-mixed

estuary with a deep central channel where summer hypoxia mostly occurs. Hypoxia in Chesapeake Bay experienced dramatic expansion due to nutrient enrichment between 1950s and 1980s, but has stabilized since the mid-1990s (Hagy et al., 2004). Water-column oxygen consumption accounts for most of the oxygen demand and drives the interannual variations of hypoxia in the bay (Kemp et al., 1997; Li et al., 2016). Freshwater discharge sustains the stratification that contributes to the formation of summer low-oxygen water (Zhou et al., 2014; Scully, 2016b). Chesapeake Bay has experienced rapid climate change in recent decades, including rapid warming and accelerating relative sea level rise (Ding and Elmore, 2015; Boon and Mitchell, 2015). Therefore, there is increasing recognition and concern about climate change impacts on Chesapeake Bay (Najjar et al., 2010).

Two recent modeling studies have examined the impacts of climate change on hypoxia in Chesapeake Bay, but they were forced by simplified changes from climate model projections. Wang et al. (2017) investigated the individual and combined effects of warming and sea level rise by 2050. Summer anoxic volume was estimated to increase by 1.4% due to warming, but sea level rise resulted in a 12% reduction in the anoxic volume. In addition to warming and sea level rise, Irby et al. (2018) considered the effects of altered river flows. They found that warming reduced oxygen solubility year around, changes in precipitation and river flow fueled increased primary production, and sea level rise increased bottom water O_2 but decreased O_2 at mid-depths. Irby et al. (2018) found that the overall impact of climate change will be to

lower O_2 in Chesapeake Bay, but its potential impact is significantly smaller than the improvement in O_2 due to planned nutrient reductions.

The Baltic Sea studies of Meier et al. (2011) and Saraiva et al. (2019b) presented results from ensemble simulations to account for climate uncertainty. This multi-model projection would generate probabilistic and practical impact assessment. However, this approach has not yet been implemented in Chesapeake Bay; previous studies were only based on sensitivity analyses to individual climate change factors or their combined effects (Wang et al., 2017; Irby et al., 2018). They cannot be directly used to make projections for estuarine hypoxia for the future climate. The natural climate variability and connections within the climate system (e.g., the relationship between temperature, precipitation/evapotranspiration, and river discharge change) were also missing in their studies. Therefore, this study utilizes multiple bias-corrected climate projections from high-resolution regional climate models to drive a coupled physical-biogeochemical model and assess the impacts of future climate change on Chesapeake Bay hypoxia. As a large eutrophic estuary with a long history of seasonal hypoxia, Chesapeake Bay is well suited as a representative study site, and the climate downscaling modeling approach developed here is applicable to other estuaries and coastal oceans.

4.2 Description of climate modeling framework and estuarine model

To project future changes in Chesapeake Bay hypoxia, we used a coupled physical-biogeochemical model that was shown to be skillful in hindcast simulations (Testa et al., 2014; Li et al., 2016), and forced it primarily with downscaled climate

projections from the North American Regional Climate Change Assessment Program (NARCCAP) (Mearns et al., 2007). NARCCAP uses a dynamic climate downscaling approach by embedding fine-resolution (about 50 km) regional climate models (RCMs) of North America into global climate models (GCMs) from the Coupled Model Intercomparison Project Phase 3 (CMIP3) (Figures 4.1a-4.1b, Table 4.1). Simulations are available for a historical period (1971-2000) and the mid-21st century (2041-2070) under the medium-high A2 greenhouse gas emissions scenario (Nakićenović et al., 2000). Although GCMs results from CMIP5 (Phase 5) are now available, some high-resolution RCMs outputs needed for driving the estuarine model are not yet available (Giorgi & Gutowski, 2015).

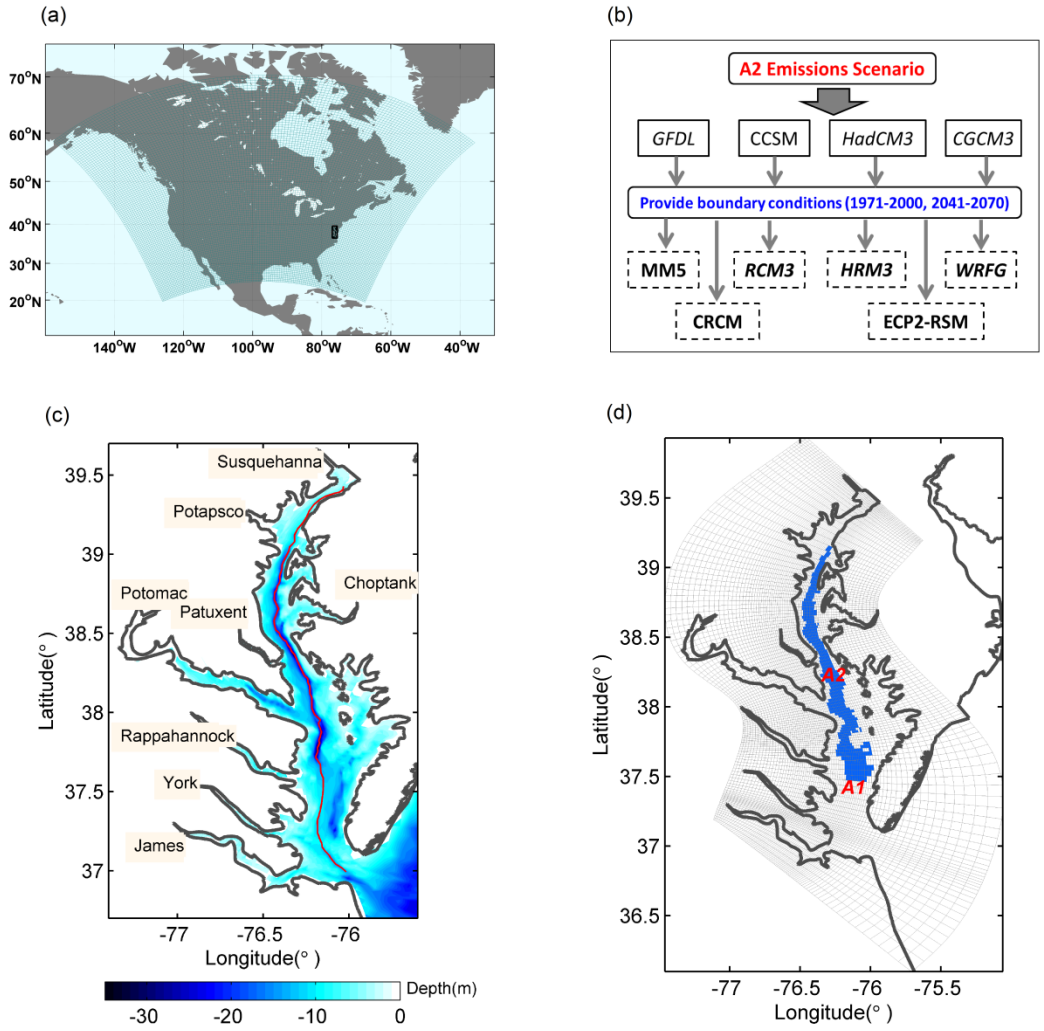

Figure 4.1 (a) NARCCAP Regional Climate Model domain in North America. The black box indicates the location of Chesapeake Bay. (b) NARCCAP modeling framework, including global climate models (in rectangles with solid line) and regional climate models (bold font, in rectangles with dashed line). The model names in italics indicate the model used in this study. The full model names and references are listed in Table 4.1. (c) Chesapeake Bay bathymetry. The solid red line marks the along-channel section used to plot the O_2 distributions in Figure 4.4. (d) The grid for the ROMS-RCA model. The blue area marks the control volume used in oxygen budget analysis in Figure 4.7 and Figure 4.11.

The Chesapeake Bay model consists of two sub-models. The physical model, based on the Regional Ocean Modeling System (ROMS, Shchepetkin & McWilliams, 2005; Haidvogel et al., 2008), has 82×122 grid points (~1 km resolution) in the

horizontal direction and 20 vertical layers with the maximum depth of 40 m in the deep channel (Figures 4.1c-4.1d, Li et al., 2005). ROMS is forced by daily river flows at eight major tributaries, by wind stress and heat fluxes at the sea surface, and by sea level and climatologies of temperature and salinity at the open boundary. At the offshore boundary, the sea level consists of tidal and non-tidal forcing (Egbert & Erofeeva, 2002; Li et al., 2005) (Table 4.2). RCM projections for meteorological variables are at 3-hourly intervals, and include surface air pressure, relative humidity and air temperature at 2 m above the surface, downwelling longwave radiation and net shortwave radiation at surface, wind speed at 10 m above the surface. These variables were used to calculate the air-sea fluxes of momentum and heat using the standard bulk formulae (Fairall et al., 2003). To correct the biases in the NARCCAP meteorological outputs, we applied the empirical quantile mapping method, using historical data from the North American Regional Reanalysis (NARR) as the observational reference (Gudmundsson et al., 2012; Wood et al., 2004; Mesinger et al., 2006). The cumulative distribution functions and quantile functions were constructed separately for each calendar season (December-February, March-May, June-August, September-November) for the historical period. For wind, the bias correction was only made on the wind speed magnitude due to larger uncertainty in the climate model projections for wind direction (Morrison et al., 2014) and the univariate nature of the quantile mapping method.

Table 4.1 RCMs and GCMs in NARCCAP (from Mearns et al., 2012).

	Abbr.	Full name	Reference
RCM	CRCM	Canadian Regional Climate Model	Caya and LaPrise 1999
	MM5	The Fifth generation Pennsylvania State University–National Center for Atmospheric Research (NCAR) Mesoscale Model	Grell et al. 1993
	HRM3	The Met Office Hadley Centre's regional climate model version 3	Jones et al. 2003
	RCM3	Regional Climate Model version 3	Giorgi et al. 1993a,b; Pal et al. 2000, 2007
	ECP2	Scripps Experimental Climate Prediction Center Regional Spectral Model	Juang et al. 1997
	WRFG	Weather Research and Forecasting model	Skamarock et al. 2005
GCM	CCSM3	NCAR Community Climate System Model, version 3	Collins et al. 2006
	CGCM3	Canadian Climate Centre Coupled General Circulation Model version 3	Scinocca and McFarlane 2004; Flato 2005
	HadCM3	The Met Office Hadley Centre's climate model version 3	Gordon et al. 2000; Pope et al. 2000
	GFDL	Geophysical Fluid Dynamics Laboratory Climate Model version 2.1	GFDL Global Atmospheric Model Development Team 2004

Table 4.2 Model forcing in the historical and future simulations

Boundary		Historical period (1989-1998)	Future period (2049-2058)
Atmosphere		NARCCAP regional climate model outputs with bias correction in 1989-1998	NARCCAP regional climate model outputs with bias correction in 2049-2058
Ocean	Sea level	Tide (TPXO7) + non-Tide (Duck) in 1989-1998	Based on historical sea level, add projected sea level change due to thermal expansion, regional dynamics, land glaciers and ice sheet and regional vertical movement
	Salinity	WOA monthly data with decadal average	Same as historical
	Temperature	WOA monthly data with decadal average	Based on historical, add monthly ocean water temperature change projected by GCMs of NARCCAP
	Nutrient	WOA monthly data with decadal average, reference values based on Filippino et al. (2011)	Same as historical
River	Discharge	USGS monitoring daily discharge in 1989-1998	Based on historical, multiply by the monthly scaling factor from NARCCAP model projection on runoff
	Temperature	CBP bi-weekly measurement in 1989-1998	Based on historical, add future temperature increases assuming at the same rate as Rice and Jastram (2015) for 1961-2010
	Nutrient	CBP bi-weekly measurement in 1989-1998	Same as historical

The biogeochemical model is based on the Row-Column Aesop (RCA) model, which consists of a water-column component (Isleib et al., 2007) and a sediment diagenesis component (Di Toro, 2001; Testa et al., 2013; Brady et al., 2013). RCA includes two phytoplankton groups, particulate and dissolved forms of organic carbon and nutrients (nitrogen, phosphorus and silicon), and O_2. The sediment model, which exchanges materials with the water column model, has one aerobic layer and one anaerobic layer, and simulates the cycling of carbon, O_2, nitrogen, phosphorus and sulfur. The RCA model for Chesapeake Bay is described in detail in Testa et al. (2014). To simulate the historical period as a baseline to make future projections, the river inputs of phytoplankton, particulate and dissolved organic carbon, and organic and inorganic nutrients were obtained from Chesapeake Bay Program bi-weekly monitoring data at eight major tributaries (https://www.chesapeakebay.net/what/data). The ocean boundary inputs were acquired from the World Ocean Atlas (WOA) 2013 and Filippino et al. (2011) (Table 4.2). Atmospheric deposition was not considered in this study.

To simulate the mid-21st century, GCM projections for the Northwest Atlantic Ocean were used to prescribe changes in the offshore boundary condition for ROMS-RCA. The relative sea level rise was set to be the sum of the CMIP3 sea level projection for the region (Slangen, et al., 2012; Mitrovica et al., 2009; Mitrovica et al., 2011) and the local sea level rise due to land subsidence (Zervas, 2009; Miller et al., 2013), following Boesch et al. (2013) and Lee et al. (2017) (Table 4.2). To set the temperature condition, we calculated the difference of monthly mean water temperature between

1971-2000 and 2041-2070 from the GCM outputs and added this difference to the historical climatology (Table 4.2). The GCM resolution mostly ranges from 1° to 2° in latitude and 2° to 4° in longitude which is too coarse to fully resolve nearshore physical and biological processes (Chapman & Beardsley, 1989; Fennel et al., 2006). One process is the northward shift of the Gulf Stream which may influence the hydrography and biogeochemistry of Chesapeake Bay (Saba et al., 2016). In this study the salinity and nutrient concentrations were assumed to remain the same at the offshore boundary (Table 4.2).

RCMs in NARCCAP include basic land-surface schemes that interact with the atmosphere to generate surface runoff (Milly and Dunne, 2011), but they do not include hydrological models or river routing models that can simulate streamflow. Here we assumed that future changes in river discharge Q can be approximated by changes in the integrated runoff R over the watershed (Table 4.2). Climate-induced changes in riverine nutrient and organic matter loading were assumed to be caused by changes in the river flows only. Potential impacts of nutrient management strategies (Linker et al., 2013) and climate-induced changes in watershed denitrification (Howarth et al., 2006; Schaefer et al., 2007) were not considered.

4.3 Climate downscaling projections and numerical experiment

There is a total of 12 RCM-GCM combinations in NARCCAP (Table 4.1, Mearns et al., 2012, 2013). Six of these combinations have a complete data set available over Chesapeake Bay and its watershed. The projected changes in surface air temperature over Chesapeake Bay and the winter-spring Susquehanna River flow

between the late 20th and mid-21st century are shown in Figure 4.2. All six models predict substantial increases in the annual mean air temperature, with the ensemble mean of about 1.68 °C and a range from 1.35 to 1.95 °C (Figure 4.2a). The January-May Susquehanna River flow shows increases in five models, ranging from a low of 92 $m^3 s^{-1}$ in RCM3_gfdl to a high of 600 $m^3 s^{-1}$ in ECP2_gfdl (Figure 4.2a). Figures 4.2b and 4.2c show the projected changes in monthly mean surface air temperature and monthly mean Susquehanna River flow among the models. There are substantial seasonal variations in the changes of temperature and river flow between the late 20th and mid-21st century. Warming in air during the summer is greatest and has smaller inter-model differences than other seasons (Figure 4.2b). The river flow is projected to increase up to 40% during the winter months (December-February) (Figure 4.2c). The spring flow is also projected to increase but there are large uncertainties among the models. Most models predict a moderate decrease in river flow in summer, with a 5-10% decline in the model ensemble mean.

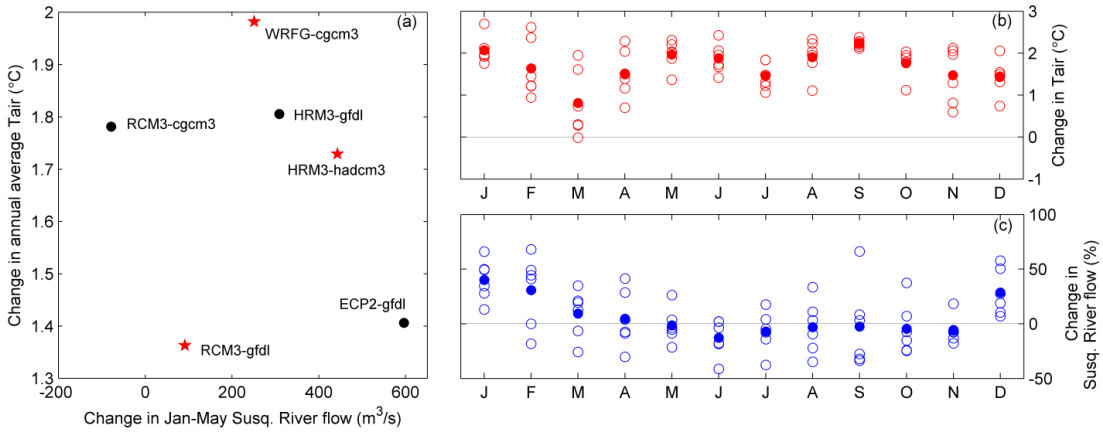

Figure 4.2 (a) Projected change in the annual mean air temperature (at 2 m above the surface) over Chesapeake Bay versus projected change in Jan-May average Susquehanna River discharge between the late 20th and mid-21st century, obtained from six GCM-RCM models in the NARCCAP ensemble. GCMs are labeled with lowercase letters and RCMs are labeled with capital letters. The full model names and references

are listed in Table 4.1. The red stars mark three GCM-RCMs used for the hypoxia projections. Scatter plots of projected changes in monthly mean air temperature (b) and monthly mean Susquehanna River flow (c). In (b) and (c), open circles indicate the value of each model in (a); solid circles indicate the ensemble mean.

For the climate downscaling projections for Chesapeake Bay hypoxia, we selected RCM3_gfdl, HRM3_hadcm3 and WRFG_cgcm3 which capture the spreads among the NARCCAP ensemble members (Figure 4.2a). RCM3_gfdl is the Regional Climate Model version 3 (RCM3, Pal et al., 2007) driven by the Geophysical Fluid Dynamics Laboratory model (GFDL, Delworth et al., 2006), projecting relatively low temperature and streamflow changes. HRM3_hadcm3 is the Hadley Regional Climate Model (HRM3, Jones et al., 2003) driven by the Hadley Centre Coupled Model version 3 (HadCM3, Gordon et al., 2000), projecting moderate temperature increase but large streamflow increase. WRFG_cgcm3 is the Weather Research and Forecasting Grell model (WRFG; Skamarock et al., 2005) driven by the Third Generation Coupled Global Climate Model (CGCM3; Flato, 2005), projecting large temperature increase but moderate streamflow increase. Figure 4.3 shows the projected monthly changes in air temperature and the Susquehanna River flow from the three RCMs. WRFG_cgcm3 projects large temperature increases (about 1.9 ^{o}C) with weak seasonal variations. It also predicts the river flow to increase in winter and spring, decrease slightly in summer and increase substantially in the fall. RCM3_gfdl predicts smaller warming (about 1.4 ^{o}C) with strong seasonal variations. It also projects an increase in the winter river discharge but mostly decreases in other seasons. HRM3_hadcm3 predicts moderate increases in temperature (about 1.7 ^{o}C) but with strong seasonal variations, and large increases in winter river flows but small changes of either sign during other seasons.

These three GCM-RCM combinations are not only representative of the ensemble mean projection but also capture the spreads within the NACCARP ensemble.

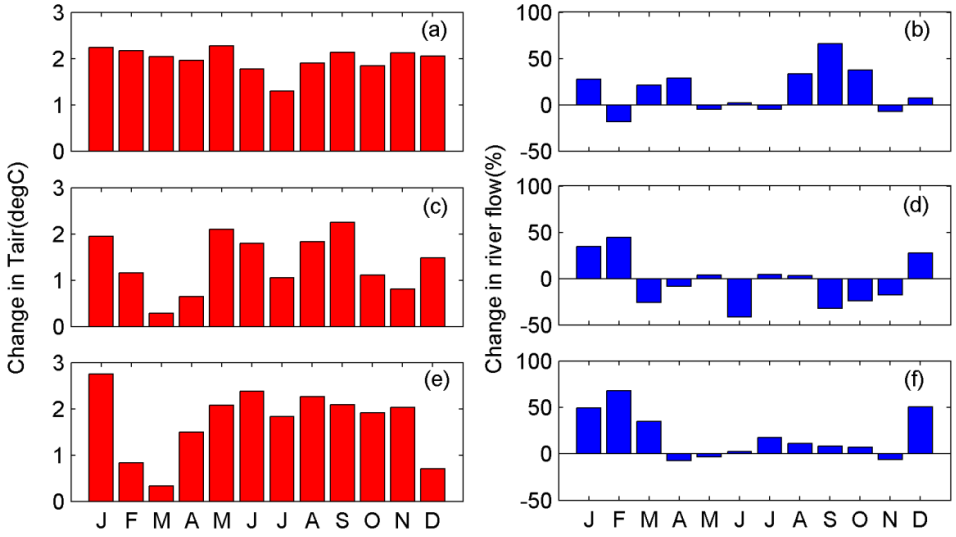

Figure 4.3 Projected changes in surface air temperature over Chesapeake Bay (left column) and Susquehanna River discharge (right column) between the late 20th century and mid-21st century, obtained from WRFG_cgcm3 (a, b), RCM3_gfdl (c, d) and HRM3_hadcm3 (e, f).

Hypoxia in Chesapeake Bay experienced dramatic expansion due to eutrophication between 1950 and the 1980s, but has stabilized since the mid-1990s (Hagy et al., 2004). We chose ten years (1989-1998) in the late 20th century within the NARCCAP historical period to conduct ROMS-RCA reference simulations. ROMS-RCA future simulations were conducted for ten years (2049-2058) in the mid-21st century. The ROMS hydrodynamic model was spun up for two years to reach a quasi-steady state, and then run continuously for the late 20th century (1989-1998) and mid-21st century (2049-2058) simulations, respectively. The initial condition of the RCA biogeochemical model was based on Chesapeake Bay Program monitoring data for the historical period but adjusted to include the effects of warming on decreasing oxygen solubility in the mid-21st century. Specifically, oxygen saturation concentration is

calculated using temperature and salinity from the historical and future ROMS model runs. Adding the difference in the oxygen saturation concentration to the initial O_2 condition in the historical RCA run then sets the initial condition for the future RCA run.

4.4 Simulated O_2 change

To show O_2 changes between the late 20th and mid-21st century, we calculated the climatological mean (10-year average) O_2 concentration for the summer months (June-August) and plotted its distribution along the center deep channel (its location marked in Figure 4.1c). For comparison, observed O_2 at a number of monitoring stations managed by Chesapeake Bay Program (https://www.chesapeakebay.net) were interpolated onto the model grids along the deep channel of the estuary (Figure 4.4, obs). ROMS-RCA produced realistic simulations of the observed O_2 distribution in 1989-1998: the hypoxic water occupies the deep channel in the mid-Bay (Figures 4.4a, 4.4d, 4.4g). The Taylor diagram (Taylor, 2001) provides a quantitative evaluation of the model's skill in predicting the time series of the surface and bottom O_2 at a mid-Bay monitoring station (CB 4.3C) as well the time series of the hypoxic ($O_2 < 2$ mg L^{-1}) and anoxic ($O_2 < 0.2$ mg L^{-1}) volumes in the Bay (Figure 4.5). These thresholds of hypoxia and anoxia are chosen according to hypoxia-related ecological effects (Hagy et al., 2004). The correlation coefficient varies from 0.90 to 0.95, indicating that ROMS-RCA accurately captures the phase information in the O_2 time series. The normalized standard derivation straddles around 1, indicating that the model does a good job in reproducing the amplitude of variations in the observed time series. The model's performance is nearly as good as a hindcast simulation of 1989-1998 forced

by the reanalysis product NARR and shows an improved skill when compared with previous modeling efforts (e.g. Irby et al., 2016).

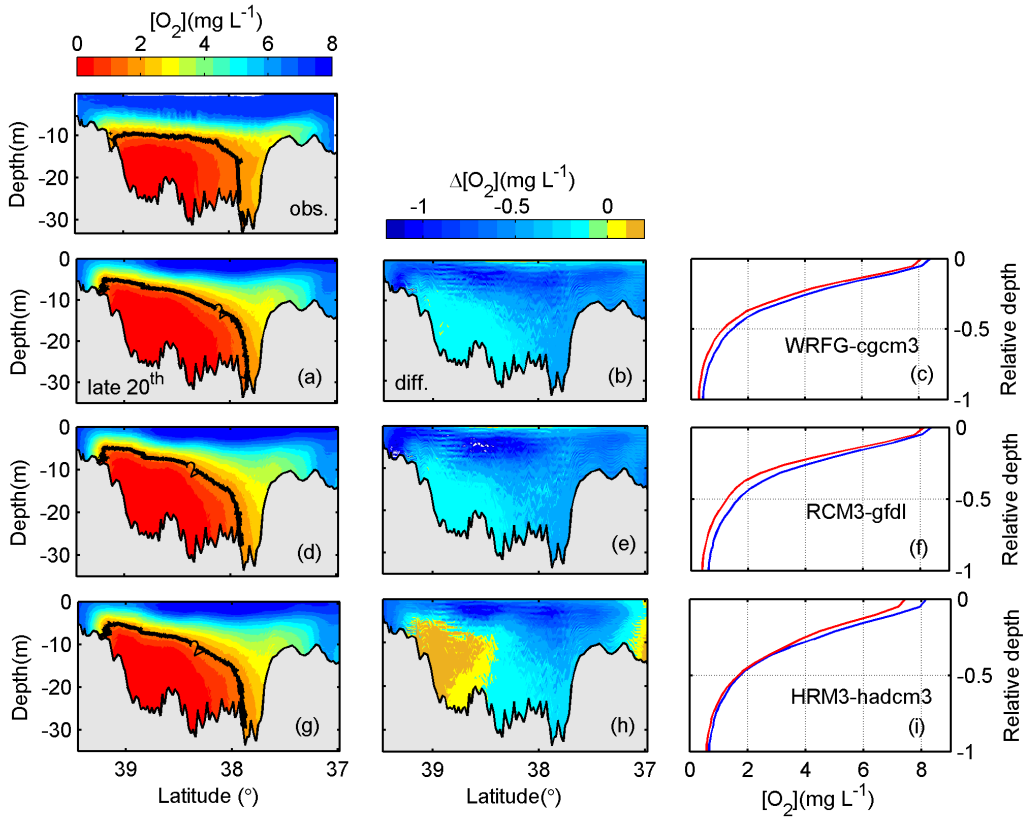

Figure 4.4 Observed (top panel) and (a, d, g) simulated climatological mean distribution of the summer O_2 concentration along the center deep channel of Chesapeake Bay in the late 20th century. The thick black line is the O_2=2 mg L^{-1} contour which defines the threshold oxygen concentration for hypoxia. (b, e, h) O_2 changes between the late 20th and mid-21st century. (c, f, i) Vertical profiles of the mean oxygen concentration of the deep water region (>20m) of Chesapeake Bay in the late 20th century (blue) and the mid-21st century (red) plotted versus the relative depth, which is defined as the depth of a layer divided by the total water depth. The RCMs are WRFG_cgcm3 (a-c), RCM3_gfdl (d-f) and HRM3_hadcm3 (g-i).

By 2049-2058, O_2 declines nearly everywhere (Figures 4.4b, 4.4e, 4.4h). The largest reduction appears in the subsurface water and in the lower bay. O_2 concentration shows a small reduction in the northern part of the hypoxic zone (between 38.6 and 39.1^{o}N) in the model runs forced by WRFG_cgcm3 and RCM3_gfdl, and even a slight

increase in the model runs forced by HRM3_hadcm3. To better quantify the O_2 changes, we plotted the vertical profiles of O_2 concentration in the deep channel (>20 m) (Figures 4.4c, 4.4f, 4.4i). O_2 concentration shifts lower at all depths, with smaller decreases in the deep water.

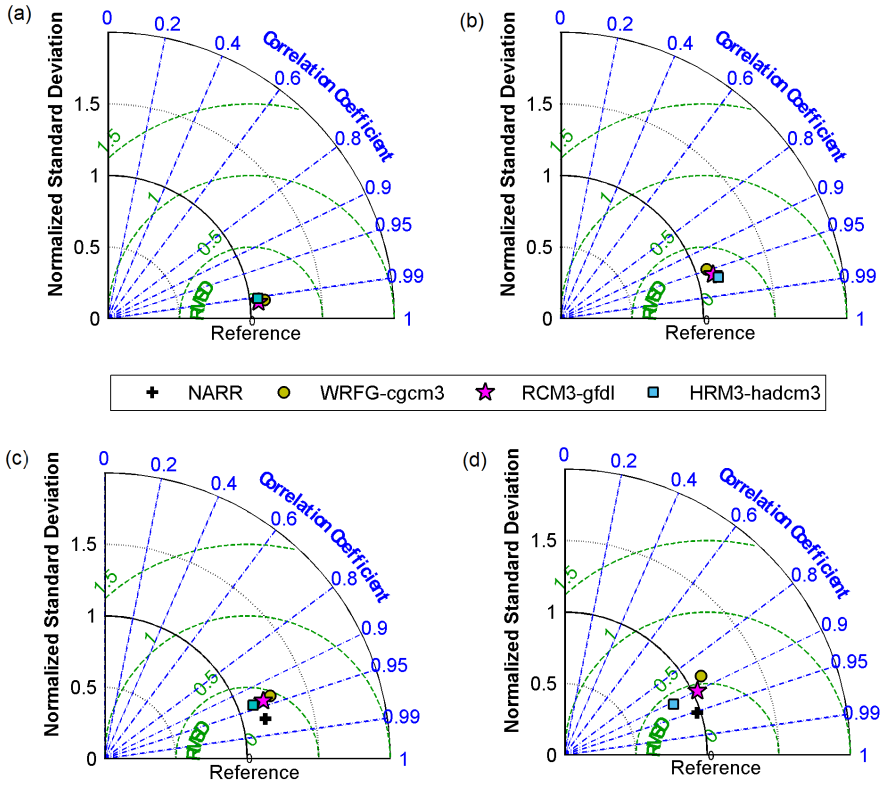

Figure 4.5 Taylor diagram for the time series for the bottom (a) and surface (b) O_2 concentration at CB4.3C (38.56°N, -76.43°W), and the hypoxic (c) and anoxic (d) volume. ROMS-RCA is forced by NARR, and RCMs (WRFG_cgcm3, RCM3_gfdl, HRM3_hadcm3). Both the model fields and observation were interpolated to 1st and 15th of each calendar month.

Compared to the late 20th century, the hypoxic area in the mid-21st century expands seaward and upward (Figures 4.6a, 4.6d, 4.6g). This leads to large increases in the hypoxic ($O_2 \leq 2$ mg L^{-1}) and anoxic ($O_2 \leq 0.2$ mg L^{-1}) volumes (Figures 4.6b, 4.6e, 4.6h and Figures 4.6c, 4.6f, 4.6i). These volumes were averaged over 1989-1998 and 2049-2058, respectively. For comparison, we also plotted the averaged observed

hypoxic and anoxic volumes for 1989-1998. ROMS-RCA captured the observed seasonal variations of the hypoxic and anoxic volumes, although the model run forced by HRM3_hadcm3 underestimated the anoxic volume (Figure 4.6i). Despite inter-model differences, all the three model runs project substantial increases in the hypoxic and anoxic volumes in the future climate (Figure 4.6 and Table 4.3). WRFG_cgcm3 and RCM3_gfdl predict larger increases (20-30%), while HRM3_hadcm3 predicts smaller increases (~10%). The expansion of the hypoxic and anoxic volumes is significantly larger in early to mid-summer (June-July) than in late summer (August and September). Another major change from the late 20th to the mid-21st century is the earlier initiation of hypoxia, from several days to nearly two weeks. RCM3_gfdl and HRM3_hadcm3 also project an earlier termination of hypoxia and a shorter hypoxia duration (Table 4.3).

Table 4.3 Model projections for the seasonal averaged water temperature, winter-spring Susquehanna River flow (averaged over January-May), relative sea level rise (RSLR), annual cumulative and averaged summer (June-August) hypoxic volume (HV) and anoxic volume (AV), the duration (days), initiation and termination days of hypoxia (day of year, threshold is set at 0.5 km^3) in the main stem of Chesapeake Bay for the late 20^{th} and mid-21^{st} century.

		WRFG_cgcm3			**RCM3_gfdl**			**HRM3_hadcm3**		
		late20^{th}	mid21^{st}	change	late20^{th}	mid21^{st}	change	late20^{th}	mid21^{st}	change
Water temperature (°C)	winter	6.3(±0.7)	8.3(±0.4)	2.0	6.1(±0.7)	7.6(±0.5)	1.5	6.1(±0.8)	7.5(±0.8)	1.4
	spring	11.9(±0.4)	13.6(±0.7)	1.7	11.3(±0.9)	12.2(±0.7)	0.9	12.2(±0.8)	12.9(±1..0)	0.7
	summer	24.8(±0.3)	26.2(±0.4)	1.4	24.1(±0.5)	25.6(±0.4)	1.5	25.1(±0.6)	26.5(±0.5)	1.4
	fall	19.4(±0.5)	21.2(±0.6)	1.8	18.5(±0.4)	20.1(±0.5)	1.6	19.4(±0.5)	21.1(±0.4)	1.7
River flow (m^3/s)	Jan-May	1794	2045	251(14%)	1794	1886	92(5%)	1794	2237	443(25%)
RSLR(m)		-	-	0.45	-	-	0.43	-	-	0.31
HV	Average (km^3)	8.5(±1.3)	10.5(±1.0)	2.0(24%)	8.1(±1.3)	10.0(±1.4)	1.9(23%)	7.6(±1.3)	8.3(±1.6)	0.7(9%)
AV		2.7(±0.8)	3.4(±0.6)	0.6(23%)	2.6(±0.7)	3.4(±0.8)	0.8(29%)	2.1(±0.7)	2.2(±0.8)	0.4(2%)
HV	Cumulative (km^3 day)	943(±161)	1231(±179)	288(31%)	883(±150)	1092(±196)	209(24%)	857(±123)	936(±181)	79(9%)
AV		273(±76)	344(±70)	71(26%)	255(±75)	330(±87)	75(29%)	209(±59)	213(±77)	4(2%)
Onset	day of year	132(±9)	120(±10)	-12	132(±11)	131(±10)	-1	129(±5)	126(±7)	-3
End		273(±9)	274(±11)	+1	271(±9)	267(±9)	-4	270(±8)	265(±10)	-5
Duration		141(±11)	154(±11)	+13	139(±14)	136(±13)	-3	141(±8)	139(±12)	-2

Note: The numbers in the parentheses indicate one standard deviation. The percentage numbers in the bracket are noted as relative

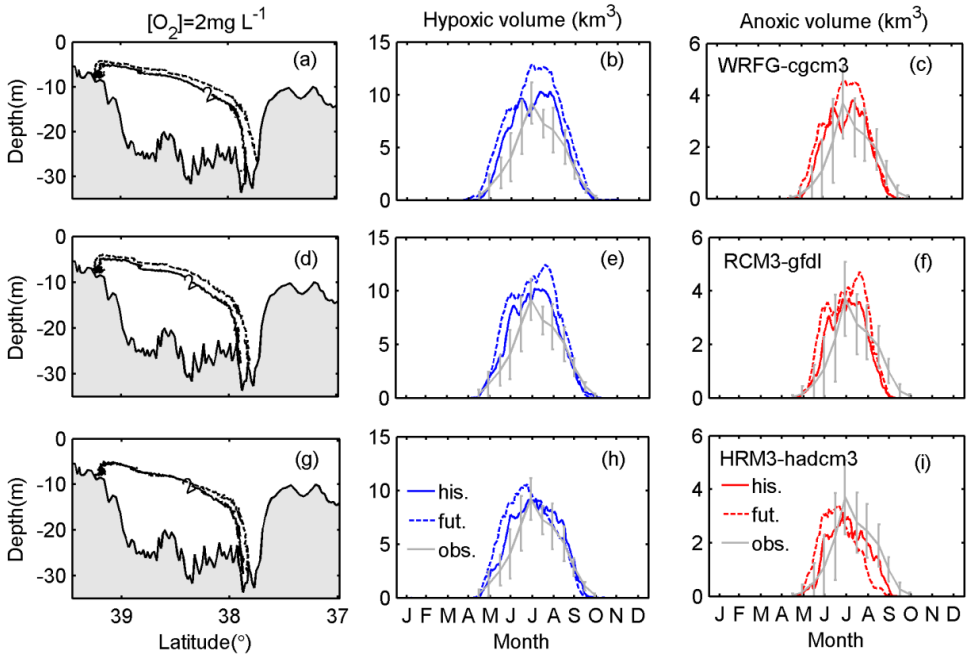

Figure 4.6 (a, d, g) Climatological mean position of the O_2=2 mg L^{-1} isoline in the along-channel section during the late 20th century (solid line) and mid-21st century (dashed line). Time series of the projected climatological mean hypoxic (second column) and anoxic (third column) volumes in Chesapeake Bay during the late 20th century (solid lines) and mid-21st century (dashed lines), projected by WRFG_cgcm3 (a-c), RCM3_gfdl (d-f) and HRM3_hadcm3 (g-i). The grey line indicates the mean and one standard deviation of the observed hypoxic and anoxic volume during the late 20th century.

4.5 Causes of oxygen decline

To determine the cause(s) for the O_2 decline, a diagnostic analysis was conducted of the O_2 budget in a fixed control volume V for the bottom water. V was selected to encompass all the waters below 10 m depth in the main stem of Chesapeake Bay, ranging between the Rappahannock River in the south and the Patapsco River in the north (Figure 4.1d). The O_2 budget over the control volume is derived from the full conservation equation given by

$$\frac{\partial O_2}{\partial t} = -u\frac{\partial O_2}{\partial x} - v\frac{\partial O_2}{\partial y} - w\frac{\partial O_2}{\partial z} + \frac{\partial}{\partial x}\left(K_H \frac{\partial O_2}{\partial x}\right) + \frac{\partial}{\partial y}\left(K_H \frac{\partial O_2}{\partial y}\right) + \frac{\partial}{\partial z}\left(K_V \frac{\partial O_2}{\partial z}\right) + WCR + SOD + F_{air-sea} + P_{phyto} \quad (4.1)$$

where *x, y* and *z* stand for the longitudinal (along-channel, namely, the major axis of the depth-averaged tidal flows), lateral (cross-channel) and vertical directions, respectively [see Xie et al. (2017) for a more detailed definition]; *u, v* and *w* represent the velocity components in these directions; K_H and K_V are the horizontal and vertical diffusivities respectively; *WCR* is the water-column O_2 uptake and includes algal respiration, organic matter oxidation, nitrification and oxidation of sulfide/methane; SOD is the sediment oxygen demand; $F_{air\text{-}sea}$ is O_2 flux across the air-sea interface; and P_{phyto} is O_2 produced by phytoplankton in the euphotic layer.

Integrating Eq. (4.1) over control volume *V* for the bottom water yields

$$\frac{\partial M_{O_2}}{\partial t} = \overbrace{\iint_{A1}(-uO_2)dydz}^{F_{\text{hadv}}} + \overbrace{\iint_{A1}\left(K_H \frac{\partial O_2}{\partial x}\right)dydz}^{F_{\text{hdiff}}} + \iint(-vO_2)dxdz + \iint\left(K_H \frac{\partial O_2}{\partial y}\right)dxdz + \overbrace{\iint_{A2}(-wO_2)dxdy}^{F_{\text{vadv}}} + \overbrace{\iint_{A2}\left(K_V \frac{\partial O_2}{\partial z}\right)dxdy}^{F_{\text{vdiff}}} + \iiint_V (WCR)dxdydz + \iint_{A3}(SOD)dxdy \quad (4.2)$$

where M_{O2} is the total O_2 content (unit=kg) in *V* (Li et al., 2015). F_{hadv} and F_{hdiff} represent the horizontal advective and diffusive influxes of O_2 into the cross-channel section (*A1*) in the lower-Bay. Since *V* intersects the bottom of the shallow upper Bay as well as the lateral boundary of the deep channel, the landward outflux and lateral fluxes are zero there (3th and 4th term in Eq.(4.2)). F_{vadv} and F_{vdiff} represent the vertical advective and diffusive fluxes across the upper boundary (*A2*) of *V*. *WCR* and *SOD* are integrated over *V* and the water-sediment interface (*A3*) separately. Since the euphotic-layer depth in the estuary is typically shallower than the 10 m depth, O_2 production due

to phytoplankton is very small in the bottom water and hence neglected in Eq. (4.2) (see also Li et al., 2015; 2016). As shown by Li et al. (2016), M_{O2} in the control volume is highly negatively correlated with the hypoxic volume. Therefore, an analysis of the O_2 budget can tell us about the physical and biogeochemical processes driving the changes in the hypoxic and anoxic volumes.

Figure 4.7 shows the time series of monthly averaged F_{hadv}, F_{hdiff}, F_{vadv}, F_{vdiff}, *WCR* and *SOD* for the two decades 1989-1998 and 2049-2058, obtained from the ROMS-RCA model run forced by WRFG_cgcm3. Over one year, three physical processes dominate the supply of O_2 to the bottom hypoxic water: the vertical diffusive F_{vdiff} and advective F_{vadv} fluxes supply O_2 to the bottom water while the horizontal advective flux F_{hadv} imports high-O_2 water in the lower Bay to the mid-Bay hypoxic region. Two biological terms *WCR* and *SOD* consume O_2, with *WCR* as the dominant consumption term. Between the late 20$^{\text{th}}$ and mid-21$^{\text{st}}$ century, F_{vdiff}, F_{vadv} and *WCR* display the largest changes. During the summer, F_{vadv} decreases by 10% and F_{vdiff} decreases by 18%, indicating that the vertical O_2 supply is reduced. F_{hadv} and F_{hdiff} have moderate reductions. On the other hand, *WCR* is substantially smaller in the future climate while *SOD* shows a small reduction. Therefore, both the physical O_2 supply and biological consumption decrease with climate change. During the winter and early spring when biological production is weak, however, *WCR* and *SOD* show slight increases. The sum of the budget terms on the right-hand side of Eq. (4.2) for both simulation periods (1989-1998 and 2049-2058) is nearly the same as the rate of change

in the O_2 content in the control volume, confirming that the numerical calculations of these budget terms are accurate.

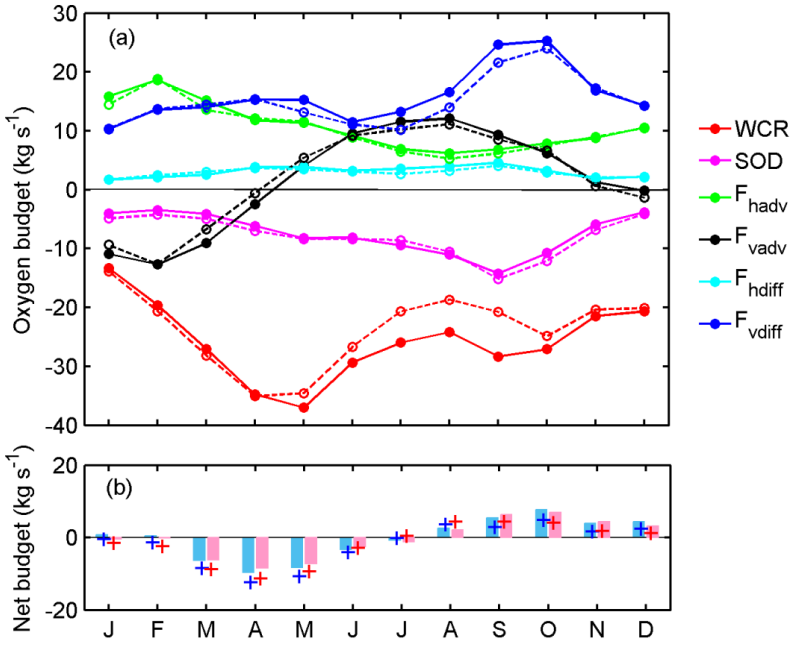

Figure 4.7 (a) Time series of the oxygen budget terms in the control volume during the late 20th century (solid lines with circles) and mid-21st century (dashed lines with circles), as projected by WRFG_cgcm3. (b) Time series of the sum of oxygen budget terms for the late 20th century (blue cross) and mid-21st century (red cross), compared with oxygen content change rate for the late 20th century (blue bar) and mid-21st century (red bar) in the control volume.

The vertical advective and diffusive fluxes of O_2 are regulated by the strength of the vertical stratification (Scully, 2010; Li et al., 2015). With sea level rise and higher winter-spring river flow in the future climate (Figure 4.3 and Table 4.3), stratification in the estuary becomes stronger (Figure 4.8). The surface salinity increases by 0.5-1 psu and the bottom salinity is 1-2 psu higher during summer (Figures 4.8a, 4.8b). In the along-channel section, saline bottom water penetrates further into the estuary while the brackish surface water spreads seaward in the lower bay (Figure 4.8d). The Brunt–Väisälä frequency (N^2) averaged over the estuary increases by 2.6×10^{-4} s^{-2}, with larger

stratification increases on the shallow shoals than in the deep channel (Figure 4.8c, Figure 4.9a). The stronger stratification suppresses turbulent mixing, resulting in weaker diffusive supply of O_2 to the bottom water in the future climate and the expansion of hypoxic region (Figure 4.9c).

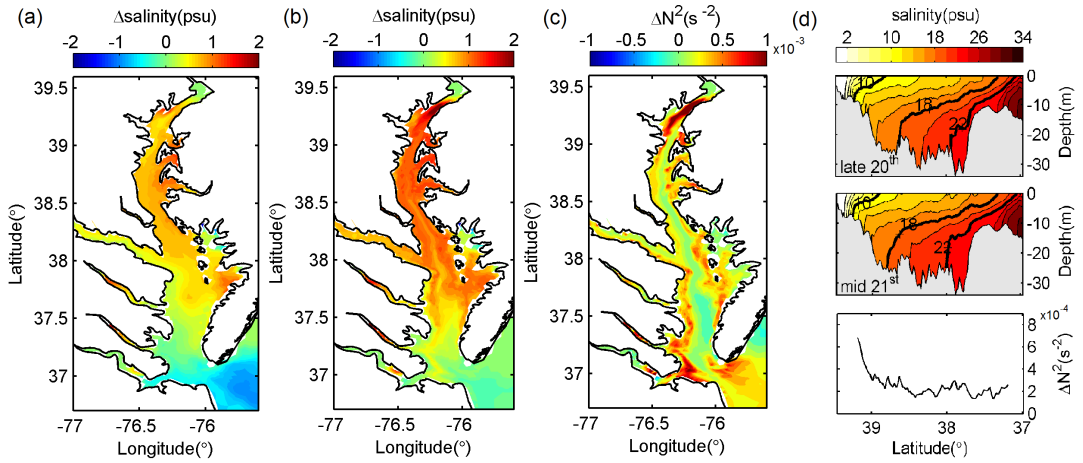

Figure 4.8 Changes in the summer averaged (a) surface salinity, (b) bottom salinity and (c) vertically averaged buoyancy frequency N^2 between the late 20th century and mid-21st century, as projected in the model simulation forced by WRFG_cgcm3. (d) The summer-averaged along-channel salinity distribution in the late 20th century (upper panel) and mid-21st century (middle panel), and changes in the vertically averaged summer stratification N^2 (lower panel) between the two periods.

It should be pointed out that the physical O_2 supply terms not only depend on the physical fields such as velocities and diffusivity but also depend on the O_2 concentration itself (see Eq. (4.2)). Part of the changes in F_{vdiff} and F_{vadv} could be related to the lower O_2 in the future climate. The reduction in the vertical diffusive flux F_{vdiff} is larger during summer (Figure 4.7), and is partly caused by the large O_2 decline in the surface layer and the associated weakening of the vertical O_2 gradient in the pycnocline (Figures 4.4b, 4.4e, 4.4h). The horizontal advective flux F_{hadv} also decreases in the future climate. The estuarine circulation is moderately stronger in the

future climate, in agreement with Hong and Shen (2012). However, the seaward expansion of the hypoxic region and O_2 reduction in the lower Bay, as shown in Figures 4.4b, 4.4e, and 4.4h, lowers the O_2 concentration in the incoming water, such that F_{hadv} (a product of u and O_2) is reduced in the future climate.

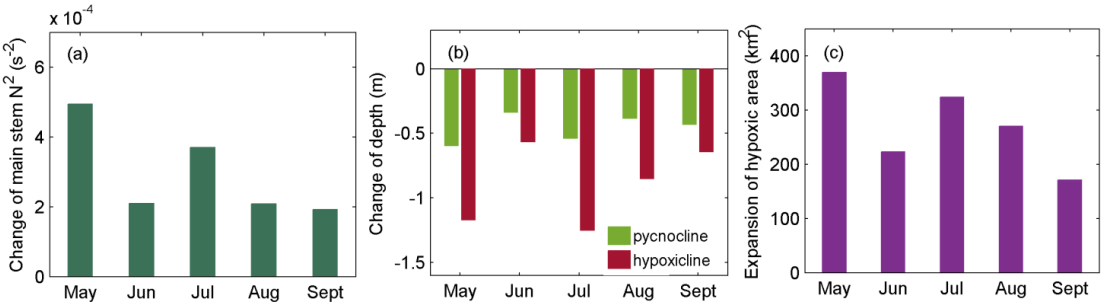

Figure 4.9 (a) Monthly averaged changes in buoyancy frequency N^2 over Chesapeake Bay from May to September. (b) Changes in the depth of pycnocline and hypoxic-line (isoline of O_2=2mg L^{-1}) from May to September. (c) Increases in the hypoxic area from May to September, as projected in the model run forced by WRFG_cgcm3.

Sea level rise may also contribute to worsening hypoxia in the future climate by increasing the volume of Chesapeake Bay and creating more space to develop hypoxia. To examine this, monthly averaged changes in the pycnocline depth and hypoxic-line depth (isoline of O_2=2mg L^{-1}) were calculated over the hypoxic region from May to September (Figure 4.9b). The pycnocline depth will be 0.3-0.6 m shallower, and hypoxic-line depth will be 1.25 m shallower, according to the model simulation forced by WRFG_cgcm3. Clearly the hypoxic water is able to fill in the extra volume created by sea level rise. Furthermore, the greater shoaling of the hypoxic-line relative to the pycnocline suggests that other processes such as *WCR* also contribute to the upward expansion of hypoxic water.

The water column respiration shows large decreases during the summer and small increases earlier in the year (Figure 4.7). *WCR* depends on the organic matter produced during the spring bloom. The winter-spring phytoplankton bloom terminates earlier (Figure 4.10a), and the total particulate organic carbon in the water column accumulates slightly faster during the spring (Figure 4.10b). Also, the temperature-dependent oxidation rate of organic matter in the water column and sediment is higher early in the year, resulting in an earlier onset of hypoxia. On the other hand, the summer phytoplankton biomass increases in early summer (May and June) but decreases in late summer and early fall (July to September) (Figure 4.10a). With the projected warming from WRFG_cgcm3, the summer water temperature will reach 26.5 °C, exceeding the optimal growth temperature (25 °C) for the summer phytoplankton species and suppressing their production. Less organic matter is produced for the export to deeper waters (Figure 4.10b), resulting in a large reduction in the summer *WCR* (Figure 4.7). These biogeochemical changes account for the earlier hypoxia onset and more rapid disintegration of hypoxia and anoxia seen in Figure 4.6.

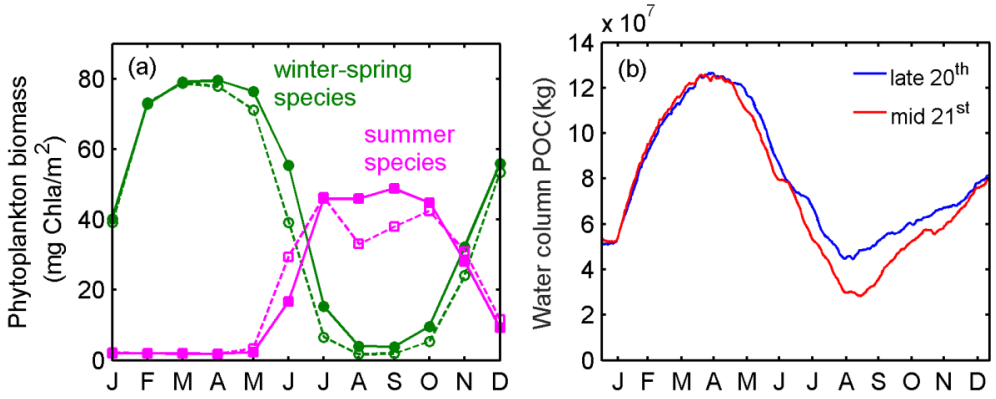

Figure 4.10 (a) Monthly averaged phytoplankton biomass in the euphotic layer during the late 20th century (solid lines) and mid-21st century (dashed lines) for the winter-spring species (green) and summer species (pink) as projected by WRFG_cgcm3. (b) Daily averaged total particulate organic carbon (POC) in the whole water column during the late 20th century (blue) and mid-21st century (red).

In addition to the physical and biological factors discussed above, decreasing O_2 solubility could contribute to the expansion of hypoxia in the future climate. The solubility effect varies seasonally: larger O_2 reductions in winter and fall and smaller reductions in summer (Figure 4.11a). Over a year, the oxygen content change due to decreasing solubility accounts for about one half of the total reduction in the bottom-water oxygen content between late 20th century and mid-21st century (Figure 4.11b). Warming not only affects solubility but also biological consumption. We conducted an additional model run for the mid-21st century that simulates the full effects of temperature increase in the RCA biogeochemical model while keeping the same hydrodynamic field as that in the late 20th century. The O_2 difference between this hypothetical model run and the historical simulation thus represents the combined effects of solubility and biological consumption due to the temperature increase between late 20th century and mid-21st century (compare the blue and black dashed lines in Figure 4.11a). During the spring, O_2 loss due to higher biological consumption is comparable to that due to the reduced solubility. During the summer and early fall, however, the biological consumption decreases and offsets the O_2 loss due to solubility, resulting in a net O_2 gain (Figure 4.11b).

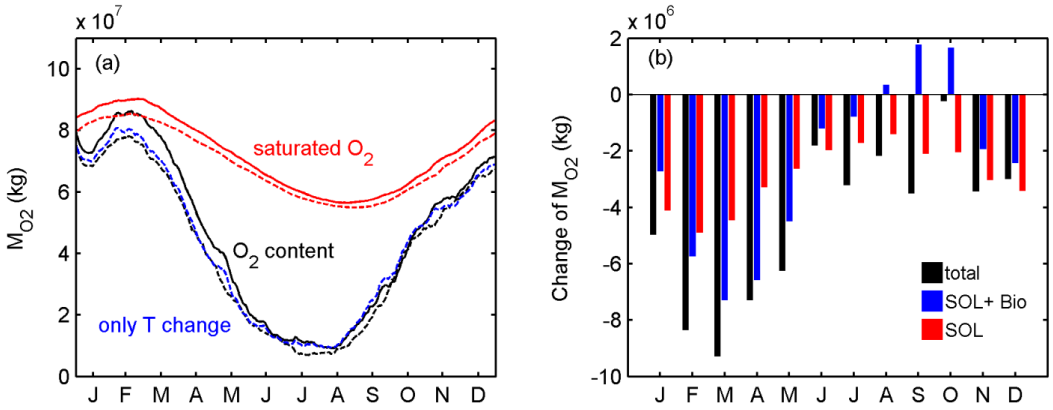

Figure 4.11 (a) The total oxygen content in the control volume (black) and hypothetical changes in the oxygen content due to solubility change (red) at the late 20th century (solid lines) and mid-21st century (dashed lines), as projected by WRFG_cgcm3. The blue line is the oxygen content calculated from a model run of the mid-21st century in which the full effects of temperature are simulated in RCA but the hydrodynamic field is kept the same as that in the historical simulation period. (b) Changes in the oxygen content of the control volume (black bar), changes due to solubility (red bar) and changes due to the combined effects of solubility and biological consumption (blue bar) between the late 20th century and mid-21st century.

Given that both the physical supply and biological consumption decrease with climate change, why is the hypoxia more severe in the future climate? An examination of the overall balance among the various terms in the budget gives us some insights. Eq. (4.2) was integrated over the entire year or over the summer (June-August) to produce the time-integrated budget terms (Figures 4.12a, 4.12c). All the physical supply terms decline in the future climate. The vertical diffusive flux experiences the largest reduction. Either the vertical advective flux or the horizontal advective flux has the second largest reduction, depending on whether the budget is integrated over the summer or the entire year. The two biological consumption terms also decrease in the future climate, with *WCR* being the bigger contributor. Despite the compensative changes in the physical supply and biological consumption, the O_2 content is lower in the mid-21st century than in the late 20th century (Figure 4.12b), consistent with the

projected increases in the hypoxic and anoxic volumes (Figure 4.6). Next we compare the total change in the bottom-water O_2 content with that due to solubility change. The solubility-induced change is equivalent to 69% of the total content change during the summer, but is larger when integrated over a year, presumably because of the large *WCR* reduction in late summer and fall. It should be pointed out that individual terms in the O_2 budget are ~1-2 orders larger than the net O_2 content change (term on the left hand of Eq.(4.2)) and the O_2 content loss due to solubility (compare Figures 4.12a and 4.12b). It also should be noted that the numerical evaluations of the O_2 budget terms contain a small (7%) error but it is considerably smaller than the changes of the individual terms (see Figure 4.7b).

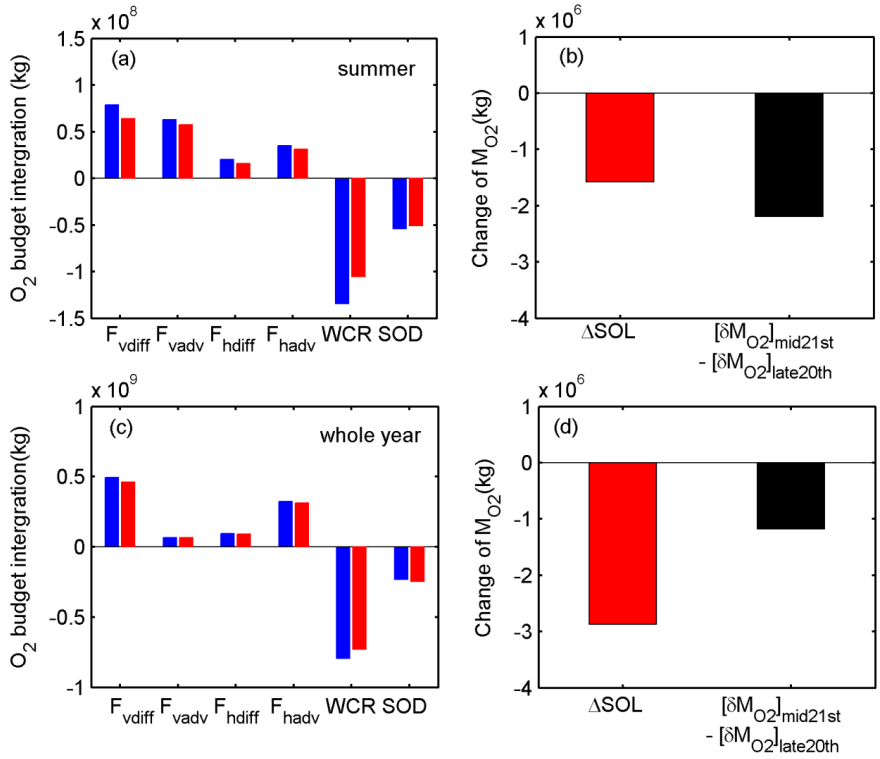

Figure 4.12 Integrated oxygen budget terms over the summer (a) and whole year (c) in the late 20th century (blue bars) and mid-21st century (red bars). The net change of oxygen content in the control volume (black bars) and the change of oxygen content due to solubility change (red bars) over summer (b) and whole year (d) between the late 20th century and mid-21st century.

4.6 Discussion and conclusion

In the open ocean, climate change brings about stronger upper-ocean stratification, reduced solubility and increased microbial respiration, all pointing to increasing deoxygenation in the future climate. Moreover, decreasing solubility was found to be the dominant driver for the O_2 decline in the upper open ocean (Schmidtko et al., 2017). In contrast, our budget analysis of bottom-water O_2 in Chesapeake Bay reveals intriguingly different physical and biogeochemical responses to climate change in a eutrophic estuary. Using the downscaled climate projections and a coupled hydrodynamic-biogeochemical model, we projected that the hypoxic and anoxic volumes in Chesapeake Bay would increase by 10-30% between the late 20th and mid-21st century. Despite the differences among the three RCM projections, the projected increases in hypoxia in this eutrophic estuary are similar. This increase of 10-30% in the hypoxic and anoxic volumes is larger than the increases obtained from the model runs that considered simplified changes from climate model projections (Wang et al., 2017; Irby et al., 2018), suggesting possible nonlinear synergistic effects among different climate change factors.

The combined effects of sea level rise and larger winter-spring runoff lead to stronger stratification in the future climate, resulting in larger reductions in the vertical diffusive and advective O_2 fluxes to the bottom water. While turbulent mixing is known to be suppressed in stratified water, previous studies (Lerzack et al., 2004; Scully, 2010; Li et al., 2015; Xie and Li, 2018) also showed that vertical advection due to lateral circulation decreases under stronger stratification. Therefore, one certain aspect about

the impact of climate change on estuarine hypoxia is the increasing stratification and decreasing vertical supply of O_2 to the bottom water. The import of high-O_2 coastal water by estuarine return flow is also a significant source of O_2 to the hypoxic region (Li et al., 2015; Li et al., 2016). According to our analysis, F_{hadv} decreases in the future climate, primarily due to the seaward expansion of hypoxia and O_2 reduction in the lower Bay.

The simplified climate change numerical experiments by Wang et al. (2017) and Irby et al. (2018) showed that sea level rise amplifies the estuarine transport and leads to stronger import of higher-O_2 coastal water to the hypoxic region in the mid-Bay. The net effect of sea level rise on estuarine hypoxia ultimately depends on the competition between the stronger vertical stratification and stronger inflows, and is the subject of an ongoing model inter-comparison study. Also, these studies superimposed the projected sea level rise onto the sea level oscillations at the offshore boundary, and did not consider the geomorphic change with sea level rise (e.g. inundation of low-lying land areas) and its effects on tidal dynamics and estuarine circulation.

Climate-induced shifts in phenology in marine ecosystems have been well documented (e.g. Edward & Richardson, 2004; Kirby et al., 2007; Nixon et al., 2009). Our model shows the earlier shifts of both winter-spring and summer phytoplankton species (Figure 4.10), in concert with the earlier initiation of hypoxia in spring and more rapid disintegration of hypoxia in late summer and early fall. These results are consistent with a recent retrospective analysis of 30-years monitoring data in

Chesapeake Bay by Testa et al. (2018) and Murphy et al. (2011). They observed an increase in winter phytoplankton biomass in landward regions, elevated early summer hypoxic volumes and a decreasing trend of late summer hypoxia. Testa et al. (2018) found that warming led to elevated rates of organic matter degradation and "speeding-up" of the typical seasonal cycle. Similar climate warming effects were observed on terrestrial ecosystems and biogeochemisty over land (Elmore et al., 2016). In the ROMS-RCA model, the phytoplankton community is represented by two functional groups: winter-spring species and summer species. Warming leads to earlier bloom of the winter-spring species and smaller biomass of the summer species. Although the retrospective data analysis by Testa et al. (2018) is consistent with our model results, one cannot rule out the possibility that new plankton species able to tolerate higher temperature may migrate to Chesapeake Bay in the future climate (Barton et al., 2016). Should this happen, the water column respiration may increase during the summer season and drive more severe hypoxia.

While ocean warming and sea level rise were considered in this study, changes of nutrient concentration in the open ocean were not considered. Such nutrient changes were found to induce 20-30% reduction of biological production on the northwest European shelf as increased stratification in a warming climate reduced oceanic nutrient supply (Holt et al., 2012; Gröger et al., 2013). However, in a eutrophic estuary like Chesapeake Bay, the nutrient loading from the rivers is 1-2 orders of magnitude larger than the nutrient input from the adjacent ocean (Nixon et al. 1987; Kemp et al. 2005). Nutrient concentration changes in the open ocean are expected to have a minor

effect on hypoxia in this estuary. Nevertheless, the northward shift of Gulf Stream, which is not fully resolved in the oceanic GCMs, may cause a greater reduction in oxygen solubility in the northwest Atlantic shelf (Claret et al., 2018). This may decrease O_2 concentration in the incoming bottom water from the shelf and exacerbate the hypoxic condition in Chesapeake Bay.

This study did not consider the effects of nutrient reductions that might be implemented to meet water quality standards. When the mandated nutrient reductions for Chesapeake Bay were considered, Irby et al. (2018) found that the negative impacts of climate change in 2050 were significantly smaller than improvements in O_2 due to the nutrient reduction. Saraiva et al. (2019a) reached a similar conclusion when studying the combined effects of changing nutrient loads from land and changing climate on the Baltic Sea during the 21st century. It would be interesting to extend our study to include the effects of different nutrient-reduction scenarios in the future.

Our goal here is not only to make climate downscaling projections on Chesapeake Bay hypoxia but also to gain better understanding of physical and biogeochemical controls of hypoxia under climate change. To make robust future projections, particularly for the late 21st century when the range of climate change scenarios is much wider, one would need to expand the uncertainty analysis by including more greenhouse gas concentration scenarios and nutrient loading scenarios, as done recently for the Baltic Sea by Saraiva et al. (2019b).

4.7 Acknowledgements

We are grateful to NSF (CBET-1360285), Pennsylvania Sea Grant (NA10OAR4170063) and NOAA-OAP (NA15NOS4780184) for the financial support. We thank two anonymous reviewers for their helpful comments. Model output is available upon request. This is UMCES contribution number 5720.

Chapter 5: Conclusion

The long-term retrospective simulation of Chesapeake Bay in this study successfully reproduces the deterioration of oxygen condition in the bottom water with increasing nutrient loading from 1950 to 1989. The summer hypoxia expands modestly from 1950s to 1960s, while the hypoxic volume increases substantially by ~65% in 1970s and maintains relatively stable in 1980s. The hypoxia duration is also prolonged by ~1 month with both earlier onset and later termination for about two weeks. The bottom oxygen concentration declines most rapidly around 1970s in the mid-Chesapeake Bay, paralleling the significant increase of winter-spring chlorophyll-a concentration from 1950s-1960s to 1970s-1980s. Therefore, a significant increase of hypoxia volume per nitrate load occurred around 1970s instead of 1986, indicating a mismatch in the timing of shift with previous observational studies which might rely on scarce biased sampling data. The possible causes for the modeled shift might include the occurrence of Tropical Storm Agnes in 1972 with consecutive years with above-average flow and relatively small summer wind speed. More thorough study on the changes of biogeochemical cycling with the expansion of hypoxia, the changes in biological and physical processes after Agnes and the impacts on hypoxia is needed in the future.

Using a coupled hydrodynamic-biogeochemical model, the hindcast simulation and additional numerical experiments between 1985 and 2016, when the riverine nutrient inputs was modest decreased, were conducted to discern the separate effects of temperature increase, sea level rise and nutrient reduction. The simulated dissolved

oxygen in the Chesapeake Bay showed a statistically significant declining trend: ~0.3 mg/L over the past three decades, which mostly occurred during winter and spring while May-August hypoxic volume showed no changes and September hypoxic volume showed a slight decrease (~0.9 km^3). Warming was found to be the dominant driver of the long-term oxygen decline whereas sea level rise had a minor effect. Although nutrient management resulted in modest increases in the oxygen concentration during spring and summer, climate warming has more than offset the benefit of nutrient reduction in Chesapeake Bay over the past three decades.

The climate downscaling projections on Chesapeake Bay hypoxia in the mid-21st century suggested that the hypoxic and anoxic volumes would increase by 10-30% when the riverine nutrient inputs maintained at high level as in 1990s. Climate change induced sea level rise and larger winter-spring runoff will generate stronger stratification and large reductions in the vertical oxygen supply to the bottom water. On the other hand, the warming lead to earlier initiation of hypoxia, accompanied by weaker summer respiration and more rapid termination of hypoxia. The future study will consider the different nutrient reduction scenarios in combination of projected future climate change in Chesapeake Bay. The uncertainties in projections should be further evaluated considering the discrepancies of estuary model, unknown future greenhouse gas concentration and climate model deficiencies.

Bibliography

Altieri, A., & Gedan, K. B. (2015). Climate change and dead zones. Global Change Biology, 21. 1395–1406. http://doi:10.1111/gcb.12754

Barton, A. D., Irwin, A. J., Finkel, Z. V, & Stock, C. A. (2016). Anthropogenic climate change drives shift and shuffle in North Atlantic phytoplankton communities. Proceedings of the National Academy of Sciences, 113(11). http://doi:10.1073/pnas.1519080113

Beck, M. W., & Murphy, R. R. (2017). Numerical and qualitative contrasts of two statistical models for water quality change in tidal waters. JAWRA Journal of the American Water Resources Association, 53(1), 197-219.

Bendtsen, J., & Hansen, J. L. S. (2013). Effects of global warming on hypoxia in the Baltic Sea – North Sea transition zone. Ecological Modelling, 264, 17–26. https://doi.org/10.1016/j.ecolmodel.2012.06.018

Bever, A. J., Friedrichs, M. A., Friedrichs, C. T., Scully, M. E., & Lanerolle, L. W. (2013). Combining observations and numerical model results to improve estimates of hypoxic volume within the Chesapeake Bay, USA. Journal of Geophysical Research: Oceans, 118(10), 4924-4944.

Boesch, D.F., W.C. Boicourt, R.I. Cullather, T. Ezer, G.E. Galloway, Jr., Z.P. Johnson, K.H. Kilbourne, M.L. Kirwan, R.E. Kopp, S. Land, M. Li, W. Nardin, C.K. Sommerfield, W.V. Sweet. 2018. Sea-level Rise: Projections for Maryland 2018, 27 pp. University of Maryland Center for Environmental Science, Cambridge, MD.

Boicourt, W. C. (1992), Influences of circulation processes on dissolved oxygen in the Chesapeake Bay, in Oxygen Dynamics in the Chesapeake Bay: A Synthesis of Recent Research, edited by D. E. Smith, M. Leffler, and G. Mackiernan, pp. 7–59, Md. Sea Grant Coll. Publ., College Park

Boon, J. D., & Mitchell, M. (2015). Nonlinear change in sea level observed at North American tide stations. Journal of Coastal Research, 31(6), 1295-1305.

Boynton, W. R., Garber, J. H., Summers, R., & Kemp, W. M. (1995). Inputs, transformations, and transport of nitrogen and phosphorus in Chesapeake Bay and selected tributaries. Estuaries, 18(1), 285-314.

Brady, D.C., Testa, J. M., Di Toro, D.M., Boynton, W. R., and Kemp, W. M. (2013). Sediment flux modeling: Calibration and application for coastal systems. Estuarine, Coastal and Shelf Science 117: 107-124. https://doi.org/10.1016/j.ecss.2012.11.003

Breitburg, D., Levin, L. A., Oschlies, A., Grégoire, M., Chavez, F. P., Conley, D. J., ... & Jacinto, G. S. (2018). Declining oxygen in the global ocean and coastal waters. Science, 359(6371), eaam7240.

Cabré, A., Marinov, I., Bernardello, R., & Bianchi, D. (2015). Oxygen minimum zones in the tropical Pacific across CMIP5 models: mean state differences and climate change trends. Biogeosciences, 12(18), 5429-5454.

Carstensen, J., Andersen, J. H., Gustafsson, B. G., & Conley, D. J. (2014). Deoxygenation of the Baltic Sea during the last century. Proceedings of the National Academy of Sciences, 111(15), 5628-5633.

Caya, D., & Laprise, R. (1999). A semi-Lagrangian semi-implicit regional climate model: The Canadian RCM. Monthly Weather Review, 127(3), 341-362.

Chapman, D.C., & Beardsley, R.C. (1989). On the origin of shelf water in the middle Atlantic Bight. Journal of Physical Oceanography, 19(3):384-391.

Cheng, P., Li, M., & Li, Y. (2013). Generation of an estuarine sediment plume by a tropical storm. Journal of Geophysical Research: Oceans, 118(2), 856-868.

Chua, V. P. and Xu, M. (2014) 'Impacts of sea-level rise on estuarine circulation: An idealized estuary and San Francisco Bay', Journal of Marine Systems. Elsevier B.V., 139, pp. 58–67. doi: 10.1016/j.jmarsys.2014.05.012.

Claret, M., Galbraith, E. D., Palter, J. B., Bianchi, D., Fennel, K., Gilbert, D., & Dunne, J. P. (2018). Rapid coastal deoxygenation due to ocean circulation shift in the northwest Atlantic. Nature climate change, 8(10), 868-872

Cloern, J. E. and Jassby, A. D. (2012) 'Drivers of change in estuarine-coastal ecosystems: Discoveries from four decades of study in San Francisco Bay', Reviews of Geophysics, 50(4), pp. 1–33. doi: 10.1029/2012rg000397.

Collins, W. D., Bitz, C. M., Blackmon, M. L., Bonan, G. B., Bretherton, C. S., Carton, J. A., ... & Kiehl, J. T. (2006). The community climate system model version 3 (CCSM3). Journal of Climate, 19(11), 2122-2143.

Conley, D. J., Bonsdorff, E., Carstensen, J., Destouni, G., Gustafsson, B. G., Hansson, L. A., Rabalais, N. N., Voss, M. and Zillén, L. (2009a) 'Tackling hypoxia in the Baltic Sea: Is engineering a solution?', Environmental Science and Technology, 43(10), pp. 3407–3411. doi: 10.1021/es8027633.

Conley, D. J., Carstensen, J., Ærtebjerg, G., Christensen, P. B., Dalsgaard, T., Hansen, J. L., & Josefson, A. B. (2007). Long_term changes and impacts of hypoxia in Danish coastal waters. Ecological Applications, 17(sp5), S165-S184.

Conley, D. J., Carstensen, J., Vaquer-Sunyer, R., & Duarte, C. M. (2009b). Ecosystem thresholds with hypoxia. In Eutrophication in coastal ecosystems (pp. 21-29). Springer, Dordrecht.

Cowan, J. L., & Boynton, W. R. (1996). Sediment-water oxygen and nutrient exchanges along the longitudinal axis of Chesapeake Bay: seasonal patterns, controlling factors and ecological significance. Estuaries, 19(3), 562-580.

Delworth, T.L., Broccoli, A.J., Rosati, A., Stouffer, R.J., Balaji, V., Beesley, J.A., et al. (2006). GFDL's CM2 global coupled climate models. Part I: formulation and simulation characteristics. Journal of Climate, 19, 643–674. http://doi:10.1175/JCLI3629.1

Deutsch, C., Brix, H., Ito, T., Frenzel, H., & Thompson, L. (2011). Climate-forced variability of ocean hypoxia. Science, 333, 336–339. http://doi:10.1126/science.1202422

Di Toro, D. M. (2001), Sediment flux modeling, 624 pp., Wiley-Interscience, New York.

Diaz, R. J. (2001). Overview of hypoxia around the world. Journal of environmental quality, 30(2), 275-281.

Diaz, R. J., & Rosenberg, R. (2008). Spreading dead zones and consequences for marine ecosystems. science, 321(5891), 926-929.

Ding, H., & Elmore, A. J. (2015). Spatio-temporal patterns in water surface temperature from Landsat time series data in the Chesapeake Bay, USA. Remote Sensing of Environment, 168, 335-348.

Du, J., Shen, J., Park, K., Wang, Y. P. and Yu, X. (2018) 'Worsened physical condition due to climate change contributes to the increasing hypoxia in Chesapeake Bay', Science of the Total Environment, 630, pp. 707–717. doi: 10.1016/j.scitotenv.2018.02.265.

Duarte, C. M., Conley, D. J., Carstensen, J., & Sánchez-Camacho, M. (2009). Return to Neverland: shifting baselines affect eutrophication restoration targets. Estuaries and Coasts, 32(1), 29-36.

Edwards, M., & Richardson, A. J. (2004). Impact of climate change on marine pelagic phenology and trophic mismatch. Nature, 430, 881–884. http://doi:10.1038/nature02808

Egbert, G. D., & Erofeeva, S. Y. (2002). Efficient inverse modeling of barotropic ocean tides. Journal of Atmospheric and Oceanic Technology, 19(2), 183-204.

Elmore, A. J., Nelson, D. M., & Craine, J. M. (2016). Earlier springs are causing reduced nitrogen availability in North American eastern deciduous forests. Nature Plants, 2(10), 1–5. http://doi:10.1038/nplants.2016.133

Engelhart SE, Horton BP, Douglas BC, Peltier WR, Törnqvist TE (2009) Spatial variability of late Holocene and 20th century sea level-rise along the Atlantic coast of the United State. Geology,37: 1115-18.

Ezer, T., & Corlett, W. B. (2012). Is sea level rise accelerating in the Chesapeake Bay? A demonstration of a novel new approach for analyzing sea level data. Geophysical Research Letters, 39(19).

Fairall, C. W., Bradley, E. F., Hare, J. E., Grachev, A. A., & Edson, J. B. (2003). Bulk parameterization of air–sea fluxes: Updates and verification for the COARE algorithm. Journal of climate, 16(4), 571-591.

Feng, Y., DiMarco, S. F., & Jackson, G. A. (2012). Relative role of wind forcing and riverine nutrient input on the extent of hypoxia in the northern Gulf of Mexico. Geophysical Research Letters, 39(9).

Fennel, K., & Testa, J. M. (2019). Biogeochemical controls on coastal hypoxia. Annual review of marine science, 11, 105-130.

Fennel, K., Wilkin, J., Levin, J., Moisan, J., O'Reilly, J., Haidvogel, D. (2006). Nitrogen cycling in the Middle Atlantic Bight: results from a three-dimensional model and implications for the North Atlantic nitrogen budget. Global Biogeochemical Cycles, 20 (3), http://doi: 10.1029/2005GB002456

Filippino, K. C., Mulholland, M. R., & Bernhardt, P. W. (2011). Nitrogen uptake and primary productivity rates in the Mid-Atlantic Bight (MAB). Estuarine, Coastal and Shelf Science, 91(1), 13-23.

Flato, G. M. (2005). The third generation coupled global climate model (CGCM3). Environment Canada Canadian Centre for Climate Modelling and Analysis note. Retrieved from http://www.ec.gc.ca/ccmac-cccma/default.asp?n=1299529F-1

Flemer, D. A., Mackiernan, G. B., Nehlsen, W., Tippie, V. K., Biggs, R. B., Blaylock, D., ... & Taft, J. L. (1983). Chesapeake Bay: A profile of environmental change. US Environmental Protection Agency, Washington, DC, 199.

GFDL Global Atmospheric Model Development Team, 2004: The new GFDL global atmospheric and land model AM2-LM2: Evaluation with prescribed SST simulations. Journal of Climate, 17, 4641–4673.

Giani, M., Djakovac, T., Degobbis, D., Cozzi, S., Solidoro, C., & Umani, S. F. (2012). Recent changes in the marine ecosystems of the northern Adriatic Sea. Estuarine, Coastal and Shelf Science, 115, 1-13.

Gilbert, D., Rabalais, N. N., Diaz, R. J., & Zhang, J. (2010). Evidence for greater oxygen decline rates in the coastal ocean than in the open ocean. Biogeosciences, 7(7), 2283-2296.

Gilbert, R.O. 1987. Statistical Methods for Environmental Pollution Monitoring, Wiley, NY.

Giorgi, F., & Gutowski Jr, W. J. (2015). Regional dynamical downscaling and the CORDEX initiative. Annual Review of Environment and Resources, 40, 467–490. http://doi:10.1146/annurev-environ-102014-021217

Giorgi, F., Marinucci, M. R., & Bates, G. T. (1993a). Development of a second-generation regional climate model (RegCM2). Part I: Boundary-layer and radiative transfer processes. Monthly Weather Review, 121(10), 2794-2813.

Giorgi, F., Marinucci, M. R., Bates, G. T., & De Canio, G. (1993b). Development of a second-generation regional climate model (RegCM2). Part II: Convective processes and assimilation of lateral boundary conditions. Monthly Weather Review, 121(10), 2814-2832.

Gordon, C., Cooper, C., Senior, C.A., Banks, H., Gregory, J.M., Johns, T.C., et al. (2000). The simulation of SST, sea ice extents and ocean heat transports in a version of the Hadley Centre coupled model without flux adjustments. Climate Dynamics, 16 (2–3): 147–168. http://doi:10.1007/s003820050010

Greening, H., & Janicki, A. (2006). Toward reversal of eutrophic conditions in a subtropical estuary: Water quality and seagrass response to nitrogen loading reductions in Tampa Bay, Florida, USA. Environmental management, 38(2), 163-178.

Grell, G. A., Dudhia, J., & Stauffer, D. R. (1993). A description of the fifth-generation Penn State/NCAR mesoscale model (MM5). NCAR Tech. Note NCAR/TN-398,107 pp.

Gröger, M., Maier-Reimer, E., Mikolajewicz, U., Moll, A., & Sein, D. (2013). NW European shelf under climate warming: implications for open ocean–shelf exchange, primary production, and carbon absorption. Biogeosciences, 10, 3767-3792.

Große, F., Greenwood, N., Kreus, M., Lenhart, H.-J., Machoczek, D., Pätsch, J., et al. (2016). Looking beyond stratification: a model-based analysis of the biological drivers of oxygen deficiency in the North Sea. Biogeosciences, 13, 2511-2535. http://doi.org/10.5194/bg-13-2511-2016

Gudmundsson, L., Bremnes, J. B., & Haugen, J. E. (2012). Technical Note_: Downscaling RCM precipitation to the station scale using statistical

transformations – a comparison of methods. Hydrology and Earch System Sciences, 16, 3383–3390. http://doi:10.5194/hess-16-3383-2012

Gurbisz, C., & Kemp, W. M. (2014). Unexpected resurgence of a large submersed plant bed in Chesapeake Bay: Analysis of time series data. Limnology and Oceanography, 59(2), 482-494.

Hagy, J. D., Boynton, W. R., Keefe, C. W. and Wood, K. V. (2004) 'Hypoxia in Chesapeake Bay, 1950-2001: Long-term change in relation to nutrient loading and river flow', Estuaries, 27(4), pp. 634–658. doi: 10.1007/BF02907650.

Haidvogel, D.B., Arango,H., Budgell, W.P., Cornuelle, B.D., Curchitser, E., Di Lorenzo, E., et al. (2008). Ocean forecasting in terrain-following coordinates: formulation and skill assessment of the regional ocean modeling system. Journal of Computational Physics, 227(7):3595-3624. http://doi:10.1016/j.jcp.2007.06.016

Harding Jr, L. W., & Perry, E. S. (1997). Long-term increase of phytoplankton biomass in Chesapeake Bay, 1950-1994. Marine Ecology Progress Series, 157, 39-52.

Harding, L. W., Gallegos, C. L., Perry, E. S., Miller, W. D., Adolf, J. E., Mallonee, M. E., & Paerl, H. W. (2016). Long-term trends of nutrients and phytoplankton in Chesapeake Bay. Estuaries and Coasts, 39(3), 664-681.

Hastie, T. & Tibshirani, R. (1986). Generalized additive models (with discussion). Statistical Science, 1, 297-318.

Hastie, T. & Tibshirani, R. (1990). Generalized Additive Models. Chapman & Hall.

Hetland, R. D., & DiMarco, S. F. (2008). How does the character of oxygen demand control the structure of hypoxia on the Texas–Louisiana continental shelf?. Journal of Marine Systems, 70(1-2), 49-62.

Hirsch, R. M., Moyer, D. L., & Archfield, S. A. (2010). Weighted regressions on time, discharge, and season (WRTDS), with an application to Chesapeake Bay river inputs 1. JAWRA Journal of the American Water Resources Association, 46(5), 857-880.

Holt, J. T., Butenschon, M., Wakelin, S. L., Artioli, Y., & Allen, J. I. (2012). Oceanic controls on the primary production of the northwest European continental shelf: model experiments under recent past conditions and a potential future scenario. Biogeosciences, 9, 97-117.

Hong, B., & Shen, J. (2012). Responses of estuarine salinity and transport processes to potential future sea-level rise in the Chesapeake Bay. Estuarine, Coastal and Shelf Science, 104, 33-45.

Howarth, R.W., Swaney, D.P., Boyer, E.W., Marino, R., Jaworski, N., Goodale, C. (2006). The influence of climate on average nitrogen export from large watersheds in the Northeastern United States. Biogeochemistry, 79, 163-186.

Irby, I. D., Friedrichs, M. A. M., Da, F., & Hinson, K. E. (2018). The competing impacts of climate change and nutrient reductions on dissolved oxygen in Chesapeake Bay. Biogeosciences, 15, 2649–2668.

Irby, I. D., Friedrichs, M. A., Friedrichs, C. T., Bever, A., Hood, R. R., Lanerolle, L. W., ... & Shen, J. (2016). Challenges associated with modeling low-oxygen waters in Chesapeake Bay: a multiple model comparison. Biogeosciences, 13(7), 2011-2028.

Isleib, R. P. E., J. J. Fitzpatrick, and J. Mueller (2007). The development of a nitrogen control plan for a highly urbanized tidal embayment, Proceedings of the Water Environment Federation, 5, 296–320.

Jaworski, N. A., Romano, B., Buchanan, C., & Jaworski, C. (2007). The Potomac River Basin and its Estuary: landscape loadings and water quality trends, 1895–2005. Potomac Integrative Analysis Online Collection at www.potomacriver.org.

Jones, R., Hassell, D., Hudson, D., Wilson, S., Jenkins, G., and Mitchell, J.(2003). Generating high resolution climate change scenarios using PRECIS. UNDP National Communications Unit Workbook, 34 pp.

Juang, H. M. H., Hong, S. Y., & Kanamitsu, M. (1997). The NCEP regional spectral model: An update. Bulletin of the American Meteorological Society, 78(10), 2125-2144.

Justic, D., Rabalais, N. N., & Turner, R. E. (2002). Modeling the impacts of decadal changes in riverine nutrient fluxes on coastal eutrophication near the Mississippi River Delta. Ecological Modelling, 152, 33–46.

Justic, D., Rabalais, N. N., & Turner, R. E. (2003). Simulated responses of the Gulf of Mexico hypoxia to variations in climate and anthropogenic nutrient loading. Journal of Marine Systems, 42, 115–126. doi:10.1016/S0924-7963(03)00070-8

Kauppila, P., Weckström, K., Vaalgamaa, S., Korhola, A., Pitkänen, H., Reuss, N., & Drew, S. (2005). Tracing pollution and recovery using sediments in an urban estuary, northern Baltic Sea: are we far from ecological reference conditions?. Marine Ecology Progress Series, 290, 35-53.

Keeling, R. F., Arne, K., & Gruber, N. (2010). Ocean Deoxygenation in a Warming World. Annual Review of Marine Science, 2, 199–229. doi:10.1146/annurev.marine.010908.163855

Kemp, W. M., Boynton, W. R., Adolf, J. E., Boesch, D. F., Boicourt, W. C., Brush, G., ... & Harding, L. W. (2005). Eutrophication of Chesapeake Bay: historical trends and ecological interactions. Marine Ecology Progress Series, 303, 1-29.

Kemp, W. M., Smith, E. M., Marvin-DiPasquale, M., & Boynton, W. R. (1997). Organic carbon balance and net ecosystem metabolism in Chesapeake Bay. Marine Ecology Progress Series, 150, 229-248.

Kemp, W. M., Testa, J. M., Conley, D. J., Gilbert, D., & Hagy, J. D. (2009). Temporal responses of coastal hypoxia to nutrient loading and physical controls. Biogeosciences, 6(12), 2985-3008.

Kendall, M.G. 1975. Rank Correlation Methods, 4th edition, Charles Griffin, London.

Kirby, R. R., Beaugrand, G., Lindley, J. a, Richardson, A. J., Edwards, M., & Reid, P. C. (2007). Climate effects and benthic-pelagic coupling in the North Sea Climate effects and benthic – pelagic coupling in the North Sea. Marine Ecology Progress Series, 330, 31–38. http://doi:10.3354/meps330031

Lake, S. J. and Brush, M. J. (2015) Modeling estuarine response to load reductions in a warmer climate: York River Estuary, Virginia, USA', Marine Ecology Progress Series, 538, 81–98. doi: 10.3354/meps11448.

Laurent, A., Fennel, K., Ko, D. S., & Lehrter, J. (2018). Climate change projected to exacerbate impacts of coastal eutrophication in the northern Gulf of Mexico.

Journal of Geophysical Research:Oceans, 123, 1–19. http://doi:10.1002/2017JC013583

Lee, S. B., Li, M., & Zhang, F. (2017). Impact of sea level rise on tidal range in Chesapeake and Delaware Bays. Journal of Geophysical Research: Oceans, 122(5), 3917-3938. http://doi:10.1002/2016JC012597

Lefcheck, J. S., Orth, R. J., Dennison, W. C., Wilcox, D. J., Murphy, R. R., Keisman, J., Gurbisz, C., Hannam, M., Brooke Landry, J., Moore, K. A., Patrick, C. J., Testa, J., Weller, D. E. and Batiuk, R. A. (2018) Long-term nutrient reductions lead to the unprecedented recovery of a temperate coastal region, Proceedings of the National Academy of Sciences of the United States of America, 115(14), 3658–3662. doi: 10.1073/pnas.1715798115.

Lentz, S. J. (2017). Seasonal warming of the Middle A tlantic B ight C old P ool. Journal of Geophysical Research: Oceans, 122(2), 941-954.

Lerczak, J. A., & Geyer, W. R. (2004). Modeling the lateral circulation in straight , stratified estuaries. Journal of Physical Oceanography, 34, 1410–1428.

Levin, L. A. (2018). Manifestation, drivers, and emergence of open ocean deoxygenation. Annual Review of Marine Science, 10, 229-260. https://doi.org/10.1146/annurev-marine-121916-063359.Li, M., Zhong, L., & Boicourt, W. C. (2005). Simulations of Chesapeake Bay estuary_: Sensitivity to turbulence mixing parameterizations and comparison with observations. Geophysical Research Letters, 110, 1–22. http://doi:10.1029/2004JC002585

Li, M., & Zhong, L. (2009). Flood–ebb and spring–neap variations of mixing, stratification and circulation in Chesapeake Bay. Continental Shelf Research, 29(1), 4-14.

Li, M., Lee, Y. J., Testa, J. M., Li, Y., Ni, W., Kemp, W. M., & Toro, D. M. Di. (2016). What drives interannual variability of hypoxia in Chesapeake Bay: Climate forcing versus nutrient loading? Geophysical Research Letters, 43, 2127–2134. http://doi:10.1002/2015GL067334

Li, M., Zhong, L., & Boicourt, W. C. (2005). Simulations of Chesapeake Bay estuary: Sensitivity to turbulence mixing parameterizations and comparison with observations. Journal of Geophysical Research: Oceans, 110(C12).

Li, M., Zhong, L., Boicourt, W. C., Zhang, S., & Zhang, D. L. (2007). Hurricane-induced destratification and restratification in a partially-mixed estuary. Journal of Marine Research, 65(2), 169-192.

Li, Y., Li, M., & Kemp, W. M. (2015). A budget analysis of bottom-water dissolved oxygen in Chesapeake Bay. Estuaries and Coasts, 38(6), 2132–2148. http://doi:10.1007/s12237-014-9928-9

Linker, L.C., Batiuk, R.A., Shenk, G.W. and Cerco, C.F. (2013). Development of the Chesapeake Bay watershed total maximum daily load allocation. Journal of the American Water Resources Association, 49(5):986-1006.

Lomas, M. W., Glibert, P. M., Shiah, F. K. and Smith, E. M. (2002) 'Microbial processes and temperature in Chesapeake Bay: Current relationships and potential impacts of regional warming', Global Change Biology, 8(1), pp. 51–70. doi: 10.1046/j.1365-2486.2002.00454.x.

Malone, T. C., W. M. Kemp, H. W. Ducklow, W. R. Boynton, J. H. Tuttle, and R. B. Jonas (1986), Lateral variation in the production and fate of phytoplankton in a

partially stratified estuary, Mar. Ecol. Prog. Ser., 32(2-3), 149–160, doi:10.3354/meps032149

Mann, H.B. 1945. Non-parametric tests against trend, Econometrica 13:163-171.

McCrackin, M. L., Jones, H. P., Jones, P. C. and Moreno-Mateos, D. (2017) 'Recovery of lakes and coastal marine ecosystems from eutrophication: A global meta-analysis', Limnology and Oceanography, 62(2), pp. 507–518. doi: 10.1002/lno.10441.

Mearns, L. O., Arritt, R., Biner, S., Bukovsky, M. S., McGinnis, S., Sain, S., … Snyder, M. (2012). The North American regional climate change assessment program: overview of phase I results. Bulletin of the American Meteorological Society, 93(9), 1337–1362. https://doi.org/10.1175/BAMS-D-11-00223.1

Mearns, L. O., Sain, S., Leung, L. R., Bukovsky, M. S., McGinnis, S., Biner, S., … Sloan, L. (2013). Climate change projections of the North American Regional Climate Change Assessment Program (NARCCAP). Climatic Change, 120(4), 965–975. https://doi.org/10.1007/s10584-013-0831-3

Mearns, L.O., et al., (2007), updated 2014. The North American Regional Climate Change Assessment Program dataset, National Center for Atmospheric Research Earth System Grid data portal, Boulder, CO. http://doi:10.5065/D6RN35ST

Mee, L. (2006). Reviving dead zones. Scientific America, 295, 78-85.

Meier, H. E. M., Andersson, H. C., Eilola, K., Gustafsson, B. G., Kuznetsov, I., Neumann, T., et al. (2011). Hypoxia in future climates_: A model ensemble study for the Baltic Sea. Geophysical Research Letters, 38: L24608. http://doi:10.1029/2011GL049929

Meier, H. E. M., Eilola, K., Almroth-Rosell, E., Schimanke, S., Kniebusch, M., Höglund, A., Pemberton, P., Liu, Y., Väli, G. and Saraiva, S. (2019) Disentangling the impact of nutrient load and climate changes on Baltic Sea hypoxia and eutrophication since 1850, Climate Dynamics. Springer Berlin Heidelberg, 53(1–2), 1–22. doi: 10.1007/s00382-018-4296-y.

Meier, H. E. M., Höglund, A., Eilola, K., & Almroth-Rosell, E. (2017). Impact of accelerated future global mean sea level rise on hypoxia in the Baltic Sea. Climate Dynamics, 49(1-2), 163-172.

Meire, L., Soetaert, K. E. R., & Meysman, F. J. R. (2013). Impact of global change on coastal oxygen dynamics and risk of hypoxia. Biogeosciences, 10, 2633–2653. http://doi:10.5194/bg-10-2633-2013

Mesinger, F., DiMego, G., Kalnay, E., Mitchell, K., Shafran, P.C., Ebisuzaki, W., et al. (2006). North American Regional Reanalysis. Bulletin of the American Meteorological Society, 87, 343–360. http://doi:10.1175/BAMS-87-3-343

Miller, K.G., Kopp, R.E., Horton, B.P., Browning, J.V., Kemp, A.C. (2013). A geological perspective on sea-level rise and its impacts along the U.S. mid-Atlantic coast. Earth's Future,1(1):3-18. http://doi:10.1002/2013EF000135

Milly, P.C.D., Dunne, K.A. (2011). On the hydrologic adjustment of climate-model projections: The potential pitfall of potential evapotranspiration. Earth Interactions 15, 1-14. http://doi.org/10.1175/2010EI363.1

Mitrovica, J. X., Gomez, N., & Clark, P. U. (2009). The sea-level fingerprint of west Antarctic collapse. Science, 323(2), 753. https://doi.org/10.1126/science.1166510

Mitrovica, J. X., Gomez, N., Morrow, E., Hay, C., Latychev, K., & Tamisiea, M. E. (2011). On the robustness of predictions of sea level fingerprints. Geophysical Journal International, 187(2), 729–742. https://doi.org/10.1111/j.1365-246X.2011.05090.x

Morrison, J., Callendar, W., Foreman, M. G. G., Masson, D., Fine, I., Morrison, J., et al. (2014). A model simulation of future oceanic conditions along the British Columbia continental shelf . Part I_: Forcing fields and initial conditions. Atmosphere-Ocean, 52(1), 1–19. http://doi:10.1080/07055900.2013.868340

Murphy, R. R., Kemp, W. M. and Ball, W. P. (2011) Long-Term Trends in Chesapeake Bay Seasonal Hypoxia, Stratification, and Nutrient Loading, Estuaries and Coasts, 34(6), 1293–1309. doi: 10.1007/s12237-011-9413-7.

Murphy, R. R., Perry, E., Harcum, J., & Keisman, J. (2019). A Generalized Additive Model approach to evaluating water quality: Chesapeake Bay case study. Environmental Modelling & Software, 118, 1-13.

Najjar, R. G., Pyke, C. R., Adams, M. B., Breitburg, D., Hershner, C., Kemp, M., ... & Sellner, K. (2010). Potential climate-change impacts on the Chesapeake Bay. Estuarine, Coastal and Shelf Science, 86(1), 1-20.

Najjar, R. G., Walker, H. A., Anderson, P. J., Barron, E. J., Bord, R. J., Gibson, J. R., ... & Polsky, C. D. (2000). The potential impacts of climate change on the mid-Atlantic coastal region. Climate Research, 14(3), 219-233.

Naki_enovi_, N., Alcamo, J., Davis, G, de Vries, B., Fenhann, J., Gaffin, S., et al. (2000). Emission scenarios. A Special Report of Working Group III of the Intergovernmental Panel on Climate Change. Cambridge University Press, p 599.

Newcombe, C. L., and W. A. Horne. 1938. Oxygen-poor waters in Chesapeake Bay. Science 88: 80-81

Ni, W., Li, M., Ross, A.C., Najjar, R.G. (2019). Large projected decline in dissolved oxygen in an eutrophic estuary due to climate change. Journal of Geophysical Research: Oceans, https://doi.org/10.1029/2019JC015274

Nixon, S. W. (1987). Chesapeake Bay nutrient budgets—a reassessment. Biogeochemistry, 4(1), 77-90.

Nixon, S. W., Fulweiler, R. W., Buckley, B. a., Granger, S. L., Nowicki, B. L., & Henry, K. M. (2009). The impact of changing climate on phenology, productivity, and benthic-pelagic coupling in Narragansett Bay. Estuarine, Coastal and Shelf Science., 82(1), 1–18. http://doi:10.1016/j.ecss.2008.12.016

O'Donnell, J., Dam, H. G., Bohlen, W. F., Fitzgerald, W., Gay, P. S., Houk, A. E., ... & Howard_Strobel, M. M. (2008). Intermittent ventilation in the hypoxic zone of western Long Island Sound during the summer of 2004. Journal of Geophysical Research: Oceans, 113(C9).

Pal, J. S., Small, E. E., & Eltahir, E. A. (2000). Simulation of regional scale water and energy budgets: Representation of subgrid cloud and precipitation processes within RegCM. Journal of Geophysical Research: Atmospheres, 105(D24), 29579-29594.

Pal, J.S., Giorgi, F., Bi, X., Elguindi, N., Solmon,F., Gao, X., et al. (2007). Regional climate modeling for the developing world: The ICTP RegCM3 and RegCNET, Bulletin of American Meteorological Society, 88(9),1395–1409.

Pope, V. D., Gallani, M. L., Rowntree, P. R., & Stratton, R. A. (2000). The impact of new physical parametrizations in the Hadley Centre climate model: HadAM3. Climate Dynamics, 16(2-3), 123-146.

Qian, W., Gan, J., Liu, J., He, B., Lu, Z., Guo, X., ... & Dai, M. (2018). Current status of emerging hypoxia in a eutrophic estuary: The lower reach of the Pearl River Estuary, China. Estuarine, Coastal and Shelf Science, 205, 58-67.

Rabalais, N. N., & Turner, R. E. (2001). Coastal hypoxia: consequences for living resources and ecosystems. American Geophyical Union.

Rabalais, N. N., Diaz, R. J., Levin, L. A., Turner, R. E., Gilbert, D., & Zhang, J. (2010). Dynamics and distribution of natural and human-caused hypoxia. Biogeosciences.7,585-619.

Rabalais, N. N., Turner, R. E. and Wiseman, W. J. (2002) Gulf of Mexico hypoxia, a.k.a. "The dead zone", Annual Review of Ecology and Systematics, 33, 235–263. doi: 10.1146/annurev.ecolsys.33.010802.150513.

Rabalais, N., Conley, J., Slomp, P., & Turner, E. (2014). Eutrophication-driven deoxygenation in the coastal ocean. Oceanography, 27(1), 172–183.

Rice, K. C., & Jastram, J. D. (2015). Rising air and stream-water temperatures in Chesapeake Bay region, USA. Climatic Change, 128(1-2), 127-138.

Saba, V. S., Griffies, S. M., Anderson, W. G., Winton, M., Alexander, M. A., Delworth, T. L., et al. (2016). Enhanced warming of the Northwest Atlantic Ocean under climate change. Journal of Geophysical Research:Oceans, 121, 118–132. http://doi:10.1002/2015JC011346

Sanford, L. P., K. G. Sellner, and D. L. Breitburg (1990), Covariability of dissolved oxygen with physical processes in the summertime Chesapeake Bay, J. Mar. Res., 48, 567–590.

Saraiva S., Meier, H. E. M., Andersson, H., Höglund, A, Dieterich, C., Groger,, M., Hordoir, R. and Eiola, K. (2019a). Baltic Sea ecosystem response to various nutrient load scenarios in present and future climates. Climate Dynamics,52:3369. https ://doi.org/10.1007/s00382-01804330-0

Saraiva S, Meier, H..E..M., Andersson, H., Höglund, A., Dieterich, C., Hordoir, R., Eilola, K. (2019b). Uncertainties in projections of the baltic sea ecosystem driven by an ensemble of global climate models. Frontiers in Earth Science, 6:244. https ://doi:10.3389/feart.2018.00244

Scavia, D., Bertani, I., Obenour, D. R., Turner, R. E., Forrest, D. R., & Katin, A. (2017). Ensemble modeling informs hypoxia management in the northern Gulf of Mexico. Proceedings of the National Academy of Sciences, 114(33), 8823-8828.

Schaefer, S.& Alber, M. (2007). Temperature controls a latitudinal gradient in the proportion of watershed nitrogen exported to coastal ecosystems. Biogeochemistry, 85:333-346. http://doi: 10.1007/s10533-007-9144-9

Schmidtko, S., Stramma, L., & Visbeck, M. (2017). Decline in global oceanic oxygen content during the past five decades. Nature, 542(7641), 335–339. http://doi:10.1038/nature21399

Schubel, J. R., & Cronin, W. B. (1977). Effects of Agnes on the distribution of dissolved oxygen along the main axis of the Bay. The Chesapeake Research Consortium, Inc.(Eds) The Effects of Tropical Storm Agnes on the Chesapeake Bay Estuarine System, 335-347.

Scinocca, J. F., & McFarlane, N. A. (2004). The variability of modeled tropical precipitation. Journal of the Atmospheric Sciences, 61(16), 1993-2015.

Scully, M. E. (2010). Wind modulation of dissolved oxygen in Chesapeake Bay. Estuaries and Coasts, 33, 1164–1175. http://doi:10.1007/s12237-010-9319-9

Scully, M. E. (2013). Physical controls on hypoxia in Chesapeake Bay_: A numerical modeling study. Journal of Geophysical Research: Oceans, 118(3), 1239–1256. http://doi:10.1002/jgrc.20138

Scully, M. E. (2016). The contribution of physical processes to interannual variations of hypoxia in Chesapeake Bay: A 30_yr modeling study. Limnology and Oceanography, 61(6), 2243-2260.

Seliger, H. H., & Boggs, J. A. (1988). Long term pattern of anoxia in the Chesapeake Bay. Understanding the estuary: advances in Chesapeake Bay research. Publication, 129, 570-583.

Sen, Pranab Kumar (1968), Estimates of the regression coefficient based on Kendall's tau, Journal of the American Statistical Association, 63 (324):

Shchepetkin, A.F., & McWilliams, J.C.(2005). The regional oceanic modeling system (ROMS): a split-explicit, free-surface, topography-following-coordinate oceanic model. Ocean modelling, 9(4):347-404. http://doi:10.1016/j.ocemod.2004.08.002

Shen, C., Testa, J. M., Li, M., Cai, W. J., Waldbusser, G. G., Ni, W., ... & Su, J. (2019). Controls on Carbonate System Dynamics in a Coastal Plain Estuary: A Modeling Study. Journal of Geophysical Research: Biogeosciences, 124(1), 61-78.

Sherwood, E. T., Greening, H. S., Janicki, A. J. and Karlen, D. J. (2016) Tampa Bay estuary: Monitoring long-term recovery through regional partnerships, Regional Studies in Marine Science. Elsevier B.V., 4, 1–11. doi: 10.1016/j.rsma.2015.05.005.

Skamarock, W. C., Klemp, J. B., Dudhia, J., Gill, D. O., Barker, D. M., Wang, W., et al. (2005). A description of the advanced research WRF version 2 (No. NCAR/TN-468+ STR). National Center for Atmospheric Research Boulder Co Mesoscale and Microscale Meteorology Div.

Slangen, A. B. A., Katsman, C. A., Vermeersen, L. L. A., & Riva, R. E. M. (2012). Towards regional projections of twenty-first century sea-level change based on IPCC SRES scenarios. Climate Dynamics, 38, 1191–1209. https://doi.org/10.1007/s00382-011-1057-6

Smolarkiewicz, P. K., & Margolin, L. G. (1998). MPDATA: A finite-difference solver for geophysical flows. Journal of Computational Physics, 140(2), 459-480.

Soetaert, K., Middelburg, J. J., Heip, C., Meire, P., Van Damme, S., & Maris, T. (2006). Long_term change in dissolved inorganic nutrients in the heterotrophic Scheldt estuary (Belgium, The Netherlands). Limnology and Oceanography, 51(1part2), 409-423.

Staniec, A., & Vlahos, P. (2017). Timescales for determining temperature and dissolved oxygen trends in the Long Island Sound (LIS) estuary. Continental Shelf Research, 151, 1-7.

Stramma, L., Johnson, G. C., Sprintall, J., & Mohrholz, V. (2008). Expanding oxygen-minimum zones in the tropical oceans. Science, 320, 655–659.

Stramma, L., Schmidtko, S., Levin, L. A., & Johnson, G. C. (2010). Ocean oxygen minima expansions and their biological impacts. Deep Sea Research Part I: Oceanographic Research Papers, 57(4), 587-595.

Taft, J. L., W. R. Taylor, E. O. Hartwig, and R. Loftus (1980), Seasonal oxygen depletion in Chesapeake Bay, Estuaries, 3(4), 242–247, doi:10.2307/1352079

Taylor, K. E. (2001). Summerizing multiple aspects of model performance in a single diagram. Journal of Geophysical Research, 106(D7), 7183–7192. https://doi.org/10.1029/2000JD900719

Testa, J. M., & Kemp, W. M. (2012). Hypoxia_induced shifts in nitrogen and phosphorus cycling in Chesapeake Bay. Limnology and Oceanography, 57(3), 835-850.

Testa, J. M., Li, Y., Lee, Y. J., Li, M., Brady, D. C., Di, D. M., et al. (2014). Quantifying the effects of nutrient loading on dissolved O 2 cycling and hypoxia in Chesapeake Bay using a coupled hydrodynamic – biogeochemical model. Journal of Marine System., 139, 139–158. http://doi:10.1016/j.jmarsys.2014.05.018

Testa, J. M., Murphy, R. R., Brady, D. C., & Kemp, W. M. (2018). Nutrient- and climate-induced shifts in the phenology of linked biogeochemical cycles in a temperate estuary. Frontiers of Marine Science, 5(114). http://doi:10.3389/fmars.2018.00114

Testa, J.M., Brady, D.C., Di Toro, D.M., Boynton, W.R., and Kemp, W.M.(2013). Sediment flux modeling: Nitrogen, phosphorus and silica cycles. Estuarine, Coastal and Shelf Science, 131:245-263.

Theil, H. (1950), A rank-invariant method of linear and polynomial regression analysis. I, II, III, Nederl. Akad. Wetensch., Proc., 53: 386–392, 521–525, 1397–1412, MR 0036489.

USEPA, (2010).Chesapeake Bay Total Maximum Daily Load for Nitrogen, Phosphorus and Seidment.

Van Meter, K. J., Van Cappellen, P. and Basu, N. B. (2018) 'Legacy nitrogen may prevent achievement of water quality goals in the Gulf of Mexico', Science, 360(6387), pp. 427–430. doi: 10.1126/science.aar4462.

Wang, P., Linker, L., Wang, H., Bhatt, G., Yactayo, G., Hinson, K., & Tian, R. (2017). Assessing water quality of the Chesapeake Bay by the impact of sea level rise and warming. IOP Conference Series: Earch and Environmental Science, 82(012001).

Warner, J. C., Geyer, W. R., & Lerczak, J. A. (2005). Numerical modeling of an estuary: A comprehensive skill assessment. Journal of Geophysical Research: Oceans, 110(C5).

Welsh, B. L. and Eller, F. C. (1991) 'Mechanisms Controlling Summertime Oxygen Depletion in Western Long Island Sound', Estuaries, 14(3), pp. 265–278.

Wilcox, Rand R. (2001). Fundamentals of Modern Statistical Methods: Substantially Improving Power and Accuracy. Springer-Verlag, pp. 207-210.

Williams, M. R., Filoso, S., Longstaff, B. J. and Dennison, W. C. (2010) 'Long-Term Trends of Water Quality and Biotic Metrics in Chesapeake Bay: 1986 to 2008', Estuaries and Coasts, 33(6), pp. 1279–1299. doi: 10.1007/s12237-010-9333-y.

Wilson, R. E., Swanson, R. L., & Crowley, H. A. (2008). Perspectives on long_term variations in hypoxic conditions in western Long Island Sound. Journal of Geophysical Research: Oceans, 113(C12).

Wood, A. W., Leung, L. R., Sridhar, V., & Lettenmaier, D. P. (2004). Hydrologic implications of dynamical and statistical approaches to downscaling climate model outputs. Climate Change, 62, 189–216.

Wood, S.A. (2006). Generalized Additive Models: An Introduction with R. Boca Raton, FL: CRC press.

Xie, X., & Li, M. (2018). Effects of Wind Straining on Estuarine Stratification: A Combined Observational and Modeling Study. Journal of Geophysical Research: Oceans, 123(4), 2363–2380. http://doi:10.1002/2017JC013470.

Xie, X., M. Li, M. Scully, and W.C. Boicourt. 2017. Generation of internal solitary waves by lateral circulation in a stratified estuary. Journal of Physical Oceanography, 47, 1789–1797.

Xu, J., Long, W., Wiggert, J. D., Lanerolle, L. W., Brown, C. W., Murtugudde, R., & Hood, R. R. (2012). Climate forcing and salinity variability in Chesapeake Bay, USA. Estuaries and Coasts, 35(1), 237-261.

Yu, L., Fennel, K., & Laurent, A. (2015). A modeling study of physical controls on hypoxia generation in the northern Gulf of Mexico. Journal of Geophysical Research: Oceans, 120, 5019–5039. http://doi:10.1002/2014JC010634

Zervas, C., (2009). Sea level variations of the United States 1854-2006. NOAA Technical Report NOS CO-OPS 053.

Zhai, W. D., Su, J. L., Liu, P. F., Li, Y. W., & Zheng, N. (2019). Emergence of summertime hypoxia and concurrent carbonate mineral suppression in the central Bohai Sea, China. Journal of Geophysical Research: Biogeosciences.

Zhang, J., Gilbert, D., Gooday, A., Levin, L., Naqvi, S. W. A., Middelburg, J. J., ... & Oguz, T. (2010). Natural and human-induced hypoxia and consequences for coastal areas: synthesis and future development.

Zhang, Q., Brady, D. C., & Ball, W. P. (2013). Long-term seasonal trends of nitrogen, phosphorus, and suspended sediment load from the non-tidal Susquehanna River Basin to Chesapeake Bay. Science of the Total Environment, 452, 208-221.

Zhang, Q., Brady, D. C., Boynton, W. R., & Ball, W. P. (2015). Long_Term Trends of Nutrients and Sediment from the Nontidal Chesapeake Watershed: An Assessment of Progress by River and Season. JAWRA Journal of the American Water Resources Association, 51(6), 1534-1555.

Zhong, L., & Li, M. (2006). Tidal energy fluxes and dissipation in the Chesapeake Bay. Continental Shelf Research, 26(6), 752-770.

Zhou, Y., Scavia, D., & Michalak, A. M. (2014). Nutrient loading and meteorological conditions explain interannual variability of hypoxia in Chesapeake Bay. Limnology and Oceanography, 59(2), 373-384.

Zillén, L., Conley, D. J., Andrén, T., Andrén, E., & Björck, S. (2008). Past occurrences of hypoxia in the Baltic Sea and the role of climate variability, environmental change and human impact. Earth-Science Reviews, 91(1-4), 77-92.